

Reference governors: Theoretical extensions and practical applications

by

Uroš Kalabić

A dissertation submitted in partial fulfillment
of the requirements for the degree of
Doctor of Philosophy
(Aerospace Engineering)
in The University of Michigan
2015

Doctoral Committee:

Professor Ilya V. Kolmanovsky, Chair
Professor Dennis S. Bernstein
Julia H. Buckland, Ford Motor Company
Emeritus Professor Elmer G. Gilbert
Professor Jessy W. Grizzle

The painter Kramskoy has a remarkable painting entitled *The Contemplator*: it depicts a forest in winter, and in the forest, standing all by himself on the road, in deepest solitude, a stray little peasant in a ragged caftan and bast shoes; he stands as if he were lost in thought, but he is not thinking, he is “contemplating” something. If you nudged him, he would give a start and look at you as if he had just woken up, but without understanding anything. It’s true that he would come to himself at once, and yet, if he were asked what he had been thinking about while standing there, he would most likely not remember, but would most likely keep hidden away in himself the impression he had been under while contemplating. These impressions are dear to him, and he is most likely storing them up imperceptibly and even without realizing it—why and what for, he does not know either; perhaps suddenly, having stored up his impressions over many years, he will drop everything and wander off to Jerusalem to save his soul, or perhaps he will suddenly burn down his native village, or perhaps he will do both.

There are a good many “contemplatives” among our peasants. And Smerdyakov was probably one of them. And he was probably greedily hoarding up his impressions, hardly knowing why.

—Dostoyevsky, *The Brothers Karamazov*

© Uroš Kalabić 2015

All Rights Reserved

To my parents,
Vojko and Dušanka,
with gratitude;

and to my family,
from Ostružnja to Ann Arbor,
with love

ACKNOWLEDGMENTS

During my doctoral studies, I have surmounted a number of difficulties and I am greatly indebted to many for helping me reach the end of the Prussian educational journey.

Firstly and most importantly, I thank my adviser, Prof. Kolmanovsky, for his guidance and example, for enabling opportunities within the research community, and for giving me the opportunity to do both theoretical and applied research. Most of all, I am thankful for having the opportunity over the past five years to sit at the other end of the desk and learn from his brilliance.

Secondly, I thank my committee for guiding me in writing this dissertation and helping me present my research. I especially thank Dr. Buckland and Prof. Gilbert for working closely with me and providing mentorship during the early part of my doctoral studies.

I also acknowledge all of my co-authors and co-workers, who have helped me in accomplishing my research goals. From Ford: Adam, Amey, Henry, Mrdjan, Nikos, Stephen, and Suzanne; from MERL: Avi and Stefano; from the University: Alexey, Asad, Prof. Bloch, Prof. Cesnik, Chris, Gerardo, Hyeongjun, Jin, John, Kevin, Khaled, Matt, Prof. McClamroch, Phillip, Ray, Ricardo, Rohit, Wenbo, Yash, Ye, Young, and Zhao; and from elsewhere: Prof. Vermillion. I heartfully acknowledge the personal support of my two friends, Alexey and Khaled.

The final acknowledgement is reserved for my wife, Marija, for her love and support.

TABLE OF CONTENTS

DEDICATION	ii
ACKNOWLEDGMENTS	iii
LIST OF FIGURES	vii
LIST OF TABLES	x
LIST OF ABBREVIATIONS	xi
LIST OF SYMBOLS	xii
CHAPTER	
Introduction	1
Overview of reference governors	1
Literature review	7
Contributions and dissertation outline	8
Part I Developments in the theory of reference governors	
1. Reduced-order reference and extended command governors	11
1.1 Introduction	11
1.2 Reduced order governors based on decomposition into fast and slow modes	12
1.3 Main results	19
1.4 Accounting for observer error	22
1.5 Example 1: Turbocharged gasoline engine	24
1.6 Example 2: Flexible beam	26
2. Reference governors for decentralized systems	34
2.1 Introduction	34
2.2 Decentralized reference governors with state reconstruction	35

2.2.1	RG development	36
2.2.2	Decentralized RGs with an observer	38
2.3	Example 1: Aircraft engine	39
2.4	Decentralized reference governors for large-scale systems	41
2.4.1	Constraint sets	44
2.4.2	Decentralized RG design	48
2.5	Example 2: Double mass-spring-damper	49
3.	Command governors for prioritized constraints and reference governors for prioritized references	53
3.1	Introduction	53
3.2	Problem motivation	53
3.3	Command governors for prioritized constraint sets	54
3.3.1	Theoretical results	57
3.3.2	Numerical example	58
3.4	Reference governors for prioritized references	62
3.4.1	Theoretical results	63
3.4.2	Numerical example	64
4.	Reference governors for linear systems subject to nonlinear constraints	68
4.1	Introduction	68
4.2	Reference governors for nonlinear constraints	69
4.2.1	Output prediction	70
4.2.2	Convex constraints	70
4.2.3	Quadratic constraints	72
4.2.4	Mixed logical-dynamic constraints	73
4.2.5	Concave constraints	74
4.3	Example 1: Satellite rendezvous and proximity maneuvering	75
4.3.1	Problem formulation	75
4.3.2	Simulation results	78
4.4	Example 2: Electromagnetically actuated mass-spring-damper system	80
4.4.1	Problem formulation	81
4.4.2	Simulation results	82
5.	Reference and command governors for systems with slowly time-varying references and time-dependent constraints	85
5.1	Introduction	85
5.2	Robustly λ -contractive sets	86
5.3	Slowly-varying references	87
5.4	Slowly-varying constraints	90

5.5	Example 1: Slowly-varying reference	91
5.6	Example 2: Slowly-varying constraint	92
Part II Practical applications of reference governors		
6.	Reference governors for the enforcement of compressor surge constraints	99
6.1	Introduction	99
6.2	Surge constraint	100
6.3	Engine model	102
6.4	Inner-loop reference governor	103
6.4.1	Linear control development	105
6.4.2	Nonlinear control development and analysis	105
6.4.3	Vehicle implementation and experimental results	112
6.5	Outer-loop reference governor	113
6.5.1	Vehicle implementation and experimental results	116
6.6	Discussion	119
7.	Reference governors for airborne wind energy systems	120
7.1	Introduction	120
7.2	Longitudinal dynamic model	122
7.3	Baseline controller design	126
7.4	Linear model simulation	127
7.5	Nonlinear model simulation	130
8.	Reference governors for constrained spacecraft attitude control on $\text{SO}(3)$	134
8.1	Introduction	134
8.2	Constrained LGVI dynamics	135
8.3	Reference governor for $\text{SO}(3)$	136
8.3.1	Unconstrained closed-loop control law	137
8.3.2	Determining $\mathbf{V}(t)$	137
8.4	Numerical simulation results	140
Conclusions and future work 144		
	Conclusions	144
	Future work	147
BIBLIOGRAPHY 149		

LIST OF FIGURES

Figure

0.1	RG schematic	2
1.1	Schematic of a turbocharged gasoline engine.	24
1.2	Responses of a fully measured system of order 3 with varying values of ε plotted on a compressor map	26
1.3	Throttle responses of a fully measured system of order 3 with varying values of ε	27
1.4	Responses of a system of varying order with fixed $\varepsilon = 0.05$ plotted on a compressor map	27
1.5	Throttle responses of a system of varying order with fixed $\varepsilon = 0.05$.	28
1.6	Responses of a system with varying observer gain with fixed $\varepsilon = 0.25$ plotted on a compressor map	28
1.7	Throttle responses of a system with varying observer gain with $\varepsilon = 0.25$	29
1.8	Governed and ungoverned responses of the beam height	32
1.9	Governed and ungoverned responses of the tip deflection plotted along with deflection constraint	33
2.1	Decentralized aircraft engine schematic	41
2.2	Top: Ordinary RG response; Bottom: Decentralized RG response .	42
2.3	Response of the governed $\Delta VSV(t)$, $\Delta VB V(t)$, using ordinary and decentralized RGs	42
2.4	Response of $\Delta W_F(t)$ using ordinary and decentralized RGs	43
2.5	Response of $\Delta T_{48}(t)$ using ordinary and decentralized RGs	43
2.6	Response of $\Delta HPC(t)$ using ordinary and decentralized RGs	44
2.7	Double mass-spring-damper schematic	49
2.8	Distance between the two masses with ordinary and decentralized RGs	51
2.9	Force applied to each mass with ordinary and decentralized RGs . .	52
3.1	Time history of $v(t)$ for three different cases	59
3.2	Time history of $x_1(t)$ for three different cases	60
3.3	Time history of $u(t)$ for three different cases	60
3.4	Time history of $\varepsilon_1(t)$ for two different cases	61
3.5	Time history of $\varepsilon_2(t)$ in the case of $Q_{\varepsilon,3}$	61
3.6	Top: First order of priority; Middle: Second order of priority; Bottom: Ordinary RG	66

3.7	Responses of $\delta_e(t)$ corresponding to the first and second orders of priority	67
3.8	Responses of $\delta_f(t)$ corresponding to the first and second orders of priority	67
4.1	Trajectories of the Deputy in the 1-2 and 2-3 planes of the Hill frame	78
4.2	Close-up views of the trajectories of the Deputy in the 1-2 and 2-3 planes of the Hill frame	79
4.3	Thrust force plotted against the thrust constraint	79
4.4	Along-track position and the relative velocity in the Hill frame . . .	80
4.5	The upper limit on the control $u(t)$	82
4.6	Mass position responses for the three cases	83
4.7	Current responses for the three cases	83
4.8	Control responses for two cases	84
5.1	An illustration of set inclusions	88
5.2	$\hat{\delta}_e(t)$ and $\hat{\delta}_f(t)$ responses	93
5.3	Top: $\theta(t)$ responses with CG based on O_∞^λ ; Bottom: Difference between desired and commanded	93
5.4	Top: $\gamma(t)$ responses with CG based on O_∞^λ ; Bottom: Difference between desired and commanded	94
5.5	Top: $\theta(t)$ responses with CG based on O_∞ ; Bottom: Difference between desired and commanded	94
5.6	Responses corresponding to moving constraint $a(t)$ with $\omega = 0.350\text{rad/s}$	96
5.7	Responses corresponding to moving constraint $a(t)$ with $\omega = 0.637\text{rad/s}$	97
5.8	Responses corresponding to moving constraint $a(t)$ with $\omega = 0.800\text{rad/s}$	97
5.9	Responses corresponding to moving constraint $a(t)$ with $\omega = 0.800\text{rad/s}$ and use of the CG	98
6.1	Typical tip-in/tip-out trajectory with manufacturer's surge constraint and approximate linearized constraint	101
6.2	Engine schematic	103
6.3	Input commands	104
6.4	Comparison of vehicle and model responses	104
6.5	Reference and governed throttle commands based on nonlinear model simulation	106
6.6	Reference and governed throttle commands with surge margin offset based on nonlinear model simulation	107
6.7	Response trajectory with surge margin offset based on nonlinear model simulation	107
6.8	Tip-in/tip-out response on a compressor map using a high-flow OP	108
6.9	Governed and reference throttle inputs using a high-flow OP	109
6.10	Tip-in/tip-out response on a compressor map using a low-flow OP .	109
6.11	Governed and reference throttle inputs using a low-flow OP	110
6.12	Tip-in/tip-out response on a compressor map using scheduled RGs .	111
6.13	Governed and reference throttle inputs using scheduled RGs	111
6.14	Inner-loop RG schematic	112

6.15	Vehicle data: Ungoverned and governed tip-in/tip-out responses on a compressor map using the inner-loop RG	113
6.16	Vehicle data: Ungoverned and governed compressor flow responses using the inner-loop RG	114
6.17	Vehicle data: Ungoverned and governed boost pressure responses using the inner-loop RG	114
6.18	Vehicle data: Ungoverned and governed desired and actual cylinder flow responses using the inner-loop RG	115
6.19	Vehicle data: Ungoverned and governed engine speed responses using the inner-loop RG	115
6.20	Outer-loop RG schematic	116
6.21	Vehicle data: Ungoverned and governed tip-in/tip-out response on a compressor map using the outer-loop RG	117
6.22	Vehicle data: Ungoverned and governed compressor flow response using the outer-loop RG	117
6.23	Vehicle data: Ungoverned and governed boost pressure response using the outer-loop RG	118
6.24	Vehicle data: Ungoverned and governed desired and actual cylinder flow response response using the outer-loop RG	118
7.1	Photograph of Altaeros's proof-of-concept system	121
7.2	Horizontal and vertical wind speeds	125
7.3	Projections of O_∞ onto the α - q and θ - q planes	127
7.4	Desired and governed reference inputs for $z_{g,d}(t)$ and $\theta_d(t)$	128
7.5	z_g and θ ungoverned and governed responses	128
7.6	$\alpha(t)$ ungoverned and governed responses	129
7.7	Forward and aft tension ungoverned and governed responses	129
7.8	$\bar{u}_1(t)$ and $\bar{u}_2(t)$ ungoverned and governed responses	130
7.9	Nonlinear simulation: z_g and θ responses plotted against governed set-point $r(t)$	131
7.10	Nonlinear simulation: $\alpha(t)$ responses	132
7.11	Nonlinear simulation: Forward and aft tension responses	132
7.12	Nonlinear simulation: $\bar{u}_1(t)$ and $\bar{u}_2(t)$ responses	133
8.1	$\ T(t)\ _2$ response	141
8.2	$\Omega_1(t)$, $\Omega_2(t)$, and $\Omega_3(t)$ responses	142
8.3	$\kappa(t)$ response	142
8.4	Orientation maneuver plotted at 10s increments	143

LIST OF TABLES

Table

1.1	Number of required constraint variables	26
2.1	Decentralized aircraft engine example data	40
5.1	Table of parameters for the function $a(t)$	95
7.1	Key shroud model variables	122
7.2	Nominal Operating Point for Linearized Model	124

LIST OF ABBREVIATIONS

CBV	Compressor bypass valve
CG	Command governor
ECG	Extended command governor
ECU	Engine control unit
HCW	Hill-Clohessy-Wiltshire
LGVI	Lie group variational integrator
LOS	Line-of-sight
LQR	Linear-quadratic regulator
MLD	Mixed logical-dynamic
MPC	Model predictive control
PCM	Powertrain control module
PRG	Prioritized reference governor
RG	Reference governor
ROM	Read-only memory

LIST OF SYMBOLS

- \mathbb{R} : Set of real numbers
 \mathbb{R}^n : Set of n -dimensional vectors of real elements
 $\mathbb{R}^{n \times m}$: Set of n -by- m matrices of real elements
 \mathbb{Z}_+ : The set of non-positive integers
- Let $A, B \subset \mathbb{R}^n$ and $c, x \in \mathbb{R}^n$
- \subset : $A \subset B$ signifies that A is a subset of B , *i.e.*, $a \in A \implies a \in B$
 \supset : $A \supset B$ signifies that A is a superset of B , *i.e.*, $a \in A \longleftarrow a \in B$
 int : $\text{int } A$ signifies the interior of the set A
 \oplus : Minkowski addition, *i.e.*, $A \oplus B = \{a + b : a \in A, b \in B\}$
 \sim : Pontryagin subtraction, *i.e.*, $A \sim B = \{c \in \mathbb{R}^n : c + b \in A, \forall b \in B\}$
 h_A : Support function, *i.e.*, $h_A(c) = \sup_{x \in A} c^T x$
 $\|x\|_p$: p -norm, *i.e.*, $\|x\|_p^p = \sum_{i=1}^n |x_i|^p$ for $1 \leq p < \infty$
 $\|x\|_Q$: Q -norm, *i.e.*, $\|x\|_Q^2 = \frac{1}{2} x^T Q x$ for positive-definite $Q \in \mathbb{R}^{n \times n}$
 \mathcal{B}_n : n -dimensional ball of unit radius centered at the origin, *i.e.*, $\{x \in \mathbb{R}^n : \|x\|_2 \leq 1\}$
 I_n : n -by- n identity matrix, *i.e.*, the element satisfying $I_n P = P I_n = P$ for all $P \in \mathbb{R}^n$
 $\mathbf{1}_n$: n -dimensional vector of all-ones, *i.e.*, $[\mathbf{1}_n]_i = 1$ for all $1 \leq i \leq n$
 δ : Dirac delta function, *i.e.*, $\delta(t) = 1$ if $t = 0$ and 0 otherwise
 $\text{SO}(3)$: 3-dimensional special orthogonal group, *i.e.*, the set of all orthogonal matrices with determinant equal to 1, $\{P \in \mathbb{R}^{3 \times 3} : P^T P = I_3, \det P = 1\}$
 \cdot^\times : The map from elements of \mathbb{R}^3 to elements of $\mathbb{R}^{3 \times 3}$ which preserves the cross product under multiplication, *i.e.*, if $X = a^\times$, then $a \times b = Xb$ for any $b \in \mathbb{R}^3$, where \times is the cross-product

Introduction

All control systems are subject to constraints. These constraints can include physical actuator and safety limits as well as other design requirements. Often, control schemes are designed without rigorously taking constraints into account and the focus of the design is instead placed on transient system performance. However, as systems become downsized and performance is stretched to its physical limitations, it becomes increasingly important to develop mechanisms that enforce constraints while preserving desirable characteristics of the transient response. In such a case, to protect system components from damage and to enforce other requirements, it is desirable to implement a constrained control scheme that modifies input signals to closed-loop controllers in order to ensure constraint enforcement. The reference governor is such a scheme. It modifies input signals to closed-loop control systems only if it predicts present or future constraint violation; otherwise it preserves the unconstrained system response.

This dissertation describes recent developments in reference governor theory and applications. In this chapter, we provide an overview of reference governors, as well as the closely related extended command governors, and summarize the contributions we have made. Note that the developments presented herein will be referred to frequently throughout the dissertation.

Overview of reference governors

Reference governors (RGs) and the related command governors (CGs) and extended command governors (ECGs) are add-on predictive control schemes that enforce pointwise-in-time state and control constraints in discrete-time, closed-loop systems. Unlike conventional model predictive control (MPC) schemes [1], which enforce constraints and ensure system stability, RGs are used to augment systems with closed-loop controllers that may have been designed without taking constraints into account. Ordinarily, the placement of RGs follows the schematic shown in Fig. 0.1. In

the schematic, the RG utilizes the measured or estimated state $x(t)$ in order to form a prediction of future constraint violation and, if required, modify the reference input from the desired $r(t)$ to the constraint-admissible $v(t)$ so that the output constraint $y(t) \in Y$ is satisfied for all present and future time instants $t \in \mathbb{Z}_+$, and any possible set-bounded disturbance sequence $\{w(t)\} \in W$.

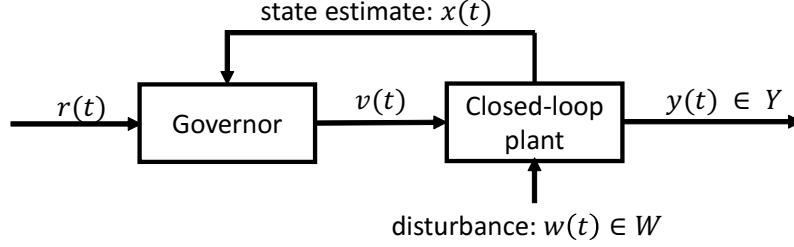


Figure 0.1: RG schematic

The focus of this dissertation is primarily on RGs and related governor schemes whose design is based on linear system models; such RGs are referred to as “linear RGs.” In several applications, these linear RGs will be applied to nonlinear systems, sometimes with modifications intended to compensate for the differences between linear and nonlinear models. In general, there also exist RGs for the case where the closed-loop model is nonlinear, *i.e.*, “nonlinear RGs” [2, 3]. Their application will be considered in Chapter 8 to the problem of enforcing constraints for models whose dynamics evolve on a smooth manifold.

Linear RGs are designed based on the discrete-time system,

$$x(t+1) = Ax(t) + Bv(t) + B_w w(t), \quad (0.1a)$$

$$y(t) = Cx(t) + Dv(t) + D_w w(t) \in Y, \quad (0.1b)$$

where $x(t) \in \mathbb{R}^n$ is the state, $v(t) \in \mathbb{R}^m$ is the admissible reference input, $w(t) \in \mathbb{R}^\ell$ is the disturbance input, and $y(t)$ is the constrained output that must satisfy constraints $y(t) \in Y \subset \mathbb{R}^p$ subject to any set-bounded disturbance sequence $\{w(t)\} \in W$. The matrix A is Schur, *i.e.*, all eigenvalues are in the unit disk, and the pair (C, A) is observable. The set Y satisfies the Minkowski assumptions, *i.e.*, it is compact, convex, and contains 0 in its interior; the set W is compact and contains 0. Unless otherwise specified, the full state $x(t)$ is assumed to be known; when it is not, we design an observer. The observer error may be accounted for in the design of the RG [4], and we do so in some of the subsequent theoretical developments.

The goal of the RG is to enforce constraints while ensuring that the reference input

$v(t)$ is close to the desired reference input $r(t)$. The RG does this by varying $v(t)$ along the line segment connecting the previously constraint-admissible input $v(t-1)$ and the desired input $r(t)$,

$$v(t) = v(t-1) + \kappa(t)(r(t) - v(t-1)), \quad (0.2)$$

where the parameter $\kappa(t) \in [0, 1]$ is maximized so that $v(t)$ is constraint admissible and close to $r(t)$ at each time instant t .

The RG relies on the model (0.1) in order to predict future constraint violation. This prediction of future constraint violation is performed by exploiting an approximation to the set,

$$O_\infty = \{(x, v) : x(0) = x, v(t) = v, \quad (0.1) \text{ are satisfied for all } t \in \mathbb{Z}_+ \text{ and } \{w(t)\} \in W\}, \quad (0.3)$$

which is computed offline. The set O_∞ is the set of all initial state and reference input pairs such that, when the reference is held constant, the constraints are satisfied for all present and future time instants and for any possible set-bounded sequence of disturbances.

Note that given an initial condition $x(0) = x$ and constant reference input $v(t) \equiv v$, the solution to (0.1b) is given by,

$$y(t) = CA^t(x - \Gamma v) + (C\Gamma + D)v + CA^t B_w w(0) + \dots + CAB_w w(t-1) + D_w w(t) \in Y, \quad (0.4)$$

where $\Gamma = (I_n - A)^{-1}B$ is the map from the constant reference v to the steady-state solution $\lim_{t \rightarrow \infty} x(t)$ in the disturbance-free case where $w(t) \equiv 0$. The set O_∞ is then the set of pairs (x, v) such that $CA^t x + (C\Gamma + D)v \subset Y \sim CA^t B_w W \sim \dots \sim C_B w \sim D_w W$ for all $t \in \mathbb{Z}_+$. It can be computed using the following recursive algorithm,

$$Y_{t+1} = Y_t \sim CA^t B_w W, \quad (0.5a)$$

$$O_{t+1} = O_t \cap X_{t+1}, \quad (0.5b)$$

where $X_t = \{(x, v) : CA^t x + (C\Gamma + D)v \in Y_t\}$ and the sets Y_0 and O_0 are initialized to $Y_0 = Y \sim D_w W$ and $O_0 = X_0$. If there exists a time $t^* \in \mathbb{Z}_+$ such that $O_{t^*} = O_{t^*+1}$, then $O_{t^*} = O_{t^*+k}$ for all $k \in \mathbb{Z}_+$ and $O_\infty = O_{t^*}$ is finitely determined. If O_∞ is not finitely determined, a finitely determined inner approximation can be obtained by steady-state constraint tightening [5]. Specifically, to compute this finitely determined

approximation, we introduce a constraint $v(t) \in \Omega$, where Ω is an inner approximation to the set of all constraint admissible steady-state references, *i.e.*, $\Omega \subset \text{int } \Omega_d$ where,

$$\Omega_d = \{r \in \mathbb{R}^m : (C\Gamma + D)r \in Y_\infty\}, \quad (0.6)$$

where $Y_\infty = \lim_{t \rightarrow \infty} Y_t$. This approximation has all the required properties of O_∞ such as constraint admissibility and positive invariance, and it replaces O_∞ in all the subsequent developments.

If Y is polyhedral, then there exists a straightforward computational procedure for performing the updates in (0.5). Suppose Y is of the form,

$$Y = \{y : Sy \leq s\}. \quad (0.7)$$

Then the step (0.5a) becomes,

$$Y_t \sim CA^t B_w W = \{y : Sy \leq s^{(i)}\}, \quad (0.8)$$

where the columns $s_k^{(i)}$ of $s^{(i)}$ are determined by,

$$s_k^{(i+1)} = s_k^{(i)} - h_W((CA^t B_w)^T S_k^T), \quad (0.9)$$

where h_W is a support function, S_k is the k -th row of S and $s_k^{(0)} = s_k - h_W(D_w^T S_k^T)$. Note that if W is polyhedral with vertices w^q , $q = 1, \dots, n_w$, then for $\eta \in \mathbb{R}^\ell$, $h_w(\eta) = \max_{q=1, \dots, n_w} \eta^T w^q$. The step (0.5b) becomes,

$$O_{t+1} = \{(x, v) : H_x^{(t+1)} + H_v^{(t+1)}v \leq h^{(t+1)}\}, \quad (0.10)$$

where $H_x^{(t+1)}$, $H_v^{(t+1)}$, and $h^{(t+1)}$ are recursively growing matrices,

$$H_x^{(t+1)} = \begin{bmatrix} H_x^{(t)} \\ SC A^t \end{bmatrix}, \quad H_v^{(t+1)} = \begin{bmatrix} H_v^{(t)} \\ SCT\Gamma + D - SC A^t \Gamma \end{bmatrix}, \quad h^{(t+1)} = \begin{bmatrix} h^{(t)} \\ s^{(t)} \end{bmatrix},$$

and are initialized to,

$$H_x^{(0)} = \begin{bmatrix} SC \\ 0 \end{bmatrix}, \quad H_v^{(0)} = \begin{bmatrix} 0 \\ SCT\Gamma + D \end{bmatrix}, \quad h^{(0)} = \begin{bmatrix} s^{(0)} \\ s^\infty \end{bmatrix},$$

where $s^\infty \leq \lim_{t \rightarrow \infty} s^{(t)}$ is an approximation to the limit of $s^{(t)}$ as $t \rightarrow \infty$ [6].

The RG solves the following optimization problem,

$$\max \kappa(t) \in [0, 1], \quad (0.11a)$$

$$\text{sub. to } v(t-1) + \kappa(t)(r(t) - v(t-1)) \in \Pi(x(t)), \quad (0.11b)$$

where $\Pi(x)$ is a slice of O_∞ at x ,

$$\Pi(x) = \{v : (x, v) \in O_\infty\}. \quad (0.12)$$

The optimization (0.11) is computed by solving a finite sequence of scalar divisions and logical comparisons [7]. An alternative to (0.11) is to compute $v(t)$ by performing a bijection search for $\kappa(t)$ over the interval $[0, 1]$ while, for each candidate $\kappa(t)$, simulating the system over a sufficiently long enough horizon to predict constraint violation [3].

The closely related ECG is a version of the RG that computes $v(t)$ by solving a quadratic programming problem. The ECG is more flexible than the RG because it does not restrict the update of the reference $v(t)$ to the line segment connecting $v(t-1)$ and $r(t)$; furthermore, it has a larger domain of attraction than the RG [8]. In the ECG, the reference $v(t)$ is the output of an auxiliary system which has been designed offline,

$$\bar{x}(t+1) = \bar{A}\bar{x}(t), \quad (0.13a)$$

$$v(t) = \bar{C}\bar{x}(t) + \rho(t), \quad (0.13b)$$

where $\bar{x}(t) \in \mathbb{R}^{\bar{n}}$ is the auxiliary state, $\rho(t) \in \mathbb{R}^m$ is the steady-state offset, \bar{A} is an asymptotically stable matrix and the pair (\bar{C}, \bar{A}) is observable. When the auxiliary dynamics (0.13) are coupled with the dynamics (0.1), the full system dynamics become,

$$\begin{bmatrix} \tilde{x}(t+1) \\ \rho(t+1) \end{bmatrix} = \begin{bmatrix} \tilde{A} & \tilde{B} \\ 0 & I_m \end{bmatrix} \begin{bmatrix} \tilde{x}(t) \\ \rho(t) \end{bmatrix} + \begin{bmatrix} \tilde{B}_w \\ 0 \end{bmatrix} w(t), \quad (0.14a)$$

$$y(t) = \begin{bmatrix} \tilde{C} & D \end{bmatrix} \begin{bmatrix} \tilde{x}(t) \\ \rho(t) \end{bmatrix} + D_w w(t) \in Y, \quad (0.14b)$$

where,

$$\tilde{x}(t) = \begin{bmatrix} x(t) \\ \bar{x}(t) \end{bmatrix}, \tilde{A} = \begin{bmatrix} A & B\bar{C} \\ 0 & \bar{A} \end{bmatrix}, \tilde{B} = \begin{bmatrix} B \\ 0 \end{bmatrix}, \tilde{B}_w = \begin{bmatrix} B_w \\ 0 \end{bmatrix}, \tilde{C} = \begin{bmatrix} C & D\bar{C} \end{bmatrix}.$$

The corresponding maximal output admissible set (0.3) is,

$$O_\infty^{\text{aug}} = \{(x, \bar{x}, \rho) : x(0) = x, \bar{x}(0) = \bar{x}, \rho(0) = \rho, \quad (0.14) \text{ are satisfied for all } t \in \mathbb{Z}_+ \text{ and } \{w(t)\} \in W\}. \quad (0.15)$$

Let $\Pi^{\text{aug}}(x)$ be the slice of O_∞^{aug} at x ,

$$\Pi^{\text{aug}}(x) = \{(\bar{x}, \rho) : (x, \bar{x}, \rho) \in O_\infty^{\text{aug}}\}. \quad (0.16)$$

The quadratic programming problem that is solved by the ECG is,

$$\min \|\bar{x}(t)\|_{\bar{S}}^2 + \|r(t) - \rho(t)\|_S^2, \quad (0.17a)$$

$$\text{sub. to } (\bar{x}(t), \rho(t)) \in \Pi^{\text{aug}}(x(t)), \quad (0.17b)$$

where \bar{S} and S are positive definite matrices and \bar{S} satisfies the Lyapunov condition, $\bar{A}^T \bar{S} \bar{A} - \bar{S} = -Q$ for some positive definite matrix Q .

The final example of scheme closely related to the RG that is considered in this dissertation is the CG. The CG is a version of the ECG in which $\bar{n} = 0$, *i.e.*, the auxiliary dynamics are empty. Consequently there is no gain in domain of attraction as compared to the RG, however the flexibility of the ECG update policy is preserved. Since $v(t) = \rho(t)$, the optimization (0.17) is,

$$\min \|r(t) - v(t)\|, \quad (0.18a)$$

$$\text{sub. to } v(t) \in \Pi(x(t)), \quad (0.18b)$$

where the norm to be minimized is not necessarily quadratic [3].

RGs, ECGs, and CGs exhibit the properties of recursive feasibility for the optimizations (0.11), (0.17), (0.18), finite-settling time for the case where $r(t)$ is held constant, and convergence of the state $x(t)$ to an attractor set that depends on the size of the disturbance set W . These results are presented in detail in [7] for RGs and [8] for ECGs and CGs and we summarize them in the following. To do this, we need to introduce a few additional definitions.

Let,

$$F_\infty(r) = \{\Gamma r\} \oplus F_\infty, \quad F_\infty = \lim_{t \rightarrow \infty} F_t, \quad F_t = \bigoplus_{i=0}^{t-1} A^i B_w W, \quad F_0 = \{0\}. \quad (0.19)$$

The set $F_\infty(r)$ is the attractor set for (0.1a) when $v(t) \equiv r$. Specifically, $F_\infty(r)$ is compact and, for all $x(0)$ and all $\varepsilon > 0$, there exists a $\bar{t} \in \mathbb{Z}_+$ such that $x(t) \in F_\infty(r) \oplus \varepsilon \mathcal{B}_n$ for all $t \geq \bar{t}$. Define,

$$\mathcal{X} = \{x : \exists v \text{ s.t. } (x, v) \in O_\infty\}, \quad (0.20)$$

$$\mathcal{X}^{\text{aug}} = \{x : \exists (\bar{x}, \rho) \text{ s.t. } (x, \bar{x}, \rho) \in O_\infty^{\text{aug}}\}. \quad (0.21)$$

These sets are respectively the projections of O_∞ and O_∞^{aug} onto \mathbb{R}^n and correspond to the domains of attraction for the RG or CG and the ECG. By their definition, it is clear that $\mathcal{X}^{\text{aug}} \supset \mathcal{X}$. This means that the ECG, as a result of its more flexible design through the addition of auxiliary variables, has a larger domain of attraction than the RG and CG.

We state the main RG and ECG theorems. The first is a portion of the main results of [7]. The second is the main result of [8].

Theorem 0.1 (Reference governor). *Consider the system (0.1) with $\{r(t)\} \in \mathbb{R}^m$, $\{w(t)\} \in \mathcal{W}$, $v(t)$ defined by (0.2), (0.11), and $x(0) \in \mathcal{X}$. Then: (i) $x(t)$, $v(t)$, and $y(t)$ are defined for all $t \in \mathbb{Z}_+$; (ii) $y(t) \in Y$ and $x(t) \in \mathcal{X}$ for all $t \in \mathbb{Z}_+$. Suppose further there exists $t_s \in \mathbb{Z}_+$ such that $r(t) = r_s \in \Omega$ for all $t \geq t_s$. Then (iii) there exists $t_f \in \mathbb{Z}_+$ such that $v(t) = r_s$ for all $t \geq t_f$; (iv) given $\varepsilon > 0$, there exists a $t_\varepsilon \in \mathbb{Z}_+$ such that $x(t) \in F_\infty(r_s) \oplus \varepsilon \mathcal{B}_n$ for all $t \geq t_\varepsilon$.*

Theorem 0.2 (Extended command governor). *Consider the system (0.1) with $\{r(t)\} \in \mathbb{R}^m$, $\{w(t)\} \in \mathcal{W}$, $v(t)$ defined by (0.13b), (0.17), and $x(0) \in \mathcal{X}^{\text{aug}}$. Then: (i) $x(t)$, $v(t)$, and $y(t)$ are defined for all $t \in \mathbb{Z}_+$; (ii) $y(t) \in Y$ and $x(t) \in \mathcal{X}^{\text{aug}}$ for all $t \in \mathbb{Z}_+$. Suppose further there exists $t_s \in \mathbb{Z}_+$ such that $r(t) = r_s$ for all $t \geq t_s$. Define $r_s^* = \arg \min_{r \in \Omega} \|r - r_s\|_S^2$. Then (iii) there exists $t_f \in \mathbb{Z}_+$ such that $v(t) = r_s^*$ for all $t \geq t_f$; (iv) given $\varepsilon > 0$, there exists a $t_\varepsilon \in \mathbb{Z}_+$ such that $x(t) \in F_\infty(r_s^*) \oplus \varepsilon \mathcal{B}_n$ for all $t \geq t_\varepsilon$.*

Literature review

RGs were originally proposed as constraint-enforcing mechanisms for application to continuous-time systems in [9, 10, 11]. In [9], the authors introduced a RG-like

method for application to stable systems and in [10], they considered applications to unstable systems by placing the governor inside the control loop.

Thereafter, [12, 13] considered discrete-time RG formulations by introducing what is now called the static RG, where the design was based on the update equation $v(t) = \kappa(t)r(t)$ instead of (0.2). In [14, 15], these ideas were refined into the form of RGs that are considered in this dissertation, with the exception that disturbances were not considered; this is equivalent to the RG with $W = 0$. The authors then refined this approach by introducing an RG in [7] that was robust to disturbances and that was based on the theory of robustly invariant sets developed previously in [5]. This theory forms the basis for the type of RGs that are considered in this dissertation.

Concurrent with the above developments, a different version of the RG was also under development. This version is similar to the CG and was developed for discrete-time systems; however the prediction is based on online simulations instead of maximal output admissible sets. This version of the RG was first presented in [16], followed by further developments in [17, 18, 3, 19, 20].

The development of RG theory was further pursued in [2], where the authors developed a nonlinear version of the RG which used constraint admissible and not necessarily invariant sets, similar to the linear RG. A parameter governor, which varied system parameters as opposed to the reference input, was considered in [21]. An RG for piecewise affine systems was proposed in [22]. The ECG was introduced in [8]. Examples of more recent theoretical developments include that of CGs for the case where the state is not directly estimated [23, 24] and RGs for network control systems [25, 26]. Recent survey papers on RGs and related topics include [27] and [28]. In addition, the technical report [6] is a comprehensive introductory reference that considers the computational aspects of maximal output admissible sets.

Applications of RGs, CGs, and ECGs have also been reported in the literature. These include the application of governors to a magnetically actuated mass-spring-damper system [29], an inverted pendulum [20], cable robots [30], and spacecraft guidance [31]. Automotive applications include rollover [32], fuel-cell systems [33, 34, 35], and HCCI engines [36, 37], with experimental results reported in [36, 37].

Contributions and dissertation outline

This dissertation is split into two parts. Part I considers new developments in the theory of RGs and Part II considers their practical applications.

In Part I, the theoretical contributions generally consist of various new RG schemes, which are modifications of the ordinary RG and for which we develop new theory. In Part II, we consider the application of the ordinary RG to practical systems subject to constraints. The majority of the contents of this dissertation has been published or submitted to scientific journals [38, 39] or refereed conference proceedings [40, 41, 42, 43, 44, 45, 46, 47]. Related developments that are not included in the dissertation have appeared in or have been submitted to journal papers [48, 49] and conference papers [27, 50, 51].

The individual contributions are listed below in order of their corresponding chapters.

Part I, Chapter 1 [38, 40]: Reduced-order RG and ECG schemes have been developed. These schemes take advantage of the modal decomposition of a system into slow and fast subsystems. The underlying predictive model is based on the slow states of the full-order system and approximates the fast states as if they were at steady-state. This results in a reduced complexity of the predictive model and reduced the memory required to store O_∞ and O_∞^{aug} . Under suitable assumptions, the schemes have been shown to enforce constraints and converge to a steady-state reference.

Chapter 2 [41]: RG schemes have been developed for decentralized systems. These schemes are based on ideas related to the reduced-order RG of the previous chapter in the sense that RGs are designed for the subsystems of the decentralized systems. These subsystem RGs operate such that constraint enforcement is assured for the system as a whole.

Chapter 3 [42]: Prioritized RG schemes have been developed for systems subject to constraints of different priorities and for systems with prioritized reference inputs. The prioritized constraint handling scheme utilizes a slack parameter that is used as padding to the constraints, with the lower priority constraint allowing for higher values of padding. The prioritized reference scheme computes the admissible reference $v(t)$ element by element, maximizing the higher priority elements before considering elements of lower priority.

Chapter 4 [43]: Various RG approaches have been considered for cases when the set Y is not polyhedral and therefore not given by a set of linear inequalities. Specifically, four different cases are discussed where the constraints are one of: convex, quadratic, mixed logical-dynamics, or concave. Algorithms for computing $v(t)$ have been developed for all four cases and illustrated with simulation results.

Chapter 5 [44]: RG and CG schemes have been developed for systems that track a time-varying reference $r(t)$ and that are subject to time-dependent constraints, *i.e.*,

the case where $Y = Y_t$. The schemes are based on a contractive version of the set O_∞ , which is different from the ordinary, invariant design. When the CG constraint set is contractive, the CG scheme has been shown to track references that vary with time. When the RG constraint set is contractive, the RG scheme has been shown to enforce constraints that depend on time.

Part II, Chapter 6 [39, 45]: The RG has been applied to the enforcement of the compressor surge constraint for turbocharged engines. Surge is an unstable and undesirable flow process and tends to occur inside what is called the surge region on a compressor map. Avoiding this region using the RG leads to the mitigation of surge. Experimental vehicle data has been presented that shows the efficacy of the RG for enforcement of the surge constraint.

Chapter 7 [46]: The RG has been applied to the control of a tethered airborne wind energy system. These systems take advantage of the higher power density available at high altitude, but are subject to constraints on parameters such as tether tension and angle of attack, which ensure that the system remains airborne. We have developed a linear controller for tracking set-point commands and coupled it with an RG that ensures constraint enforcement. Nonlinear simulations have been presented that show the successful operation of the RG in enforcing constraints.

Chapter 8 [47]: The RG has been applied to the constrained control of spacecraft attitude, whose configuration space is $SO(3)$. The RG updates $v(t)$ by utilizing the underlying group structure of $SO(3)$. This scheme has been analyzed and demonstrated to have global rest-to-rest reorientation properties on $SO(3)$. Numerical simulations have been reported that show the enforcement of attitude constraints using the RG.

Part I

Developments in the theory of reference governors

CHAPTER 1

Reduced-order reference and extended command governors

1.1 Introduction

The complexity of the RG, ECG, and CG optimizations, (0.11), (0.17), and (0.18) respectively, are directly related to the dimension of the system n . The purpose of this chapter is to present an approach for reducing this complexity. It takes advantage of decomposing the state of system (0.1) into *slow* and *fast* states, as characterized by magnitude of the eigenvalues of A , and modeling (0.1) by an appropriate, reduced order model based on the slow subsystem. The effects of the fast states are treated as an output disturbance in the reduced order model. With appropriate constraint tightening to account for this disturbance, it follows that whenever $v(t)$ in the slow model is such that hard constraints in the reduced order model are met, then the same $v(t)$ used in (0.1) assures that the actual constraints are met. Thus, applying a governor to the reduced order model guarantees constraint satisfaction in system (0.1).

In this chapter, we first develop the theory of the reduced order RG followed by the theory of the reduced order ECG. The ideas behind the reduced order ECG are similar to those of the reduced order RG, but more complex because of the need to consider the state of the auxiliary system $\bar{x}(t)$. Because of these auxiliary states, model order

reduction is even more important for making the ECG computationally tractable. Model order reduction directly contributes to lower complexity by decreasing the number of state variables needed for the implementation of the ECG.

It is important to note that there is a trade-off in the order reduction. The errors in the system approximation must be suitably controlled and this is done by tightening constraints; the consequence of constraint tightening is that the set of recoverable initial states may be reduced and the reduced order governors may produce slower response than the ordinary RG and ECG schemes.

Two examples are considered. In the first example, we demonstrate that the surge margin constraint in a turbocharged gasoline engine can be handled based on the reduced order model for the two slowest states out of five states in total. The complexity reduction is important for this application due to limited computational capability of the Engine Control Unit (ECU). In the second example, we demonstrate that constraints on the elastic deflections of the free-free beam [52], which is an infinite-dimensional system, can be handled based on the reduced order model of the two lowest frequency modes. This example is motivated by applications to very flexible aircraft [53].

The chapter is organized as follows. Section 1.2 presents the development of the reduced order RG and ECG. Section 1.3 presents the main theorem. Section 1.4 considers the treatment of observer errors in the case where not all slow states are measured. Section 1.5 presents an application of the reduced order RG to a turbocharged gasoline engine. Section 1.6 presents an application of the reduced order RG to an example that involves an infinite-dimensional system model.

1.2 Reduced order governors based on decomposition into fast and slow modes

This section presents a model order reduction that is based on the decomposition of the system (0.1) into normal modes. Specifically, the system is decomposed according to fast and slow eigenvalues, and the RG or ECG is then designed based on the slow subsystem only. A more general decomposition [54] is possible and its development is similar, but because it does not lead to a reduction in model order, it is not explicitly considered here.

We begin by transforming the system via an appropriate coordinate transformation so that (0.1) is split into fast and slow subsystems. Consider an invertible

coordinate transformation $P : \mathbb{R}^n \rightarrow \mathbb{R}^n$ such that,

$$P^{-1}x(t) = \begin{bmatrix} x_2(t) \\ x_1(t) \end{bmatrix}, \quad P^{-1}AP = \begin{bmatrix} A_2 & 0 \\ 0 & A_1 \end{bmatrix}, \quad (1.1)$$

$$P^{-1}B = \begin{bmatrix} B_2 \\ B_1 \end{bmatrix}, \quad P^{-1}B_w = \begin{bmatrix} B_{w,2} \\ B_{w,1} \end{bmatrix}, \quad CP = \begin{bmatrix} C_2 & C_1 \end{bmatrix}, \quad (1.2)$$

where $A_1 \in \mathbb{R}^{n_1 \times n_1}$ and $A_2 \in \mathbb{R}^{n_2 \times n_2}$ are, respectively, matrices of the fast and slow dynamics; by this, we mean that the magnitudes of all eigenvalues of A_1 are small when compared to the magnitudes of all eigenvalues of A_2 . Assuming that such a transformation can be constructed, our approach is to design the governor based only on the dynamics of $x_2(t)$ and develop conditions that bound the error that is introduced by the deviation of $x_1(t)$ from steady-state.

The RG and CG dynamics are a special case of the ECG dynamics where the auxiliary system is empty; *i.e.*, $\bar{n} = 0$ implies $v(t) = \rho(t)$, so we continue the development of the reduced order governor scheme with a specific focus on the ECG. We will specialize the ECG scheme to the RG later. Let,

$$\tilde{P} = \begin{bmatrix} P & 0 \\ 0 & I_{\bar{n}} \end{bmatrix}, \quad (1.3)$$

so that,

$$\tilde{P}^{-1}\tilde{A}\tilde{P} = \begin{bmatrix} A_2 & 0 & B_2\bar{C} \\ 0 & \hat{A} \\ 0 & \end{bmatrix}, \quad (1.4)$$

wherein,

$$\hat{A} = \begin{bmatrix} A_1 & B_1\bar{C} \\ 0 & \bar{A} \end{bmatrix}, \quad \hat{B} = \begin{bmatrix} B_1 \\ 0 \end{bmatrix}, \quad \hat{\Gamma} = \begin{bmatrix} \Gamma_1 \\ 0 \end{bmatrix}, \quad \hat{B}_w = \begin{bmatrix} B_{w,1} \\ 0 \end{bmatrix}, \quad \hat{C} = \begin{bmatrix} C_1 & 0 \end{bmatrix}, \quad (1.5)$$

and $\Gamma_1 := (I_{n_1} - A_1)^{-1}B_1$. Because $x_1(t)$ represents the fast state, subsequent developments are guided by the approximation that,

$$x_1(t) \approx \Gamma_1\rho(t). \quad (1.6)$$

We introduce a modified approximate output,

$$y_2(t) = C_2 x_2(t) + C_1 \Gamma_1 \rho(t) + Dv(t) + D_w w(t). \quad (1.7)$$

To maintain the true and modified outputs close to each other, we introduce an artificial *output error set* $E_y \subset \mathbb{R}^p$, and subsequently use it as an artificial constraint on their difference, *i.e.*,

$$\hat{y}(t) = y(t) - y_2(t) \in E_y. \quad (1.8)$$

Note that,

$$\hat{y}(t) = C_1(x_1(t) - \Gamma_1 \rho(t)). \quad (1.9)$$

The choice of E_y must satisfy conditions that are determined by the modal decomposition of system (0.1): E_y is compact, convex, and satisfies,

$$E_y \subset \text{int } Y_{\infty,2}, \quad (1.10)$$

where,

$$Y_{\infty,2} = Y \sim D_w W \sim \begin{bmatrix} 0 & C_2 \end{bmatrix} F_{\infty} \supset Y_{\infty}. \quad (1.11)$$

Finally, the modified output must be constrained to a tightened form of Y ,

$$y_2(t) \in Y \sim E_y, \quad (1.12)$$

where (1.8) and (1.12) together imply that $y(t) = y_2(t) + \hat{y}(t) \in (Y \sim E_y) \oplus E_y \subset Y$.

Thus to guarantee $y(t) \in Y$ for all $t \in \mathbb{Z}_+$, the ECG can be applied to a modified system based on the dynamics of A_2 and constraints on the modified output (1.12) with the additional constraint in (1.8).

An approach to satisfying (1.8) is based on translating it to a set of sufficient conditions on $v(t)$. We define a *state error set* $E_x \subset \mathbb{R}^{n_1} \times \mathbb{R}^{\bar{n}}$, satisfying,

$$\hat{A}E_x \oplus \hat{B}_w W \subset \text{int } E_x, \quad (1.13)$$

$$\hat{C}E_x \subset E_y. \quad (1.14)$$

The condition in (1.13) implies that E_x is robustly invariant and contractive with respect to \hat{A} and is used to recursively guarantee constraint admissibility of the error dynamics and also to guarantee convergence. The condition in (1.14) relates E_x to E_y and guarantees constraint admissibility in the presence of disturbances.

If we define,

$$\hat{x}(t) = \begin{bmatrix} x_1(t) - \Gamma_1 \rho(t) \\ \bar{x}(t) \end{bmatrix}, \quad (1.15)$$

then from (1.14), $0 \in W$, and the definition of \hat{C} , it follows that $\hat{x}(t) \in E_x \implies \hat{y}(t) = C_1(x_1(t) - \Gamma_1 \rho(t)) = \hat{C}\hat{x}(t) \in \hat{C}E_x \subset E_y$.

The following proposition characterizes the predicted trajectories of the errors $\hat{x}(t)$ and $\hat{y}(t)$. The prediction of the trajectory of $\hat{y}(t)$ is needed in order to subsequently enforce the constraint (1.8).

Proposition 1.1. *The dynamics of $\hat{x}(t+k|t)$ and $\hat{y}(t+k|t)$ for $k \in \mathbb{Z}_+$ satisfy,*

$$\hat{x}(t+k+1|t) = \hat{A}\hat{x}(t+k|t) + \hat{B}_w w(t+k), \quad (1.16a)$$

$$\hat{x}(t|t) = \hat{x}(t|t-1) + \Delta\hat{x}(t),$$

$$\hat{y}(t+k+1|t) = \hat{C}\hat{x}(t+k+1|t), \quad (1.16b)$$

where,

$$\Delta\hat{x}(t) = \begin{bmatrix} -\Gamma_1 \Delta\rho(t) \\ \Delta\bar{x}(t) \end{bmatrix}, \quad (1.17)$$

$$\Delta\rho(t) = \rho(t) - \rho(t-1), \quad (1.18)$$

$$\Delta\bar{x}(t) = \bar{x}(t) - \bar{A}\bar{x}(t-1),$$

$$\hat{x}(t|t-1) = \begin{bmatrix} x_1(t) - \Gamma_1 \rho(t-1) \\ \bar{A}\bar{x}(t-1) \end{bmatrix}. \quad (1.19)$$

Proof. To show (1.16a), consider some $k \geq 0$. Then, $\hat{x}(t+k+1|t) = [(x_1(t+k+1|t) - \Gamma_1 \rho(t))^T \bar{x}(t+k+1|t)^T]^T = \hat{A}[x_1(t+k|t)^T \bar{x}(t+k|t)^T]^T + \hat{B}_w w(t+k) + \hat{B}\rho(t) - \hat{\Gamma}\rho(t) = \hat{A}[x_1(t+k|t)^T \bar{x}(t+k|t)^T]^T + \hat{B}_w w(t+k) + (I_{n_1+\bar{n}} - (I_{n_1+\bar{n}} - \hat{A})^{-1})\hat{B}\rho(t) = \hat{A}[x_1(t+k|t)^T \bar{x}(t+k|t)^T]^T + \hat{B}_w w(t+k) - \hat{A}(I_{n_1+\bar{n}} - \hat{A})^{-1}\hat{B}\rho(t) = \hat{A}\hat{x}(t+k|t) + \hat{B}_w w(t+k)$.

Also,

$$\hat{x}(t|t) = \begin{bmatrix} x_1(t|t) - \Gamma_1 \rho(t) \\ \bar{x}(t|t) \end{bmatrix} = \hat{x}(t|t-1) + \Delta\hat{x}(t), \quad (1.20)$$

completing the derivation of (1.16a).

The output error equation (1.16b) follows from the fact that $\hat{y}(t+k+1|t) = C_1(x(t+k+1|t) - \Gamma_1 \rho(t)) = \hat{C}\hat{x}(t+k+1|t)$ for $k \geq 0$. \square

The following proposition provides conditions that enforce constraint admissibility

of $\hat{y}(t)$ for all future time instants.

Proposition 1.2. *Let $\hat{x}(t+k|t)$ and $\hat{y}(t+k+1|t)$ satisfy (1.16). Suppose $\hat{x}(t|t-1) \in E_x$. If,*

$$\hat{A}\Delta\hat{x}(t) \in E_x \sim \hat{A}E_x \sim \hat{B}_wW, \quad (1.21)$$

then $\hat{x}(t+k+1|t) \in E_x$, $\hat{y}(t+k+1|t) \in E_y$ for all $k \in \mathbb{Z}_+$.

Proof. The proof is by induction. Suppose $k > 1$ and assume $\hat{x}(t+k|t) \in E_x$. From (1.13) and (1.14), it follows that $\hat{x}(t+k+1|t) = \hat{A}\hat{x}(t+k|t) + \hat{B}_w w(t+k) \in \hat{A}E_x \oplus \hat{B}_wW \subset E_x$, which implies that $\hat{y}(t+k+1|t) = \hat{C}\hat{x}(t+k+1|t) \in \hat{C}E_x \subset E_y$. For $k = 1$, $\hat{x}(t+1|t) = \hat{A}\hat{x}(t|t) + \hat{B}_w w(t) = \hat{A}\hat{x}(t|t-1) + \hat{A}\Delta\hat{x}(t) + \hat{B}_w w(t) \in \hat{A}E_x \oplus (E_x \sim \hat{A}E_x \sim \hat{B}_wW) \oplus \hat{B}_wW \subset E_x$. \square

Remark 1.3. Note that Proposition 1.2 requires that $\hat{x}(t|t-1) \in E_x$. This property will always be ensured by the governor from the previous time step, provided a feasible solution to the optimization problem exists at $t = 0$. With this in mind, based on Proposition 1.2, if the governor ensures, through the selection of $\rho(t)$ and $\bar{x}(t)$, that $y_2(t+k|t) \in Y \sim E_y$ for all $k \in \mathbb{Z}_+$ and, additionally, $\Delta\hat{x}(t)$ given by (1.17) satisfies (1.21), then $y(t+k|t) \in Y$ for all $k \in \mathbb{Z}_+$.

Remark 1.4. The reduced order ECG offers most benefit when the reduction is based on a clear separation of the eigenvalues determining the fast and slow dynamics of the closed loop system. When all the eigenvalues of A_1 are much smaller in magnitude than those of A_2 , the underlying approximation in (1.6) is reasonable and $E_x \sim \hat{A}E_x \sim \hat{B}_wW$ more closely approximates $E_x \sim \hat{B}_wW$, resulting a less stringent constraint (1.21).

We use Remark 1.4 in order to help with the design procedure of the reduced order RG and ECG. We now summarize the steps used to design the reduced order governors and the online computations involved. As with the ordinary RG and ECG, the development is split into an offline and online design; the former corresponds to the construction of the appropriate constraint sets and the latter corresponds to the reduced order online control law.

Reduced order ECG offline design

Given a system (0.1), find an invertible transformation P such that the state matrix is in a split form as in (1.4). This decomposition should follow the insight of Remark 1.4, so that the eigenvalues of A_1 are relatively small in magnitude. We are

now able to form a subsystem corresponding to slow eigenvalues, which is in the form of (0.14),

$$\begin{aligned} \begin{bmatrix} x_2(t+1) \\ \bar{x}(t+1) \end{bmatrix} &= \begin{bmatrix} A_2 & B_2\bar{C} \\ 0 & \bar{A} \end{bmatrix} \begin{bmatrix} x_2(t) \\ \bar{x}(t) \end{bmatrix} + \begin{bmatrix} B_2 \\ 0 \end{bmatrix} \rho(t) + \begin{bmatrix} B_{w,2} \\ 0 \end{bmatrix} w(t), \\ y_2(t) &= \begin{bmatrix} C_2 & D\bar{C} \end{bmatrix} \begin{bmatrix} x_2(t) \\ \bar{x}(t) \end{bmatrix} + (C_1\Gamma_1 + D)\rho(t) + D_w w(t) \in Y \sim E_y. \end{aligned} \quad (1.22a)$$

This is the reduced order system with a tightened output constraint and we develop an ordinary ECG which corresponds to it, *i.e.*, we find (\bar{C}, \bar{A}) and $O_\infty^{\text{aug}} \subset \mathbb{R}^{n_2} \times \mathbb{R}^{\bar{n}} \times \mathbb{R}^m$, along with its corresponding set $\Pi^{\text{aug}}(x_2) \in \mathbb{R}^{\bar{n}} \times \mathbb{R}^m$, to use in the online algorithm.

All that is left is to handle the dynamics of A_1 , so define the matrices as in (1.5) and choose the sets $E_x \subset \mathbb{R}^{n_1} \times \mathbb{R}^{\bar{n}}$ and $E_y \subset \mathbb{R}^p$, such that,

$$\begin{aligned} E_y &\subset \text{int } Y_{\infty,2}, \\ \hat{A}E_x \oplus \hat{B}_w W &\subset \text{int } E_x, \\ \hat{C}E_x &\subset E_y, \end{aligned} \quad (1.23)$$

and define a new constraint set,

$$\mathcal{E}^{\text{aug}} = \left\{ (\Delta\bar{x}, \Delta\rho) : \hat{A} \begin{bmatrix} -\Gamma_1\Delta\rho \\ \Delta\bar{x} \end{bmatrix} \in E_x \sim \hat{A}E_x \sim \hat{B}_w W \right\}, \quad (1.24)$$

so that we can impose the following condition online,

$$(\Delta\bar{x}(t), \Delta\rho(t)) \in \mathcal{E}^{\text{aug}}, \quad (1.25)$$

where the definitions of $\Delta\bar{x}(t)$ and $\Delta\rho(t)$ are given in (1.18). This completes the specification of the offline procedure.

Reduced order RG offline design

The reduced order RG design is similar to that of the reduced order ECG, with the exception of the use of the auxiliary variables. Therefore certain variables reduce to just the slow system variables, *e.g.*, $\hat{A} = A_1$, $\hat{B}_w = B_{w,1}$, *etc.* The sets O_∞ and $\Pi(x_2)$ are defined based on the slow system, and the constraint set \mathcal{E} becomes,

$$\mathcal{E} = \{\Delta v : -A_1\Gamma_1\Delta v \in E_x \sim \hat{A}_1 E_x \sim B_{w,1} W\}, \quad (1.26)$$

which is imposed on the change in the reference $\Delta v(t) = v(t) - v(t-1)$, *i.e.*,

$$\Delta v(t) \in \mathcal{E}. \quad (1.27)$$

Reduced order ECG online design

The online mechanism for computing $v(t)$ according to the reduced order ECG is similar to that of the ordinary ECG, with the exception that the additional constraint (1.25) must be included. At each discrete time instant t , update the auxiliary system state and offset based on the estimate or measured value of the slow state $x_2(t)$ by solving the following optimization problem,

$$\min \|\bar{x}(t)\|_{\bar{S}}^2 + \|r(t) - \rho(t)\|_{\bar{S}}^2, \quad (1.28a)$$

$$\text{sub. to } (\bar{x}(t), \rho(t)) \in \Pi^{\text{aug}}(x_2(t)), \quad (1.28b)$$

$$(\bar{x}(t) - \bar{A}\bar{x}(t-1), \rho(t) - \rho(t-1)) \in \mathcal{E}^{\text{aug}}. \quad (1.28c)$$

Then the modified reference becomes,

$$v(t) = \bar{C}\bar{x}(t) + \rho(t). \quad (1.29)$$

Note that at the initial time-instant $t = 0$, for the constraint (1.28c) to be enforceable, we require that the initial variables $\bar{x}(t-1)$ and $\rho(t-1)$ satisfy,

$$\begin{bmatrix} x_1(0) - \Gamma_1 \rho(-1) \\ \bar{A}\bar{x}(-1) \end{bmatrix} \in E_x. \quad (1.30)$$

Reduced order RG online design

At each discrete time instant t , the reduced order RG solves the following optimization problem,

$$\min \kappa(t) \in [0, 1], \quad (1.31a)$$

$$\text{sub. to } v(t-1) + \kappa(t)(r(t) - v(t-1)) \in \Pi(x_2(t)), \quad (1.31b)$$

$$v(t) - v(t-1) \in \mathcal{E}. \quad (1.31c)$$

1.3 Main results

In this section, we show that the reduced order ECG exhibits similar theoretical properties to that of the ordinary ECG.

We first note that the following result is immediate by Propositions 1.1 and 1.2 and Remark 1.

Proposition 1.5. *If the problem (1.28) has a feasible solution at time $t = 0$, then it is recursively feasible, i.e., it has a feasible solution for all $t \in \mathbb{Z}_+$.*

The following theorem shows that the reduced order ECG exhibits characteristics similar to the full order version. Let Ω_2 be a set satisfying the properties of Ω along with the inclusion $\Omega_2 \subset \text{int } \Omega_{d,2}$ where,

$$\Omega_{d,2} := \{r : (CT + D)r \in Y_{\infty,2} \sim E_y\} \subset \Omega_d. \quad (1.32)$$

Furthermore define a set $\mathcal{X}_2 \subset \mathbb{R}^{n_2}$ for the system (1.22) analogously to the definition (0.20) of \mathcal{X} for the system (0.14).

Theorem 1.6. *Consider the system (1.22) with $\{r(t)\} \in \mathbb{R}^m$, $\{w(t)\} \in \mathcal{W}$, $v(t)$ given by (1.29), (1.30), and $x_2(0) \in \mathcal{X}_2$. Then: (i) $x(t)$, $v(t)$, and $y(t)$ are defined for all $t \in \mathbb{Z}_+$, and (ii) $y(t) \in Y$ and $x_2(t) \in \mathcal{X}_2$ for all $t \in \mathbb{Z}_+$. Suppose further that there exists a $t_s \in \mathbb{Z}_+$ such that $r(t) = r_s$ for all $t \geq t_s$. Define $r_s^* := \arg \min_{r \in \Omega_2} \|r - r_s\|_S^2$. Then (iii) there exists a $t_f \in \mathbb{Z}_+$ such that $v(t) = r_s^*$ for all $t \geq t_f$; (iv) given $\varepsilon > 0$, there exists a $t_\varepsilon \in \mathbb{Z}_+$ such that $x(t) \in F_\infty(r_s^*) \oplus \varepsilon B_n$ for all $t \geq t_\varepsilon$.*

The theorem shows that many of the properties of the ordinary ECG are preserved by the reduced order version. The convergence properties apply to the reduced order system described by (1.22), but the constraints are satisfied for the overall system, i.e., $y(t) \in Y$ for all present and future time instants in (0.1).

The assumptions are also restricted to a minimum. The differences from the full order ECG is that the error part of the initial condition is assumed to already be bounded, i.e., $\hat{x}(0) \in E_x$. Furthermore, the set of final admissible references is changed from Ω to Ω_2 , because of the reduction in constraint set from Y to $Y \sim E_y$.

Furthermore, as in Remark 2 of [8], the result can easily be extended to the theory of the CG, i.e., the constraint (1.25) can be used in the CG algorithm under the same assumptions by making $\bar{x}(t)$ empty and removing its dynamics from consideration. The result for the RG is analogous and is available in [40]; we consider the application of this reduced order RG to a couple of numerical examples later in this chapter.

Remark 1.7. The error sets E_x and E_y do not need to be fixed at the time of design. Instead, E_y can be replaced with a time-varying output error set by introducing a time-varying scalar parameter $0 < c(t) < 1$ and setting $E_y(t) = c(t)Y$. This makes the computation of $Y \sim E_y(t)$ convenient because $Y \sim E_y(t) = Y \sim c(t)Y = (1 - c(t))Y$. The optimization (1.28) is then modified to simultaneously minimize $c(t)$ and the cost function (1.28a). The details are not covered in this dissertation but can partly be found in our work on network reference governors (see Section 4 of [49]).

Proof. Part (i) is implied by Proposition 1.2 and the definition of \mathcal{E}^{aug} in (1.26). For (ii), the ordinary ECG guarantees that $y_2(t) \in Y \sim E_y$ for all $t \in \mathbb{Z}_+$. Proposition 1.2 implies that $\hat{y}(t+1) \in E_y$ for all $t \in \mathbb{Z}_+$. Since $\hat{y}(0) \in E_y$ by assumption, then $y(t) = y_2(t) + \hat{y}(t) \in Y \sim E_y \oplus E_y \subset Y$ for all $t \in \mathbb{Z}_+$ and the proof of (i) and (ii) is complete.

We prove the rest of the theorem by defining,

$$V(t) = \|\bar{x}(t)\|_{\bar{S}}^2 + \|\rho(t) - r_s\|_{\bar{S}}^2 \geq 0, \quad (1.33)$$

Because $(\bar{x}(t-1), \rho(t-1)) \in \Pi(x_2(t-1))$, at the next time step, $(\bar{A}\bar{x}(t-1), \rho(t-1)) \in \Pi(x_2(t))$. Due to (1.29), this implies that $V(t) \leq \|\bar{A}\bar{x}(t-1)\|_{\bar{S}}^2 + \|\rho(t-1) - r_s\|_{\bar{S}}^2$. According to the Lyapunov-like condition on \bar{S} and \bar{A} , $\|\bar{A}\bar{x}(t-1)\|_{\bar{S}} \leq \|\bar{x}(t-1)\|_{\bar{S}}$, and therefore, $V(t) \leq V(t-1)$, implying there exists a $V_m \geq 0$ such that $V(t) \rightarrow V_m$.

We now prove the following,

$$\|\Delta\bar{x}(t)\|_{\bar{S}}^2 + \|\Delta\rho(t)\|_{\bar{S}}^2 \leq V(t-1) - V(t). \quad (1.34)$$

First we state the following lemma.

Lemma 1.8. *Suppose $Z, \Delta Z \subset \mathbb{R}^q$ are closed and convex and $z_r \in Z, 0 \in \text{int } \Delta Z, z_s \in \mathbb{R}^q, 0 \prec Q \in \mathbb{R}^{q \times q}$, and $z_{op} = z_{op}(z_r, z_s) = \arg \min_{z \in Z, z - z_r \in \Delta Z} (z - z_s)^T Q (z - z_s)$. Then,*

$$\|z_r - z_{op}\|_Q^2 \leq \|z_r - z_s\|_Q^2 - \|z_{op} - z_s\|_Q^2. \quad (1.35)$$

Proof. Because Z and ΔZ are closed, $z_r \in Z$ and $0 \in \Delta Z$, z_{op} exists. Now, $\|z_r - z_s\|_Q^2 = \|z_r - z_{op} - (z_s - z_{op})\|_Q^2 = \|z_r - z_{op}\|_Q^2 - 2(z_r - z_{op})^T Q (z_s - z_{op}) + \|z_s - z_{op}\|_Q^2$. Because z_{op} is the optimal point, the necessary optimality condition on the gradient $\nabla(z - z_s)^T Q (z - z_s) = 2Q(z - z_s)$ implies that $-2(z - z_{op})^T Q (z_s - z_{op})$ cannot be negative for any point satisfying the constraint $z \in Z$; this yields $\|z_r - z_s\|_Q^2 \geq$

$\|z_r - z_{op}\|_Q^2 + \|z_s - z_{op}\|_Q^2$, which is an equivalent form of the result. \square

In Lemma 1.8, let $Z = \Pi^{\text{aug}}(x_2(t))$, $\Delta Z = \mathcal{E}^{\text{aug}}$, $z_r = (\bar{A}\bar{x}(t-1), \rho(t-1))$, $z_{op} = (\bar{x}(t), \rho(t))$, $z_s = (0, r_s)$, and $Q = \text{diag}(\bar{S}, S)$. Therefore,

$$\begin{aligned} \|(\Delta\bar{x}(t), \Delta\rho(t))\|^2 &= \|(\bar{A}\bar{x}(t-1) - \bar{x}(t), \rho(t-1) - \rho(t))\|^2 \\ &\leq \|(\bar{A}\bar{x}(t-1), \rho(t-1) - r_s)\|^2 - \|(\bar{x}(t), \rho(t) - r_s)\|^2 \\ &= V(t-1) - V(t), \end{aligned}$$

proving by (1.34) and $\Delta\bar{x}(t) \rightarrow 0$, $\Delta\rho(t) \rightarrow 0$.

Define $\Delta v(t) = v(t) - v(t-1)$. From the above, it follows that $\Delta v(t) \rightarrow 0$. This leads to the result that for any $\varepsilon > 0$, there exists a $t_\varepsilon \in \mathbb{Z}_+$ such that,

$$x(t) \in \{\Gamma v(t)\} \oplus F_\infty \oplus \varepsilon \mathcal{B}_n, \quad \forall t \geq t_\varepsilon. \quad (1.36)$$

To confirm this, decompose $x(t) = x_v(t) + x_w(t)$, where $x_v(t)$ is the solution of $x(t)$ with $w(t) \equiv 0$ and $x_w(t)$ is the solution of $x(t)$ with $v(t) \equiv 0$. It is apparent that $x_w(t) \in F_t \subset F_\infty$, for all $t \in \mathbb{Z}_+$. Now define, $\Delta x_v(t+1) = x_v(t+1) - x_v(t) = A\Delta x_v(t) + B\Delta v(t)$, therefore $\Delta x_v(t) \rightarrow 0$ as $\Delta v(t) \rightarrow 0$. Since $x_v(t+1) = Ax_v(t) + Bv(t) = x_v(t) + \Delta x_v(t)$, then $x_v(t) = \Gamma v(t) - (I - A)^{-1}\Delta x_v(t) \rightarrow \Gamma v(t)$. This leads to the conclusion that $x(t) = x_v(t) + x_w(t) \rightarrow \{\Gamma v(t)\} \oplus F_\infty$.

Because $(\bar{x}(t), \rho(t)) \in \Pi^{\text{aug}}(x_2(t))$, then $\rho(t) \in \Omega_2$. This implies that,

$$V_m \geq V^* := \|r_s^* - r_s\|_S^2. \quad (1.37)$$

In the proof of the theorem corresponding to the ordinary ECG [8], the next step is to show that $V_m = V^*$. The only difference between the assumptions in [8] and the assumptions herein is the addition of the constraint in (1.25). By our assumption that $0 \in \text{int } \mathcal{E}^{\text{aug}}$ in (1.25), updates to the increment of $\Delta\rho(t)$ and $\Delta\bar{x}$ are always non-zero if they would be non-zero when not considering the constraint in (1.25); this and $\Delta\rho(t) \rightarrow 0$, $\Delta\bar{x}(t) \rightarrow 0$ as $t \rightarrow \infty$ imply that the constraint (1.25) is inactive for all t sufficiently large. Consequently, we obtain the result that $V_m = V^*$.

Parts (iii) and (iv) now follow directly. In Lemma 1.8, let $z_r = (\bar{x}(t), \rho(t))$, $Z = \mathbb{R}^{\bar{n}} \times \Omega_2$, $\Delta Z = \mathcal{E}^{\text{aug}}$, $z_{op} = (0, r_s^*)$, and $z_s = (0, r_s)$. Then, $\|\bar{x}(t)\|_S^2 + \|\rho(t) - r_s^*\|_S^2 \leq V(t) - V^*$. Therefore $\bar{x}(t) \rightarrow 0$ and $\rho(t) \rightarrow r_s^*$. This and (1.36) prove part (iv). Furthermore, they imply that for sufficiently large t , $(0, r_s^*) \in \Pi^{\text{aug}}(x_2(t))$ and the constraint $(\Delta\bar{x}(t), \Delta\rho(t)) \in \mathcal{E}^{\text{aug}}$ is inactive. Therefore, (1.29) and the definition of

r_s^* imply that for all t sufficiently large, $\rho(t) = r_s^*$, proving part (iii). \square

1.4 Accounting for observer error

If we do not measure all the components of the state $x_2(t)$, then we can design an observer to generate their estimates. The observer errors can be accounted for by the ECG in an analogous manner to fast state deviations from steady-state.

Consider that a reduced order ECG has been developed for the system (1.22). Let $x_o(t)$ be the output of the observer for $x_2(t)$ with gain L ,

$$x_o(t+1) = A_2x_o(t) + B_2v(t) + L(y(t) - y_o(t)), \quad (1.38a)$$

$$y_o(t) = C_2x_o(t) + Dv(t) + C_1\Gamma_1\rho(t). \quad (1.38b)$$

where, without loss of generality, we assume that $y_o(t)$ is both a measured and constrained output. In the design of the ECG, the state $x_2(t)$ is set to $x_o(t)$.

Let,

$$\tilde{x}(t) = \begin{bmatrix} x_2(t) - x_o(t) \\ x_1(t) - \Gamma_1\rho(t) \\ \bar{x}(t) \end{bmatrix},$$

and $\tilde{y}(t) = y(t) - y_2(t)$. The following proposition characterizes the predicted trajectories of $\tilde{x}(t)$ and $\tilde{y}(t)$.

Proposition 1.9. *The dynamics of $\tilde{x}(t+k|t)$ and $\tilde{y}(t+k|t)$ for $k \in \mathbb{Z}_+$ satisfy,*

$$\tilde{x}(t+k+1|t) = \tilde{A}\tilde{x}(t+k|t) + \tilde{B}_w w(t+k), \quad (1.39a)$$

$$\tilde{x}(t|t) = \tilde{x}(t|t-1) + \Delta\tilde{x}(t),$$

$$\tilde{y}(t+k+1|t) = \tilde{C}\tilde{x}(t+k+1|t), \quad (1.39b)$$

where,

$$\tilde{A} = \begin{bmatrix} A_2 - LC_2 & -LC_1 & 0 \\ 0 & A_1 & B_1\bar{C} \\ 0 & 0 & \bar{A} \end{bmatrix}, \quad \tilde{B}_w = \begin{bmatrix} B_{w,2} - LD_w \\ B_{w,1} \\ 0 \end{bmatrix}, \quad \tilde{C} = \begin{bmatrix} C_2 & C_1 & 0 \end{bmatrix},$$

and,

$$\Delta\tilde{x}(t) = \begin{bmatrix} 0 \\ -\Gamma_1\Delta\rho(t) \\ \Delta\bar{x}(t) \end{bmatrix},$$

$$\tilde{x}(t|t-1) = \begin{bmatrix} x_2(t) - x_o(t|t-1) \\ x_1(t) - \Gamma_1\rho(t-1) \\ \bar{A}\bar{x}(t-1) \end{bmatrix}.$$

Proof. For $k \geq 0$, $x_2(t+k+1|t) - x_o(t+k+1|t) = A_2x_2(t+k|t) + B_2v(t+k|t) + B_{w,2}w(t+k) - A_2x_o(t+k|t) - B_2v(t+k|t) - L(y(t+k|t) - y_o(t+k|t)) = A_2(x_2(t+k|t) - x_o(t+k|t)) + B_{w,2}w(t+k) - L(C_2(x_2(t+k|t) - x_o(t+k|t)) + C_1(x_1(t+k|t) - \Gamma_1\rho(t)) + D_w w(t+k)) = (A_2 - LC_2)(x_2(t+k|t) - x_o(t+k|t)) - LC_1(x_1(t+k|t) - \Gamma_1\rho(t)) + (B_{w,2} - LD_w)w(t+k)$.

The rest of (1.39a) is proven by the fact that $x_2(t|t) - x_o(t|t) = x_2(t) - x_o(t)$ and Proposition 1.1.

Finally, (1.39b) follows from the choice of the initialization of $x_2(t|t)$ to $x_o(t|t-1)$. \square

Propositions 1.9 and 1.2 imply that the reduced order ECG with an observer can be developed by defining new constraint sets $\tilde{E}_x \subset \mathbb{R}^{n_2} \times \mathbb{R}^{n_1} \times \mathbb{R}^{\bar{n}}$ and $\tilde{E}_y \subset \mathbb{R}^p$ to replace E_x and E_y , respectively. These sets satisfy,

$$\begin{aligned} \tilde{E}_y &\subset \text{int } Y_{\infty,2}, \\ \tilde{A}\tilde{E}_x \oplus \tilde{B}_w W &\subset \text{int } \tilde{E}_x, \\ \tilde{C}\tilde{E}_x &\subset \tilde{E}_y. \end{aligned} \tag{1.40}$$

The constraint in (1.26) is replaced by the following constraint,

$$\begin{bmatrix} -LC_1 & 0 \\ A_1 & B_1\bar{C} \\ 0 & \bar{A} \end{bmatrix} \begin{bmatrix} -\Gamma_1\Delta\rho(t) \\ \Delta\bar{x}(t) \end{bmatrix} \in \tilde{E}_x \sim \tilde{A}\tilde{E}_x \sim \tilde{B}_w W. \tag{1.41}$$

We can use the constraint in (1.41) to restrict changes in $\bar{x}(t)$ and $\rho(t)$ analogously to the constraint in (1.21). In this way, we ensure that the observer error, in addition to the fast state deviation, does not cause constraint violation.

Response properties in Proposition 5.6 and Theorem 1.6 hold with appropriate notational modifications.

1.5 Example 1: Turbocharged gasoline engine

Our first example addresses surge constraint handling in turbocharged gasoline engines (see the schematic in Fig. 1.1). The problem description and full order RG design for the nonlinear system will be discussed in Chapter 6. Here we consider the design of the reduced order RG.

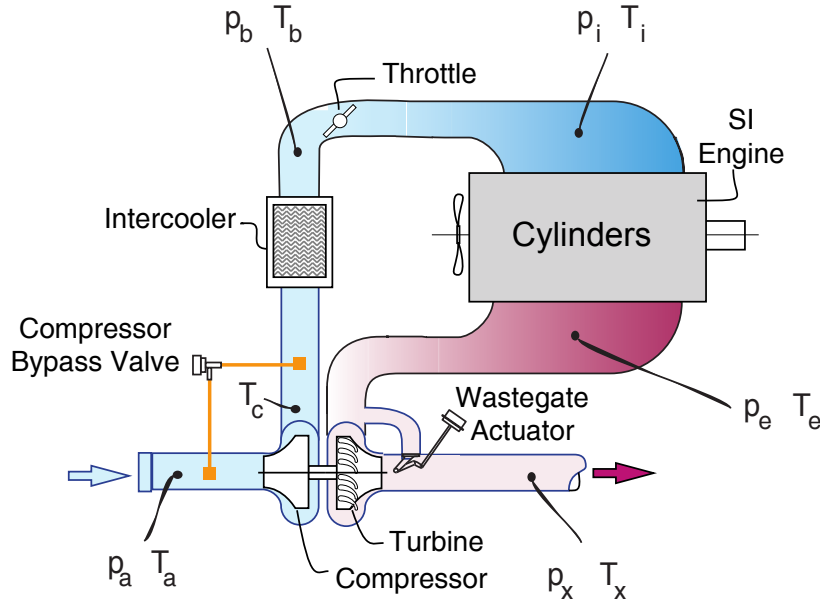


Figure 1.1: Schematic of a turbocharged gasoline engine. [45]

The engine model [45] has five states: intake manifold pressure (kPa), boost pressure (kPa), exhaust manifold pressure (kPa), turbocharger speed (rpm), and wastegate flow (g/sec). The eigenvalues of the linearized continuous-time model are,

$$\{-2.39, -3.16, -24.3, -161, -259\},$$

suggesting that the dynamics can be decomposed into a second or a third order slow subsystem and, respectively, a third or a second order fast subsystem. The model has 2 outputs $y(t)$: boost pressure (kPa), and compressor flow (g/sec) that to avoid compressor surge are constrained by an affine inequality $y(t) \in Y$ where,

$$Y = \{y : Sy \leq s\}. \quad (1.42)$$

The RG is applied to modify the throttle and wastegate command.

The linearized discrete-time model of the engine is first transformed into the form of (1.2), where the eigenvalues of A_1 are fast and the eigenvalues of A_2 are slow. Note

that for this system $D = 0$. We then proceed to define E_y by shrinking the constraint set, Y :

$$E_y = \varepsilon Y = \{y : Sy \leq \varepsilon s\}, \quad (1.43)$$

where $\varepsilon > 0$ is a scalar. Therefore,

$$Y \sim E_y = \{y : Sy \leq (1 - \varepsilon)s\}. \quad (1.44)$$

Now we define $E = \{x : SCx \leq \varepsilon s\}$. We construct a A_1 -contractive set, $E_x \subseteq E$, with the maximum output admissible set algorithm [5], computing O_∞ by replacing A with $\frac{1}{\lambda}A$ and Y with εY , thus obtaining that E is a λ -contractive set with contraction parameter λ .

In this section, we first use a reduced model of order $n_s = 3$ to investigate different choices of the set E_x , *i.e.*, choices of ε , assuming full-state measurement. We then fix a value for ε and use it to investigate different choices of n_s . Then we fix ε and n_s , introduce an observer and consider different choices of the observer gain L .

Figs. 1.2-1.3 show the results for the case when all states are directly measured, $n_s = 3$, and the parameter, ε , is varied. From the results, a larger ε requires a longer convergence time of $v(t)$ to $r(t)$. This is due to the tightening of the constraints with the increase in ε .

We next vary the order of the reduced system n_s between 1 and 4, with fixed $\varepsilon = 0.05$. The results are plotted in Figs. 1.4-1.5. Other than the case $n_s = 1$, the reduced order RGs perform comparably to the full-order RG, with similar convergence rates to the reference command, see Fig. 1.5. Since it is of most complexity reduction benefit to reduce n_s as much as possible, $n_s = 2$ is selected.

Table 1.1 show the number of variables that are required to represent the inequality constraints as function of n_s . The first two columns on the right are the number of variables used to describe the O_∞ and E_x constraint sets; they are obtained by multiplying the number of linear inequalities used to describe each set with the dimension of the set plus one more to account for the fixed variable on the right hand side of the inequality.

In the next investigation, we no longer assume full state measurement and we introduce an observer, with sets \tilde{E}_x, \tilde{E}_y and fixed $\varepsilon = 0.25$. The observer is based on the Kalman filter and to test the impact of the observer gain L , we vary the covariance matrix of the process noise. We have chosen a larger value of ε to expand \tilde{E}_x and to better accommodate observer errors. Figs. 1.6-1.7 show that the response of the

n_s	$\ell_{O_{\infty,2}} \times (n_s + m + 1)$	+	$\ell_{E_x} \times (m + 1)$	=	
1	3×4	+	109×3	=	339
2	401×5	+	31×3	=	2098
3	424×6	+	21×3	=	2607
4	431×7	+	3×3	=	3028
5	432×8	+	0×3	=	3208

Table 1.1: Number of required constraint variables

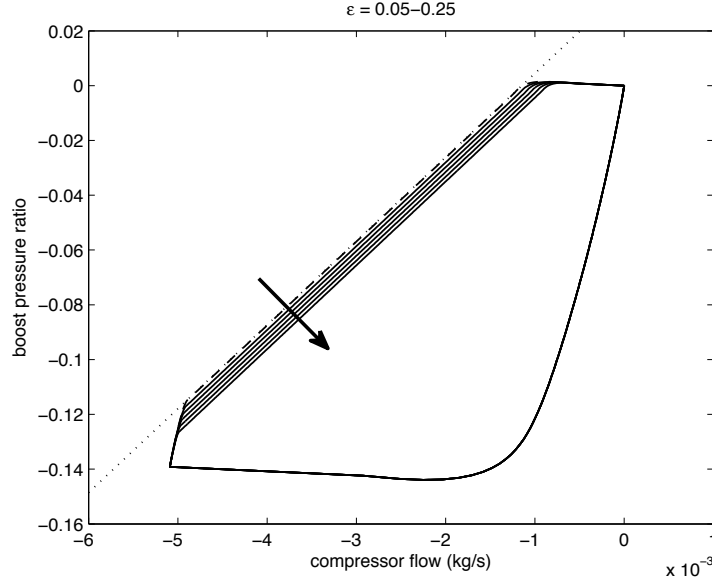


Figure 1.2: Responses (solid) of a fully measured system of order 3 with varying values of ε equally spaced between 0.05 and 0.25 plotted on a compressor map and compared to a full-order response (dashed) plotted against compressor line (dotted); the arrows indicate the direction of increasing ε

RG is slowed for higher observer gains. This happens as a more aggressive observer exhibits higher peaking, which the RG limits.

1.6 Example 2: Flexible beam

Our second example is motivated by applications to very flexible aircraft, such as [53, 55]. We consider a flexible free-free beam, serving as a simplified prototype for an aircraft wing, which can change the vertical position of the center of mass. The change in the vertical position of the center of mass creates elastic deflections in the beam. The objective is to maintain the tip deflection within the specified limits. The model of the system is infinite-dimensional. We use the theory of the reduced order RG to develop an an RG that adjusts the set-point for the vertical position of the

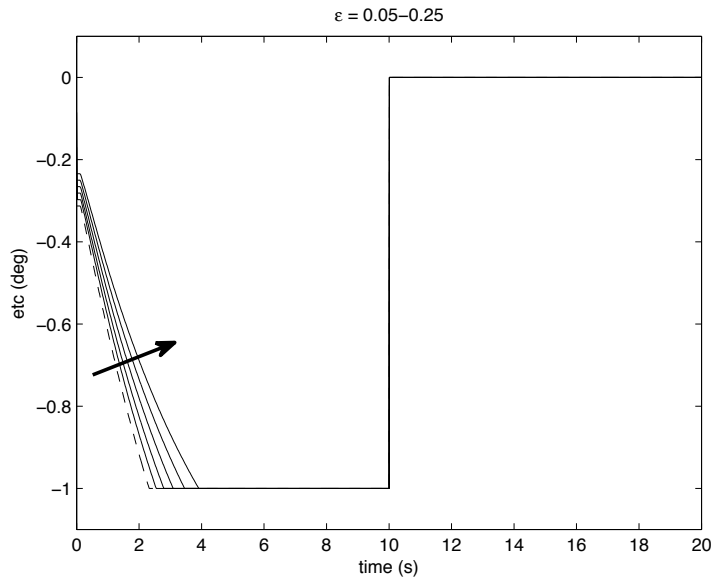


Figure 1.3: Throttle responses (solid) of a fully measured system of order 3 with varying values of ε equally spaced between 0.05 and 0.25 compared to a full order response (dashed); the arrows indicate the direction of increasing ε

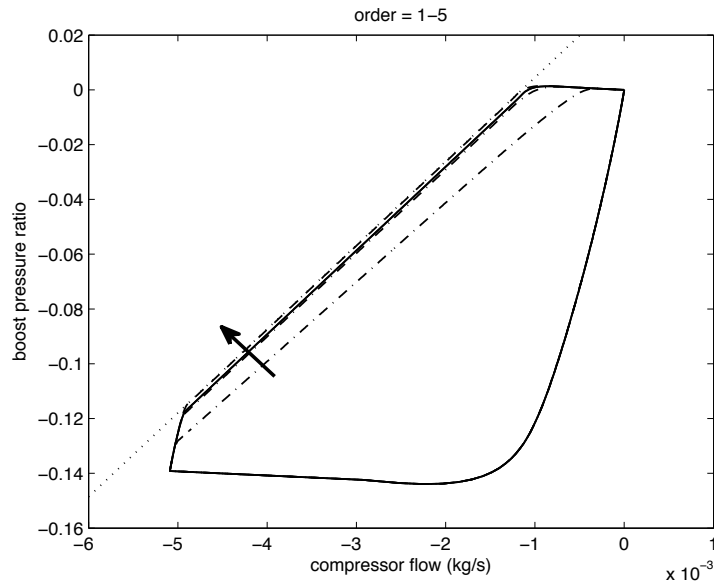


Figure 1.4: Responses of a system of order varying from 1 to 5 with fixed $\varepsilon = 0.05$ plotted on a compressor map; the lowest two reduced order (dot-dashed) compared to the next two (solid) and the full-order (dashed) responses are plotted against the compressor line (dotted); the arrows indicate the direction of increasing order

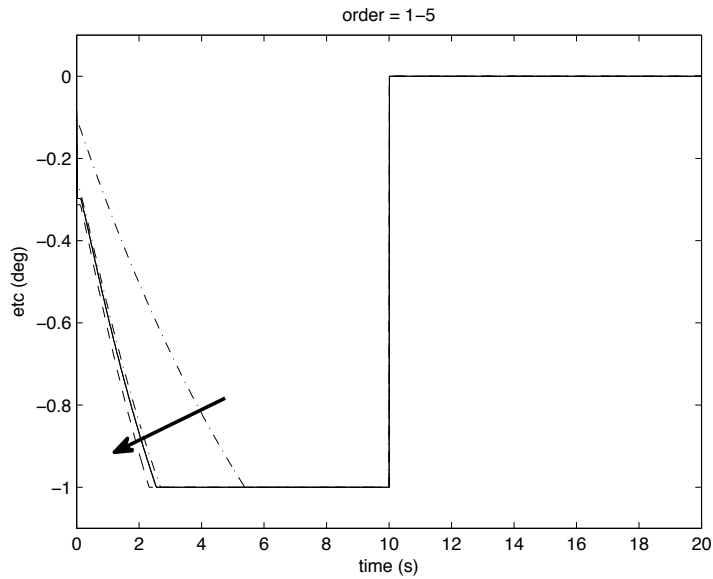


Figure 1.5: Throttle responses of a system of order varying from 1 to 5 with fixed $\varepsilon = 0.05$; the lowest two reduced order (dot-dashed) are compared to the next two (solid) and the full-order (dashed); the arrows indicate the direction of increasing order

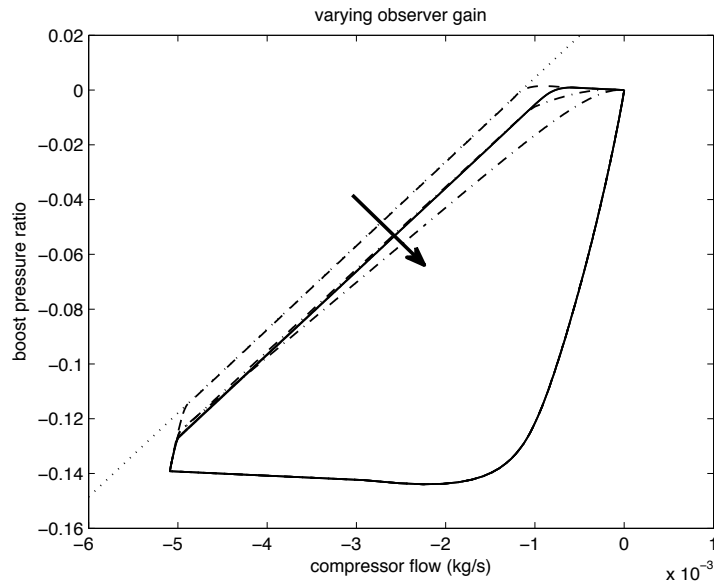


Figure 1.6: Responses of a system with varying observer gain with fixed $\varepsilon = 0.25$ plotted on a compressor map; the highest two reduced order (dot-dashed), the next two (solid), and the fully measured (dashed) responses are plotted against the compressor line (dotted); the arrows indicate the direction of increasing gain

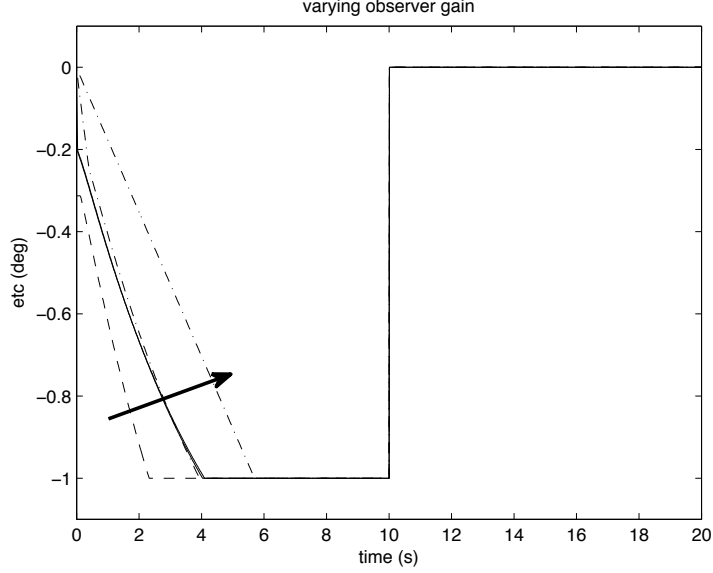


Figure 1.7: Throttle responses of a system with varying observer gain with $\varepsilon = 0.25$, with the highest two reduced order (dot-dashed), the next two (solid), and the fully measured (dashed); the arrows indicate the direction of increasing gain

center of mass based on the reduced order model for just two elastic modes of the beam.

The undamped equations of motion governing the dynamics of a free-free beam are given by the partial differential equations [52],

$$EI \frac{\partial^4 y}{\partial x^4}(x, t) + \rho \frac{\partial^2 y}{\partial t^2}(x, t) = -u(t)\delta(x), \quad (1.45)$$

with the boundary conditions,

$$\frac{\partial^2 y}{\partial x^2}(\pm \ell, t) = \frac{\partial^3 y}{\partial x^3}(\pm \ell, t) = 0, \quad (1.46a)$$

$$y(x, 0) = \frac{\partial^2 y}{\partial t^2}(x, 0) = 0, \quad (1.46b)$$

where $EI = 8.4 \cdot 10^3 \text{ Nm}^2$, $\rho = 9.0 \text{ kg/m}$, $\ell = 36 \text{ m}$.

The solution $y(x, t)$ can be decomposed into orthonormal modes [52],

$$y(x, t) = \sum_{i=0}^{\infty} w_i(x) q_i(t), \quad (1.47)$$

where

$$w_i(x) = \begin{cases} \cos(k_i x) - \frac{\sin(k_i \ell)}{\sinh(k_i \ell)} \cosh(k_i x), & i \text{ odd} \\ \sin(k_i x) - \frac{\cos(k_i \ell)}{\cosh(k_i \ell)} \sinh(k_i x), & i \text{ even} \end{cases} \quad (1.48)$$

and k_i are solutions to,

$$\cos(2\ell k_i) \cosh(2\ell k_i) = 1, \quad (1.49)$$

in increasing order of positive i . Using orthonormality and assuming that all of the modes are damped, the modal coordinates satisfy the following equations for all i ,

$$\ddot{q}_i(t) + 2\zeta\omega_i\dot{q}_i(t) + \omega_i^2 q_i(t) = -u(t) \int_{-\ell}^{\ell} w_i(x)\delta(x) dx = -w_i(0)u(t), \quad (1.50)$$

where $\omega_i^2 = \frac{EI}{\rho} k_i^4$, and the damping ratio $\zeta = 0.01$ is assumed for simplicity to be the same for all modes. We note that due to the symmetry of the problem, $w_i(0) = 0$ for even i , and hence we assume that the modal coordinates for all odd modes are zero and, furthermore, that $y(t, \ell) = y(t, -\ell)$.

The constraint on the tip deflection is that the tip can deflect no more than 1% of the half-length,

$$y(t, \pm\ell) \in Y = \{y : -0.01\ell \leq y \leq 0.01\ell\}, \quad t \in \mathbb{Z}^+. \quad (1.51)$$

The equations of motion for the vertical position of the center of mass are given by,

$$\dot{z} = \begin{bmatrix} 0 & 1 \\ 0 & 0 \end{bmatrix} z + \begin{bmatrix} 0 \\ \frac{1}{2\rho\ell} \end{bmatrix} u(t), \quad (1.52)$$

where $u(t) = Kz(t) + Qv(t)$ and $v(t)$ is the set-point for the vertical position of the center of mass prescribed by the RG. Our objective is to develop such a RG using observed modal coordinates q_1 and q_3 . We define,

$$g_5(x) = \sum_{i=5}^{\infty} -\frac{1}{\omega_i^2} w_i(x) w_i(0), \quad (1.53)$$

so that $g_5(x)u(t)$ is the contribution of modes higher than 5 to the steady-state

deflection of the beam at position $x(t)$, whenever a constant force $u(t)$ is applied. For the deflection of the tip, we can find a bound $g_{b,5}(\ell)$ on $g_5(\ell)$,

$$\begin{aligned}
g_5(\ell) &= \sum_{i=5}^{\infty} -\frac{1}{\omega_i^2} w_i(\ell) w_i(0) \leq \sum_{i=5,9,\dots}^{\infty} -\frac{1}{\omega_i^2} w_5(\ell) w_5(0) - \sum_{i=7,11,\dots}^{\infty} \frac{1}{\omega_i^2} w_{\infty}(\ell) \\
&= \frac{\rho}{EI} \sum_{i=5,9,\dots}^{\infty} -\frac{1}{k_i^4} w_5(\ell) w_5(0) - \sum_{i=7,11,\dots}^{\infty} \frac{1}{k_i^4} \sqrt{2} \\
&\leq \frac{\rho}{EI} \sum_{\substack{i=3 \\ i \text{ odd}}}^{\infty} \frac{-w_5(\ell) w_5(0)}{(ik_3/2)^4} - \frac{\sqrt{2}}{((i+1)k_3/2)^4} \\
&= \frac{\rho}{EI} \frac{16}{k_3^4} \sum_{i=3}^{\infty} -\frac{1}{i^4} w_5(\ell) w_5(0) - \sum_{\substack{i=4 \\ i \text{ even}}}^{\infty} \frac{1}{i^4} \left(-w_5(\ell) w_5(0) + \sqrt{2} \right) \\
&= \frac{16}{\omega_3^2} \left[\left(\frac{\pi^4}{90} - \frac{17}{16} \right) (-w_5(\ell) w_5(0)) - \frac{1}{16} \left(\frac{\pi^4}{90} - 1 \right) \left(-w_5(\ell) w_5(0) + \sqrt{2} \right) \right] \\
&\approx 0.2156 \frac{1}{\omega_3^2} = g_{b,5}(\ell),
\end{aligned}$$

where $w_{\infty}(\ell) = \limsup_{i \rightarrow \infty} w_i(\ell) = \sqrt{2}$.

We introduce a new constrained system with observer gain L ,

$$\dot{\hat{\xi}}(t) = A\hat{\xi}(t) + Bu(t) + L(y(t, \ell) - \hat{y}_r(t)), \quad (1.54a)$$

$$\hat{y}_r(t) = \hat{q}_1(t) + \hat{q}_3(t) + g_{b,5}(\ell)u(t) \in Y \sim E_y, \quad (1.54b)$$

where $\hat{\xi} = (\hat{z}, \dot{\hat{z}}, \hat{q}_1, \dot{\hat{q}}_1, \hat{q}_3, \dot{\hat{q}}_3)$, with A and B satisfying (1.50) and (1.52), and $\hat{y}_r(t)$ is the reduced order output. For the RG development, in order to discretize (1.54), we choose the sampling period to be twice the value of the frequency of the third mode, *i.e.*, $T = \frac{2\pi}{\omega_3}$.

To complete the development of the reduced order RG, we constrain the overshoot of the fast modes past their steady state value. Noting that the use of the bound has reduced the contributions of the infinite number of fast states to that of one variable, we choose the constraint set, $E_x = E_y := [-0.002\ell, 0.002\ell]$, and bound the overshoot of this variable by $\exp(-\frac{\zeta\pi}{\sqrt{1-\zeta^2}})g_{b,5}(\ell)\Delta u(t)$. We introduce the constraint, $\exp(-\frac{\zeta\pi}{\sqrt{1-\zeta^2}})g_{b,5}(\ell)\Delta u(t) \in E_x \sim \Delta_T E_x$ where $\Delta_T = \exp(-\omega'_5 T)$ for $\omega'_5 = \omega_5 \sqrt{1-\zeta^2}$. Therefore, if $\Delta u(t) = 0$ and the bounded overshoot $\exp(-\frac{\zeta\pi}{\sqrt{1-\zeta^2}})g_{b,5}(\ell)\Delta u(t)$ is contained in E_x at time t , it will be contained in $\Delta_T E_x$ at time $t + T$. We complete the design by following the procedure in Section 1.4. The set E is constructed using a

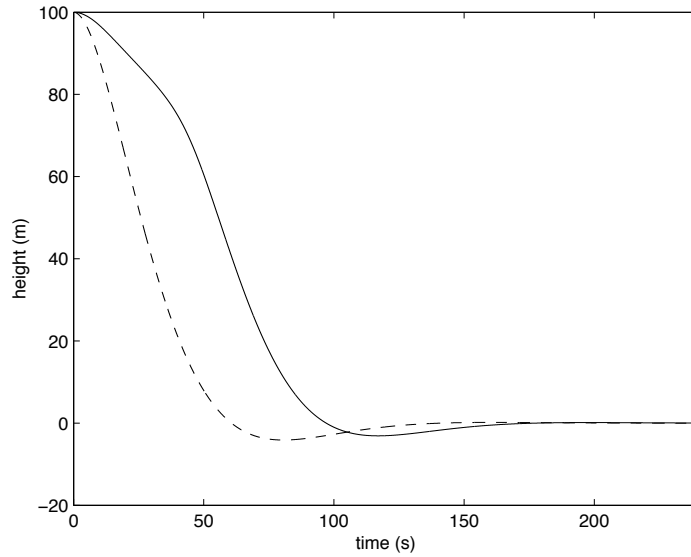


Figure 1.8: Governed (dashed) and ungoverned (solid) responses of the beam height

contractive parameter $\lambda = 0.98$ in a procedure similar to the construction of E_x in the previous example.

We perform a simulation using a much faster time constant and with initial condition set at 100m, $z(0) = (100, 0)$, controlling the position of the center of mass to a reference of 0m. We compare the responses of both the ungoverned and governed systems and plot the results in Figs. 1.8-1.9, where the RG is able to prevent the constraint violation present in the ungoverned response.

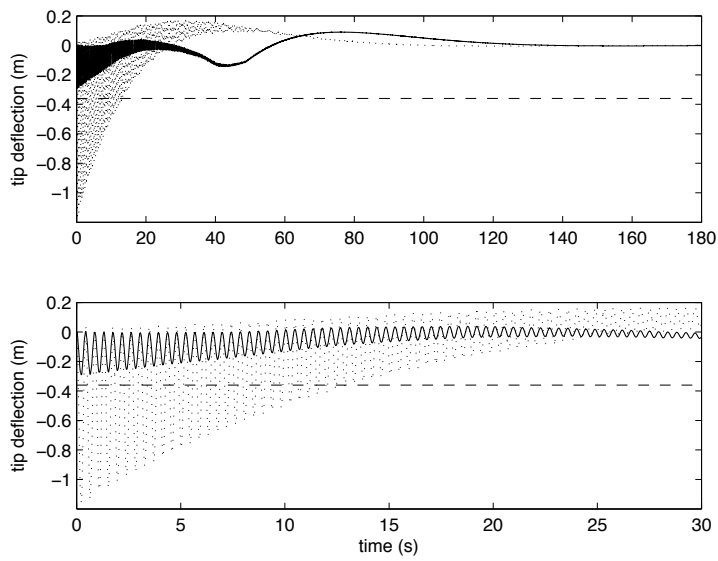


Figure 1.9: Two plots with different time axes; the governed (solid) and ungoverned (dotted) responses of the tip deflection plotted along with deflection constraint (dashed)

CHAPTER 2

Reference governors for decentralized systems

2.1 Introduction

Decentralized controllers arise in the control design for complex or large-scale systems. Large-scale systems are often too large for conventional control techniques to be effectively applied and decentralized techniques are instead exploited in order to achieve stability and other performance characteristics [56, 57, 58]. Furthermore, in order to decrease engine wiring and weight, and achieve cooling requirements and system reliability, efforts are being made to decentralize and distribute the control system design for aircraft gas turbines, which are not large-scale in the conventional sense [58, 59].

In this chapter, we consider disturbance-free, constrained linear systems of the form (0.1) with $W = 0$, for which a possibly decentralized controller has been designed to achieve suitable performance but which has not taken constraint-admissibility into account.

The focus is on developing a decentralized RG scheme that builds on the results of the previous chapter on reduced order RGs. Reduced order RGs are designed by firstly decomposing a system into fast and slow subsystems and then developing an RG for the slow subsystem, while guaranteeing bounds on the error dynamics that are induced by assuming the fast state immediately converges to steady-state. Since the fast states converge quickly, the transient error is kept small and the reduced order RG behaves similarly to the ordinary RG. In this chapter, we pursue a related approach for decentralized constrained control.

A decentralized RG is developed for each component subsystem and each decentralized RG guarantees constraint satisfaction of the system in its entirety, as long as all the other decentralized RGs function as expected. Specifically, in the language of previous developments on reduced order RGs, each decentralized RG is applied to a

system with lower fidelity than the large-scale system. Each decentralized RG then guarantees constraint-adherence within some tightened constraint set, while bounding the modeling error through the use of constraints on the rate of the change in reference. Following this procedure, the decentralized RGs guarantee constraint-adherence of the entire subsystem as a whole. This approach is similar to [60] and references therein, however we exploit invariant subsets and auxiliary constraints in bounding the errors, including observer errors.

Thus our approach is to design sub-controllers for various components and then design an RG for each controller. In one case, the sub-controllers are allowed to communicate with each other over a network but with some delay in communication; in fact, the assumptions inherent in this approach are that each subsystem has the full information of only its own component of $v(t)$ and that the rest of the components of $v(t)$ are delayed by one time-instant. In the other case presented in this paper, we treat the situation for systems that are large-scale and for which the sub-controller does not have any such information.

The chapter is organized as follows. Section 2.2 introduces the theory of decentralized RGs when applied to low-order systems. Section 2.3 presents an aircraft engine example based on the model from [61]. Section 2.4 introduces the reference governor design for large scale systems and Section 2.5 presents an example of a coupled mass-spring-damper system that illustrates these developments.

2.2 Decentralized reference governors with state reconstruction

Consider a system that is composed of q subsystems, where every i -th subsystem receives a reference input, $v_i(t)$. Generally, every subsystem is coupled to all other subsystems through both the dynamics and the output. We begin the discussion of decentralized RGs by considering such systems of lower order, for which it is not computationally expensive to form an estimate of the total state within each subsystem. In such a case, we further assume that the subsystems communicate over a network and receive the reference signals of all other RGs, subject to a one time-step delay. The full-state dynamics of such a decentralized system can be written as,

$$x(t+1) = Ax(t) + B^1v_1(t) + \cdots + B^qv_q(t), \quad (2.1a)$$

$$y(t) = Cx(t) + D^1v_1(t) + \cdots + D^qv_q(t) \in Y, \quad (2.1b)$$

where $v_i(t) \in \mathbb{R}^{m_i}$ and,

$$v(t) = \begin{bmatrix} v_1(t) \\ \vdots \\ v_q(t) \end{bmatrix}.$$

The decentralized RG theory exploits the use of the ordinary RGs by developing multiple RGs for q different reference inputs. Decentralized RGs act independently of each other, but are designed to achieve constraint satisfaction for the entire system.

2.2.1 RG development

To begin, we introduce q outputs,

$$y_i(t) = C_i x(t) + D_i^1 v_1(t) + \dots + D_i^q v_q(t) \in Y_i, \quad i = 1, \dots, q, \quad (2.2)$$

where $Y_i \subset \mathbb{R}^{p_i}$ are compact convex sets containing 0 such that,

$$y_i(t) \in Y_i, \quad i = 1, \dots, q \implies y(t) \in Y.$$

Every i -th output of the form (2.2) corresponds to a constrained system for which an RG governing $v_i(t)$ must be designed.

We denote the RG corresponding to the i -th subsystem as RG i . The RG i is designed with the assumption that all reference inputs are held constant for all future time-instants, while the inputs that it does not govern are delayed by one time-instant. In order to enforce constraints, the RG i utilizes $\hat{x}_i(t) \in \mathbb{R}^n$ and $\hat{y}_i(t) \in \mathbb{R}^{p_i}$, which are predictions of $x(t)$ and $y_i(t)$. At time-instant t , the state predictions and constraints on the predicted output are given by,

$$\hat{x}_i(t+k+1|t) = A\hat{x}_i(t+k|t) + B^i v_i(t+k|t) + \sum_{j,j \neq i} B^j v_j(t+k|t), \quad (2.3a)$$

$$\hat{y}_i(t+k|t) = C_i \hat{x}_i(t+k|t) + D_i^i v_i(t+k|t) + \sum_{j,j \neq i} D_i^j v_j(t+k|t) \in \hat{Y}_i, \quad (2.3b)$$

where $\hat{Y}_i \subset Y_i$ is a tightened version of Y_i to be defined below. The system dynamics (2.3) can be used to design an O_∞ for use in the online RG i . This set is,

$$O_\infty^i = \{(x_i, \bar{v}_i, \tilde{v}) : x_i(t|t) = x, v_i(t+k|t) \equiv \bar{v}_i, v_j(t+k|t) \equiv \tilde{v}_j, j \neq i, \quad (2.3) \text{ are satisfied}\}. \quad (2.4)$$

The RGi is designed to modify $v_i(t)$ in order to satisfy the constraint,

$$(x_i(t), v_i(t), v(t-1)) \in O_\infty^i. \quad (2.5)$$

The difference between the sets O_∞ and O_∞^i is that the latter depends on the input $v(t-1)$, whose elements may not be controlled by the RGi. We subsequently show that we can introduce constraints and assumptions on $v_j(t)$, $j \neq i$, such that the inclusion in (2.5) is satisfied.

Proposition 2.1. *Assume that at the initial time, $(x_i(0), v_i(-1), v(-1)) \in O_\infty^i$ for all $i = 1, \dots, q$. Introduce sets $E_x^i \in \mathbb{R}^n$ and $E_y^i \in \mathbb{R}^{p_i}$, that satisfy,*

$$AE_x^i \subset \text{int } E_x^i, \quad (2.6a)$$

$$C_i E_x^i \subset \text{int } E_y^i. \quad (2.6b)$$

Define $\Delta v_i(t) = v_i(t) - v_i(t-1)$ and introduce constraints,

$$B^i \Delta v_i(t) \in \lambda_i^j (E_x^j \sim AE_x^j), \quad (2.7a)$$

$$D_j^i \Delta v_i(t) \in \lambda_i^j (E_y^j \sim C_j E_x^j), \quad (2.7b)$$

where $0 < \lambda_i^i \leq 1$ and $\sum_{j, j \neq i} \lambda_j^i = 1$.

Assume that $x(0) - x_i(0) \in E_x^i$. If every RGi enforces constraint (2.5) with $\hat{Y}_i \subset Y_i \sim E_y^i$ and constraints (2.7), then for all $i = 1, \dots, q$, and $t \in \mathbb{Z}_+$, the constraints $y_i(t) \in Y_i$ are satisfied and the problem is recursively feasible, i.e., a feasible $v(t)$ exists for all t .

Proof. For arbitrary i , fix t . For $k \geq 1$, assume $x(t+k|t) - \hat{x}_i(t+k|t) \in E_x^i$. Then, because $v(t)$ is held constant over the prediction horizon, $x(t+k+1|t) - \hat{x}_i(t+k+1|t) = A(x(t+k|t) - \hat{x}_i(t+k|t)) \in AE_x^i \subset E_x^i$.

Now assume $x(t) - \hat{x}_i(t) \in E_x^i$. Then $x(t+1|t) - \hat{x}_i(t+1|t) = Ax(t|t) + B^i v_i(t) + \sum_{j, j \neq i} B^j v_j(t) - A\hat{x}_i(t|t) - B^i v_i(t) - \sum_{j, j \neq i} B^j v_j(t-1) = A(x(t+1|t) - \hat{x}_i(t+1|t)) + \sum_{j, j \neq i} B^j \Delta v_j(t) \in AE_x^i \oplus \sum_{j, j \neq i} \lambda_j^i (E_x^i \sim AE_x^i) = AE_x^i \oplus (E_x^i \sim AE_x^i) \subset E_x^i$. Therefore $x(t+k|t) - \hat{x}_i(t+k|t) \in E_x^i$ for all $k \in \mathbb{Z}_+$ by recursion.

Therefore, for all $k \in \mathbb{Z}_+$, $\hat{y}_i(t+k|t) = C_i \hat{x}_i(t+k|t) + D_i^i v_i(t) + \sum_{j, j \neq i} D_i^j v_j(t-1) + C_i(x(t+k|t) - \hat{x}_i(t+k|t)) + \sum_{j, j \neq i} D_i^j \Delta v_j(t-1) \in (Y_i \sim E_y^i) \oplus C_i E_x^i \oplus \sum_{j, j \neq i} \lambda_j^i (E_y^i \sim C_i E_x^i) = (Y_i \sim E_y^i) \oplus C_i E_x^i \oplus (E_y^i \sim C_i E_x^i) \subset Y_i$. Noting that the conventional RG guarantees recursive feasibility, recursive feasibility is proven here as well.

The choice of i was arbitrary so, because $x(0) - \hat{x}_i(0) \in E_x^i$, recursive feasibility

guarantees that the result is true for all $t \in \mathbb{Z}_+$ and $i = 1, \dots, q$. \square

2.2.2 Decentralized RGs with an observer

Suppose that, instead of assuming knowledge of the full state, we design a Luenberger observer for (2.1) with gain L_i , where we assume without loss of generality that the output $\hat{y}_i(t)$ is measured. Because the reference inputs for the j -th elements (where $j \neq i$) are delayed by one time-insant, the observer state-update equation becomes,

$$\tilde{x}_i(t+1) = A\tilde{x}_i(t) + B^i v_i(t) + \sum_{j,j \neq i} B^j v_j(t-1) + L_i(y_i(t) - \tilde{y}_i(t)), \quad (2.8a)$$

and the output equation is,

$$\tilde{y}_i(t) = C_i \tilde{x}_i(t) + D_i^i v_i(t) + \sum_{j,j \neq i} D_i^j v_j(t-1). \quad (2.8b)$$

The delay in the reference input induces an observer error, which the RG i can limit by reducing the rate of change in $v_i(t)$.

Proposition 2.2. *Assume that at the initial time, $(\tilde{x}_i(0), v_i(-1), v(-1)) \in O_\infty^i$ for all $i = 1, \dots, q$. Introduce sets, $\tilde{E}_x^i \in \mathbb{R}^n$ and $\tilde{E}_y^i \in \mathbb{R}^{p_i}$, satisfying,*

$$A\tilde{E}_x^i \subset \text{int } \tilde{E}_x^i, \quad (2.9a)$$

$$(A - L_i C_i)\tilde{E}_x^i \subset \text{int } \tilde{E}_x^i, \quad (2.9b)$$

$$C_i \tilde{E}_x^i \subset \text{int } \tilde{E}_y^i. \quad (2.9c)$$

Introduce constraints,

$$B_j^i \Delta v_i(t) \in \tilde{\lambda}_i^j (\tilde{E}_x^j \sim A\tilde{E}_x^j), \quad (2.10a)$$

$$(B^i - L_j D_j^i) \Delta v_i(t) \in \tilde{\lambda}_i^j (\tilde{E}_x^j \sim (A - L_j C_j) \tilde{E}_x^j), \quad (2.10b)$$

$$D_j^i \Delta v_i(t) \in \tilde{\lambda}_i^j (\tilde{E}_y^j \sim \tilde{C}_j \tilde{E}_x^j), \quad (2.10c)$$

where $0 < \tilde{\lambda}_j^i \leq 1$ and $\sum_{j,j \neq i} \tilde{\lambda}_j^i = 1$.

Assume that $x(0) - \tilde{x}_i(0) \in \tilde{E}_x^i$. If every RG i enforces constraint $(\tilde{x}_i(t), v_i(t), v(t-1)) \in \tilde{O}_\infty^i$ with $\hat{Y}_i \subset Y_i \sim \tilde{E}_y^i$, and constraints (2.10), then for all $i = 1, \dots, q$ and $t \in \mathbb{Z}_+$, $\hat{y}_i(t) \in Y_i$ is satisfied and $v(t)$ is recursively feasible.

Proof. By Proposition 2.1, we know that if $x(t) - \hat{x}_i(t) \in \tilde{E}_x^i$, then $x(t+k|t) - \hat{x}_i(t+$

$k|t) \in \tilde{E}_x^i$ and $\hat{y}_i(t) \in \tilde{E}_y^i$ is guaranteed for all $k \in \mathbb{Z}_+$. By the assumptions in the theorem, we set $\hat{x}_i(t|t) = \tilde{x}_i(t|t)$ at the beginning of the prediction.

Now, for arbitrary i , we fix t . For $k \geq 1$, assume $x(t+k|t) - \tilde{x}_i(t+k|t) \in \tilde{E}_x^i$. Then, since $v(t)$ is held constant on the prediction horizon, $x(t+k+1|t) - \tilde{x}_i(t+k+1|t) = (A - L_i C_i)(x(t+k|t) - \tilde{x}_i(t+k|t)) \in (A - L_i C_i)\tilde{E}_x^i \subset \tilde{E}_x^i$.

Now assume $x(t) - \tilde{x}_i(t) \in \tilde{E}_x^i$. Then $x(t+1|t) - \tilde{x}_i(t+1|t) = Ax(t|t) + B^i v_i(t) + \sum_{j,j \neq i} B^j v_j(t) - A\tilde{x}_i(t|t) - B^i v_i(t) - \sum_{j,j \neq i} B^j v_j(t-1) - (L_i C_i x(t|t) + L_i D_i^i v_i(t) + \sum_{j,j \neq i} D_i^j v_j(t) - L_i C_i \tilde{x}_i(t|t) - L_i D_i^i v_i(t) - \sum_{j,j \neq i} D_i^j v_j(t-1)) = (A - L_i C_i)(x(t+1|t) - \tilde{x}_i(t+1|t)) + \sum_{j,j \neq i} (B^j - D_i^j) \Delta v_j(t) \in (A - L_i C_i)\tilde{E}_x^i \oplus \sum_{j,j \neq i} \tilde{\lambda}_j^i(\tilde{E}_x^i \sim (A - L_i C_i)\tilde{E}_x^i) = A\tilde{E}_x^i \oplus (\tilde{E}_x^i \sim (A - L_i C_i)\tilde{E}_x^i) \subset \tilde{E}_x^i$. Therefore $x(t+k|t) - \tilde{x}_i(t+k|t) \in \tilde{E}_x^i$ for all $k \in \mathbb{Z}_+$ by recursion. Noting that the conventional RG guarantees recursive feasibility and that we set $x_i(t|t) = \tilde{x}_i(t|t)$ for all $t \in \mathbb{Z}_+$, recursive feasibility is proven here as well.

The choice of i was arbitrary so, because $x(0) - \tilde{x}_i(0) \in \tilde{E}_x^i$, recursive feasibility guarantees that the result is true for all $t \in \mathbb{Z}_+$ and $i = 1, \dots, q$. \square

Remark 2.3. The design of the RG i and the relevant sets (2.9) follows procedures similar to the ones outlined in the previous chapter. The sets can always be computed if the corresponding A matrix is asymptotically stable and the constraint set has a non-empty interior. Furthermore, the design of every RG i can be simplified if, for a particular output, the pair (C_i, A) is unobservable; in such a case, because unobservable dynamics do not affect constraint adherence [12] the design of RG i can be reduced by splitting the system into observable and unobservable dynamics and developing an RG only for the former.

2.3 Example 1: Aircraft engine

The example considered here is of an aircraft gas turbine engine actuated with three reference inputs, of which one corresponds to one constraint set and the rest to another. The linearized system model is for an aircraft at ground idle and is taken from [61]. In order to reduce the wiring, the control systems of different engine components communicate over a network and the communication is subject to a delay. The continuous states are $X(t) = (\Delta N_f(t), \Delta N_c(t))$, the inputs are $U(t) = (\Delta W_F(t), \Delta VSV(t), \Delta VBV(t))$, and the available model outputs are $y(t) = (\Delta W_F(t), \Delta T_{48}(t), \Delta HPC(t))$, where the components are detailed in Table 2.1 and Δ signifies their deviation from the operating point.

Symbol	Variable name	Ref. value
N_f	fan speed	1376 rpm
N_c	core speed	8624 rpm
W_F	fuel flow	0.33 pps
VSV	variable stator vane	-51.4°
VBV	variable bleed valve	1.00 frac
T_{48}	total temp. at HP turbine outlet	1091°R
HPC	HP compressor stall margin	37.5%

Table 2.1: Decentralized aircraft engine example data

The input and output variable constraints are given by,

$$\Delta W_F(t) \in [-0.28, 1.97], \quad (2.11a)$$

$$\Delta T_{48}(t) \in [-150, 300], \quad (2.11b)$$

$$\Delta HPC(t) \in [-10, 20], \quad (2.11c)$$

where the constraints correspond to the physically restricted range of fuel flow rate and the outlet temperature and compressor stall margin ranges that correspond to safe engine operation.

In this section, we compare the ordinary RG to the decentralized version. As a first step in the design, we discretize the system using a sampling period of 0.015s and then design a controller to track a reference for the fan speed demand, which is a reference input that is calculated from the aircraft throttle angle position via a static function [61].

We introduce error dynamics, $e(t+1) = e(t) + N_f(t) - v_1(t)$, which represents the accumulated fan speed tracking error. Ignoring all inputs other than $\Delta W_F(t)$, we use LQR techniques to design a stabilizing controller of the form,

$$\Delta W_F(t) = K_I e(t) + K_P X(t), \quad (2.12)$$

so that $N_f(t)$ tracks the reference $v_1(t)$. After computing the optimal feedback gain, we obtain discrete-time closed-loop dynamics of the form (0.1) where $x(t) = (e(t), X(t))$ and $v(t) = (\Delta N_{f,des}(t), \Delta VSV(t), \Delta VBV(t))$. We split $v(t)$ such that $v_1(t) = \Delta N_{f,des}(t)$ and $v_2(t) = (\Delta VSV(t), \Delta VBV(t))$.

The decentralized controllers are used so that $v_1(t)$ enforces the constraint on $y_1(t) = \Delta W_F(t) \in Y_1 = [-0.28, 1.97]$, while attempting to track the fan speed setpoint; $v_2(t)$ is then used to enforce the constraints on $y_2(t) = (\Delta T_{48}(t), \Delta HPC(t)) \in Y_2 = [-150, 300] \times [-10, 20]$. The system schematic is provided in Fig. 2.1. Physically,

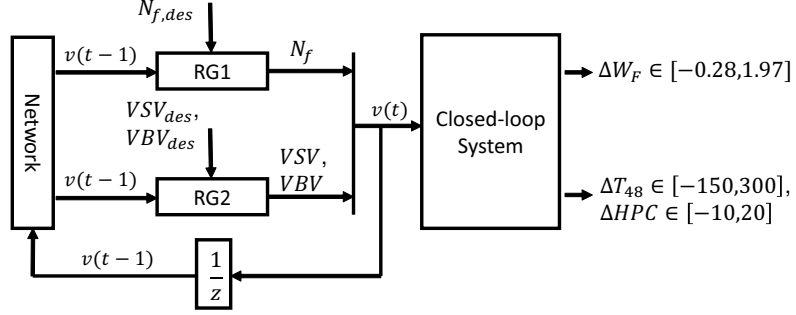


Figure 2.1: Decentralized aircraft engine schematic

the first RG is used to govern the desired fan speed, which is directly related to pilot command, while the second RG governs inputs to the compressor, VSV and VBV , which are used to prevent compressor stall and surge, respectively.

For the sets (2.6), we choose $E_y^i = 0.25Y_i$ and E_x^i to satisfy $\frac{1}{0.945}AE_x^i \subset E_x^i$ and $C_iE_x^i \subset 0.9E_y^i$.

The simulation results for conventional and decentralized RG are presented and compared in Figs. 2.2-2.6 for a constant desired reference, $r(t) \equiv (600, 15, -0.8)$. They show that the decentralized RGs behave similarly to the ordinary RG, with a slightly longer response time due to the conservativeness introduced by use of decentralization. As shown in Figs. 2.4-2.6, both versions of the RG satisfy the constraints given in (2.11). As expected, the decentralized RG has a slightly slower convergence to the desired set-point than the ordinary RG, which is shown in Fig. 2.2. This is due to the constraint-tightening involved in designing the decentralized RG.

2.4 Decentralized reference governors for large-scale systems

In this section, we develop a decentralized RG for use in large-scale linear systems. Because of the large dimensionality, it is unrealistic for every RG_i to reconstruct the full system state. We now introduce q states $x_i(t) \in \mathbb{R}^{n_i}$, $i = 1, \dots, q$, where,

$$x(t) = \begin{bmatrix} x_1(t) \\ \vdots \\ x_q(t) \end{bmatrix}.$$

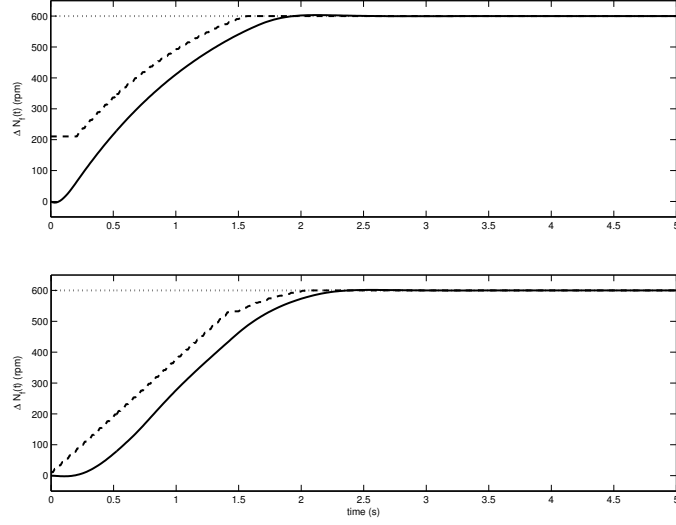


Figure 2.2: Top: Ordinary RG response with $r(t)$ (dotted), $v(t)$ (dashed), and $\Delta N_f(t)$ (solid); Bottom: Decentralized RG response with $r_1(t)$ (dotted), $v_1(t)$ (dashed), and $\Delta N_f(t)$ (solid)

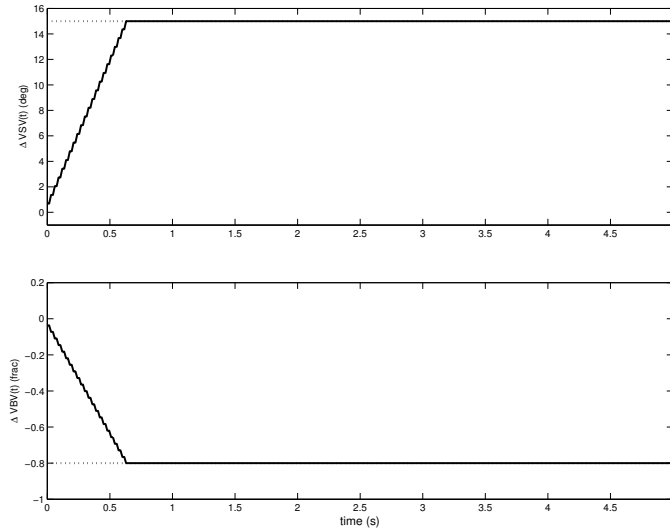


Figure 2.3: Response of the governed $\Delta VSV(t)$ (top), $\Delta VBV(t)$ (bottom), using ordinary (dashed) and decentralized (solid) RGs with corresponding reference values (dotted)

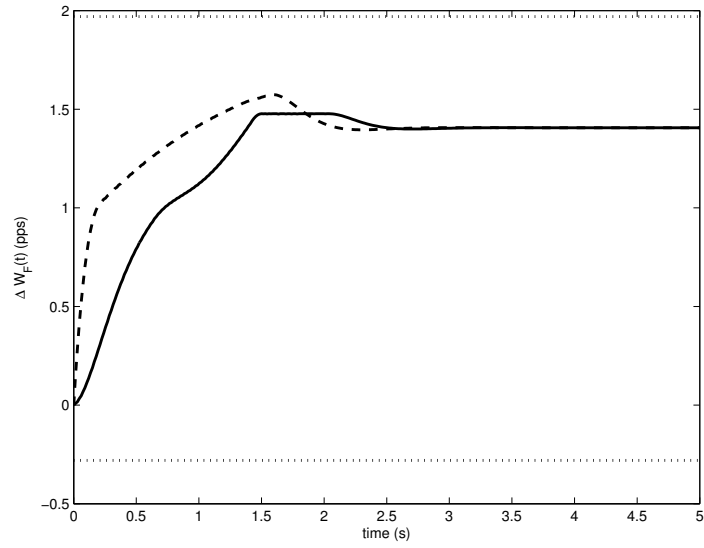


Figure 2.4: Response of $\Delta W_F(t)$ using ordinary (dashed) and decentralized (solid) RGs plotted against constraints (dotted)

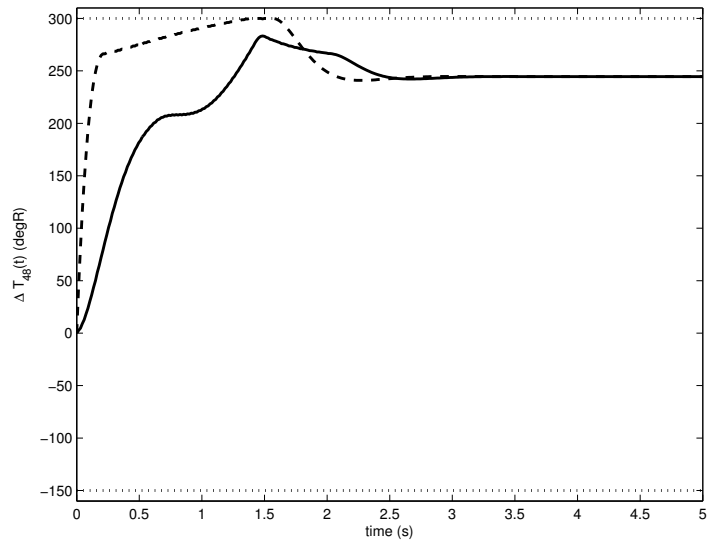


Figure 2.5: Response of $\Delta T_{48}(t)$ using ordinary (dashed) and decentralized (solid) RGs plotted against constraints (dotted)

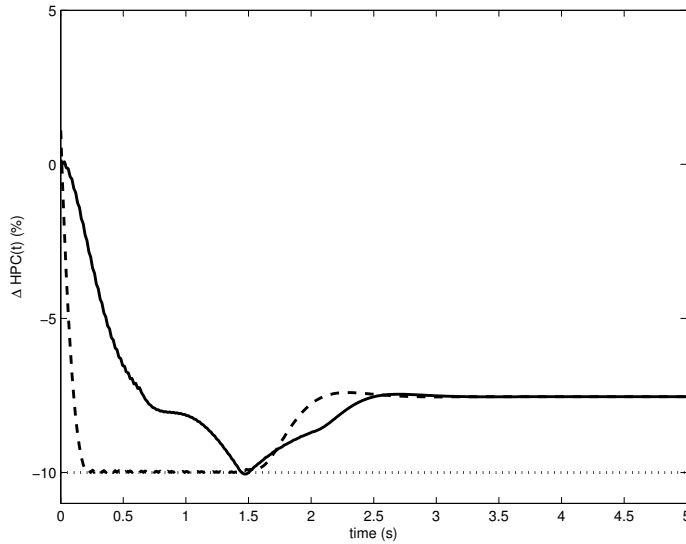


Figure 2.6: Response of $\Delta HPC(t)$ using ordinary (dashed) and decentralized (solid) RGs plotted against constraints (dotted)

The dynamics (2.1) become,

$$x_i(t+1) = A_{i1}x_1(t) + \dots + A_{iq}x_q(t) + B_{i1}v_1(t) + \dots + B_{iq}v_q(t), \quad (2.13a)$$

$$y(t) = C_1x_1(t) + \dots + C_qx_q(t) + D_1v_1(t) + \dots + D_qv_q(t) \in Y, \quad (2.13b)$$

for $i = 1, \dots, q$.

2.4.1 Constraint sets

We consider the situation, in which every RG_i is applied to the i -th subsystem and the RGs do not communicate over a network. Every RG_i is designed with the assumption that the states of all the other subsystems are close to their steady-state values. This assumption is used to help in the design of the RG but is not a requirement during system operation.

Given the i -th subsystem, let,

$$x_{(i)}(t) = \begin{bmatrix} x_1(t) \\ \vdots \\ x_{i-1}(t) \\ x_{i+1}(t) \\ \vdots \\ x_q(t) \end{bmatrix}, \quad v_{(i)}(t) = \begin{bmatrix} v_1(t) \\ \vdots \\ v_{i-1}(t) \\ v_{i+1}(t) \\ \vdots \\ v_q(t) \end{bmatrix}. \quad (2.14)$$

After rearranging in terms of the new variables, (2.13) is of the form,

$$x_i(t+1) = A_{ii}x_i(t) + A_{i(i)}x_{(i)}(t) + B_{ii}v_i(t) + B_{i(i)}v_{(i)}(t), \quad (2.15a)$$

$$x_{(i)}(t+1) = A_{(i)i}x_i(t) + A_{(i)(i)}x_{(i)}(t) + B_{(i)i}v_i(t) + B_{(i)(i)}v_{(i)}(t), \quad (2.15b)$$

$$y(t) = C_i x_i(t) + C_{(i)} x_{(i)}(t) + D_i v_i(t) + D_{(i)} v_{(i)}(t) \in Y^i. \quad (2.15c)$$

where $Y^i \subset Y$ is introduced as a constraint partition of Y that is enforced by the RG*i*. The RG*i* does not have a measurement or estimate of $x_{(i)}(t)$, so the design assumes that $x_{(i)}(t)$ instantaneously achieves steady-state after every update with $v_{(i)}(t) = 0$,

$$x_{(i)}(t) \approx \hat{A}_{(i)i}x_i(t) + \hat{B}_{(i)i}v_i(t), \quad (2.16)$$

where, $\hat{A}_{(i)i} = (I - A_{(i)(i)})^{-1}A_{(i)i}$ and $\hat{B}_{(i)i} = (I - A_{(i)(i)})^{-1}B_{(i)i}$.

Assuming that $A_{ii} + A_{i(i)}\hat{A}_{(i)i}$ are asymptotically stable and making use of the fact, $\hat{A}_{(i)i} = A_{(i)i} + A_{(i)(i)}\hat{A}_{(i)i}$, $\hat{B}_{(i)i} = B_{(i)i} + A_{(i)(i)}\hat{B}_{(i)i}$, the prediction equations governing the RG*i* become,

$$\hat{x}_i(t+k+1|t) = (A_{ii} + A_{i(i)}\hat{A}_{(i)i})\hat{x}_i(t+k|t) + (B_{ii} + A_{i(i)}\hat{B}_{(i)i})v_i(t+k|t), \quad (2.17a)$$

$$\hat{x}_{(i)}(t+k+1|t) = \hat{A}_{(i)i}\hat{x}_i(t+k|t) + \hat{B}_{(i)i}v_i(t+k|t), \quad (2.17b)$$

$$\hat{y}_i(t+k|t) = C_i\hat{x}_i(t+k|t) + C_{(i)}\hat{x}_{(i)}(t+k|t) + D_i v_i(t+k|t) \in \hat{Y}^i, \quad k \geq 1. \quad (2.17c)$$

The states, $\hat{x}_i(t)$ and $\hat{x}_{(i)}(t)$, are approximate predictions of $x_i(t)$ and $x_{(i)}(t)$, respectively, the output $\hat{y}_i(t)$ is an approximate prediction of $y(t)$, and $\hat{Y}^i \subset \mathbb{R}^p$ is a tightened version of Y^i . Note that, in the above, there are no contributions from $v_{(i)}(t+k|t)$, *i.e.*, due to the lack of information regarding the operation of other subsystems, we assume $v_{(i)}(t+k|t) \equiv 0$.

Because the RG for the i -th subsystem can only govern $v_i(t)$, this necessitates

that Y be partitioned across all subsystems so the sets Y^i are chosen to satisfy,

$$Y^1 \oplus Y^2 \oplus \dots \oplus Y^q \subset Y. \quad (2.18)$$

Therefore, if every RGi guarantees constraint satisfaction with respect to Y^i by assuming that $v_{(i)}(t+k|t) \equiv 0$, constraint satisfaction for the whole system is also guaranteed.

Specifically, given a state estimate for $x_i(t)$ and $x_{(i)}(t)$, the RGi is designed to modify $v_i(t)$ in order to enforce the following constraint,

$$(x_i(t), x_{(i)}(t), v_i(t)) \in \hat{O}_\infty^i, \quad (2.19)$$

where,

$$\hat{O}_\infty^i = \{(\hat{x}_i, \hat{x}_{(i)}, \bar{v}_i) : \hat{x}_i(t|t) = x_i, \hat{x}_{(i)}(t|t) = x_{(i)}, v_i(t+k|t) \equiv \bar{v}_i, (2.17) \text{ are satisfied}\}. \quad (2.20)$$

As in the case of the reduced order system of the previous chapter, we are able to derive a constraint on the rate of change of $v_i(t)$ in order to help ensure the constraint adherence of (2.15c).

Proposition 2.4. *Assume that at the initial time, $(x_i(0), x_{(i)}(0), v_i(-1)) \in \hat{O}_\infty^i$. Introduce compact error sets, $E_i \subset \mathbb{R}^{n_i}$, $E_{(i)} \subset \mathbb{R}^{n-n_i}$, and $E_y^i \subset \mathbb{R}^p$ satisfying,*

$$A_{ii}E_i \oplus A_{i(i)}E_{(i)} \subset \text{int } E_i, \quad (2.21a)$$

$$A_{(i)i}E_i \oplus A_{(i)(i)}E_{(i)} \subset \text{int } E_{(i)}, \quad (2.21b)$$

$$C_iE_i \oplus C_{(i)}E_{(i)} \subset \text{int } E_y^i, \quad (2.21c)$$

$$E_y^i \subset \text{int } Y_i. \quad (2.21d)$$

Define $\Delta v_i(t) = v_i(t) - v_i(t-1)$ and $\Delta \hat{x}_i(t) = \hat{x}_i(t) - \hat{x}_i(t-1)$ and introduce constraints,

$$-A_{i(i)}\hat{A}_{(i)i}\Delta \hat{x}_i(t) - A_{i(i)}\hat{B}_{(i)i}\Delta v_i(t) \in E_i \sim A_{ii}E_i \sim A_{i(i)}E_{(i)}, \quad (2.22a)$$

$$-A_{(i)(i)}\hat{A}_{(i)i}\Delta \hat{x}_i(t) - A_{(i)(i)}\hat{B}_{(i)i}\Delta v_i(t) \in E_{(i)} \sim A_{(i)i}E_i \sim A_{(i)(i)}E_{(i)}, \quad (2.22b)$$

and for $k \geq 1$,

$$-A_{i(i)}\hat{A}_{(i)i}\Delta\hat{x}_i(t+k|t) \in E_i \sim A_{ii}E_i \sim A_{i(i)}E_{(i)}, \quad (2.23a)$$

$$-A_{(i)(i)}\hat{A}_{(i)i}\Delta\hat{x}_i(t+k|t) \in E_{(i)} \sim A_{(i)i}E_i \sim A_{(i)(i)}E_{(i)}, \quad (2.23b)$$

$$-C_{(i)}\hat{A}_{(i)i}\Delta\hat{x}_i(t+k|t) \in E_y^i \sim C_iE_i \sim C_{(i)}E_{(i)}. \quad (2.23c)$$

Assume that $x_i(0) - \hat{x}_i(0) \in E_i$, $x_{(i)}(0) - \hat{A}_{(i)i}\hat{x}_i(-1) - \hat{B}_{(i)i}v_i(-1) \in E_{(i)}$. Further assume $v_{(i)}(t) \equiv 0$. If RGi enforces constraints (2.19) with $\hat{Y}^i \subset Y^i \sim E_y^i$ and constraints (2.22)-(2.23) by updating $v_i(t)$, $t \in \mathbb{Z}_+$, according to,

$$v_i(t) = v_i(t-1) + \kappa_i(t)(r_i(t) - v_i(t-1)), \quad (2.24)$$

for $\kappa_i(t) \in [0, 1]$, then $y(t) \in Y^i$ is satisfied and $v_i(t)$ is recursively feasible.

Proof. Fix t . For $k \geq 1$, assume $x_i(t+k|t) - \hat{x}_i(t+k|t) \in E_i$, and $x_{(i)}(t+k|t) - \hat{A}_{(i)i}\hat{x}_i(t+k-1|t) - \hat{B}_{(i)i}v_i(t) \in E_{(i)}$. Then, because $v_i(t)$ is held constant along the prediction horizon, $x_i(t+k+1|t) - \hat{x}_i(t+k+1|t) = A_{ii}(x_i(t+k|t) - \hat{x}_i(t+k|t)) + A_{i(i)}(x_{(i)}(t+k|t) - \hat{A}_{(i)i}\hat{x}_i(t+k-1|t) - \hat{B}_{(i)i}v_i(t)) = A_{ii}(x_i(t+k|t) - \hat{x}_i(t+k|t)) + A_{i(i)}(x_{(i)}(t+k|t) - \hat{A}_{(i)i}\hat{x}_i(t+k-1|t) - \hat{B}_{(i)i}v_i(t)) - A_{i(i)}\hat{A}_{(i)i}\Delta\hat{x}_i(t+k|t) \in A_{ii}E_i \oplus A_{i(i)}E_{(i)} \oplus (E_i \sim A_{ii}E_i \sim A_{i(i)}E_{(i)}) \subset E_i$. Furthermore, $x_{(i)}(t+k+1|t) - \hat{A}_{(i)i}\hat{x}_i(t+k|t) - \hat{B}_{(i)i}v_i(t) = A_{(i)i}x_i(t+k|t) + A_{(i)(i)}x_{(i)}(t+k|t) + B_{(i)i}v_i(t) - (A_{(i)i} + A_{(i)(i)}\hat{A}_{(i)i})\hat{x}_i(t+k|t) - (B_{(i)i} + A_{(i)(i)}\hat{B}_{(i)i})v_i(t) = A_{(i)i}(x_i(t+k|t) - \hat{x}_i(t+k|t)) + A_{(i)(i)}(x_{(i)}(t+k|t) - \hat{A}_{(i)i}\hat{x}_i(t+k-1|t) - \hat{B}_{(i)i}v_i(t)) - A_{(i)(i)}\hat{A}_{(i)i}\Delta\hat{x}_i(t+k|t) \in A_{(i)i}E_i \oplus A_{(i)(i)}E_{(i)} \oplus (E_{(i)} \sim A_{(i)i}E_i \sim A_{(i)(i)}E_{(i)}) \subset E_{(i)}$.

Now assume $x_i(t) - \hat{x}_i(t) \in E_i$, $x_{(i)}(t) - \hat{A}_{(i)i}\hat{x}_i(t-1) - \hat{B}_{(i)i}v_i(t-1) \in E_{(i)}$. Then, $x_i(t+1|t) - \hat{x}_i(t+1|t) = A_{ii}(x_i(t) - \hat{x}_i(t)) + A_{i(i)}(x_{(i)}(t) - \hat{A}_{(i)i}\hat{x}_i(t) - \hat{B}_{(i)i}v_i(t)) = A_{ii}(x_i(t) - \hat{x}_i(t)) + A_{i(i)}(x_{(i)}(t) - \hat{A}_{(i)i}\hat{x}_i(t-1) - \hat{B}_{(i)i}v_i(t-1)) - A_{i(i)}\hat{A}_{(i)i}\Delta\hat{x}_i(t) - A_{i(i)}\hat{B}_{(i)i}\Delta v_i(t) \in A_{ii}E_i \oplus A_{i(i)}E_{(i)} \oplus (E_i \sim A_{ii}E_i \sim A_{i(i)}E_{(i)}) \subset E_i$. Also, $x_{(i)}(t+1|t) - \hat{A}_{(i)i}\hat{x}_i(t) - \hat{B}_{(i)i}v_i(t) = A_{(i)i}x_i(t) + A_{(i)(i)}x_{(i)}(t) + B_{(i)i}v_i(t) - (A_{(i)i} + A_{(i)(i)}\hat{A}_{(i)i})\hat{x}_i(t) - (B_{(i)i} + A_{(i)(i)}\hat{B}_{(i)i})v_i(t) = A_{(i)i}(x_i(t) - \hat{x}_i(t)) + A_{(i)(i)}(x_{(i)}(t) - \hat{A}_{(i)i}\hat{x}_i(t-1) - \hat{B}_{(i)i}v_i(t-1)) - A_{(i)(i)}\hat{A}_{(i)i}\Delta\hat{x}_i(t) - A_{(i)(i)}\hat{B}_{(i)i}\Delta v_i(t) \in A_{(i)i}E_i \oplus A_{(i)(i)}E_{(i)} \oplus (E_{(i)} \sim A_{(i)i}E_i \sim A_{(i)(i)}E_{(i)}) \subset E_{(i)}$. Therefore $x_i(t+k|t) - \hat{x}_i(t+k|t) \in E_i$, and $x_{(i)}(t+k|t) - \hat{A}_{(i)i}\hat{x}_i(t+k-1|t) - \hat{B}_{(i)i}v_i(t) \in E_{(i)}$ for all $t \in \mathbb{Z}_+$, by recursion.

Therefore, for all $k \geq 1$, $y(t+k|t) - \hat{y}_i(t+k|t) = C_i(x_i(t+k|t) - \hat{x}_i(t+k|t)) + C_{(i)}(x_{(i)}(t+k|t) - \hat{x}_{(i)}(t+k|t)) = C_i(x_i(t+k|t) - \hat{x}_i(t+k|t)) + C_{(i)}(x_{(i)}(t+k|t) - \hat{A}_{(i)i}\hat{x}_i(t+k-1|t) - \hat{B}_{(i)i}v_i(t)) - C_{(i)}\hat{A}_{(i)i}\Delta\hat{x}_i(t) \in C_iE_i \oplus C_{(i)}E_{(i)} \oplus (E_y^i \sim C_iE_i \sim C_{(i)}E_{(i)}) \subset E_y^i$.

So $y(t) - \hat{y}_i(t) \in E_y^i$ for all $t \geq 1$, because $y(t) - \hat{y}_i(t) = y(t|t-1) - \hat{y}_i(t|t-1)$. Therefore, $y(t) = \hat{y}_i(t) + (y(t) - \hat{y}_i(t)) \in (Y^i \sim E_y^i) \oplus E_y^i \subset Y^i$. Noting that the

RG i guarantees recursive feasibility and provided that $y(0) - \hat{y}_i(0) \in E_y^i$, recursive feasibility is proven here as well. \square

2.4.2 Decentralized RG design

Having developed RGs for every individual subsystem, we are now able to complete the design of the decentralized RG scheme by showing that the interactions between the RGs of every subsystem can together enforce constraints for the system (2.13).

Proposition 2.5. *Assume that the assumptions of Proposition 2.4 have been satisfied and RG1 through RG q have been designed as in Proposition 2.4. Then $y(t) \in Y$ for all $t \in \mathbb{Z}_+$ and $v(t)$ is recursively feasible.*

Proof. Note that due to the linearity of (2.13) and by the principle of superposition, the system can be split into q parts, the i -th of which is driven by one input $v_i(t)$, with all other inputs held at 0. Because of this, we can define matrices $\bar{A}_1, \dots, \bar{A}_q$, $\bar{B}_1, \dots, \bar{B}_q$, $\bar{C}_1, \dots, \bar{C}_q$, and $\bar{D}_1, \dots, \bar{D}_q$, as above so that the system becomes,

$$\bar{x}_1(t+1) = \bar{A}_1 \bar{x}_1(t) + \bar{B}_1 v_1(t), \quad (2.25)$$

\vdots

$$\bar{x}_q(t+1) = \bar{A}_q \bar{x}_q(t) + \bar{B}_q v_q(t), \quad (2.26)$$

$$y(t) = \bar{C}_1 \bar{x}_1(t) + D_1 v_1(t) + \dots + \bar{C}_q \bar{x}_q(t) + D_q v_q(t) \in Y, \quad (2.27)$$

where,

$$\bar{x}_i(t) = \begin{bmatrix} x_i(t) \\ x_{(i)}(t) \end{bmatrix}.$$

Applying Proposition 2.4, we can guarantee $C_i \bar{x}_i(t) + D_i v_i(t) \in Y^i$ for all $i = 1, \dots, q$. Because $Y^1 \oplus \dots \oplus Y^q \subset Y$ by (2.18) and,

$$v(t) = \begin{bmatrix} v_1(t) \\ \vdots \\ v_q(t) \end{bmatrix}$$

by definition, the conclusion follows. \square

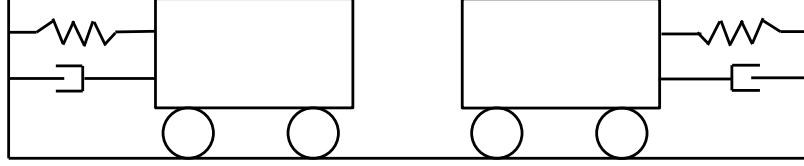


Figure 2.7: Double mass-spring-damper schematic

2.5 Example 2: Double mass-spring-damper

We illustrate the above approach by developing an decentralized RG scheme for two interconnected subsystems that are unable to communicate with each other. We show that, by applying the constraints above at the subsystem level, we are able to achieve constraint enforcement for the whole system. Although the system is not large in scale, the example is illustrative because, as we will show, component subsystems are able to enforce minimum and maximum separation constraints without communicating with each other. The particular subsystems are blocks in a double mass-spring-damper system, where each block is controlled by a force applied directly to its center of mass. The system is modeled as a two degree-of-freedom system in which two blocks are attached by a spring and damper to walls on each side and to each other, as in Fig. 2.7.

The continuous-time equations of motion are given by,

$$m_1\ddot{x}_1(t) + (c_1 + c_3)\dot{x}_1(t) - c_3\dot{x}_2(t) + (k_1 + k_3)x_1(t) - k_3x_2(t) = F_1(t), \quad (2.28a)$$

$$m_2\ddot{x}_2(t) - c_3\dot{x}_1(t) + (c_2 + c_3)\dot{x}_2(t) - k_3x_1(t) + (k_2 + k_3)x_2(t) = F_2(t), \quad (2.28b)$$

where $x_1(t)$ and $x_2(t)$ are the positions of the two masses relative to equilibrium in meters and $F_1(t)$ and $F_2(t)$ are the forces applied to each mass in Newtons. Note that k_3 and c_3 are spring and damper constants for the middle spring and damper. We impose the constraint on the relative distance between two masses,

$$y(t) = x_1(t) - x_2(t) \in Y = [-0.04, 0.04], \quad (2.29)$$

so that the minimum and maximum separation between them is 4cm from the rest configuration.

The parameter values are given as, $m_1 = 20$, $m_2 = 1$, $c_1 = c_2 = 10$, $c_3 = 0$,

$k_1 = 16$, $k_2 = 190$, and $k_3 = 1$. Let,

$$x(t) = \begin{bmatrix} x_1(t) \\ \dot{x}_1(t) \\ x_2(t) \\ \dot{x}_2(t) \end{bmatrix}, \quad v(t) = \begin{bmatrix} F_1(t) \\ F_2(t) \end{bmatrix},$$

In this case, the equations of motion become,

$$\dot{x}(t) = \begin{bmatrix} A_{11} & A_{12} \\ A_{21} & A_{22} \end{bmatrix} x(t) + \begin{bmatrix} B_{11} & 0 \\ 0 & B_{22} \end{bmatrix} v(t), \quad (2.30)$$

$$y(t) = \begin{bmatrix} C_1 & C_2 \end{bmatrix} x(t) \in Y, \quad (2.31)$$

where,

$$A_{ii} = \begin{bmatrix} 0 & 1 \\ -\frac{k_i}{m_i} & -\frac{c_i}{m_i} \end{bmatrix}, \quad B_{ii} = \begin{bmatrix} 0 \\ -\frac{1}{m_i} \end{bmatrix}, \quad (2.32)$$

for $i = 1, 2$, and,

$$A_{ij} = \begin{bmatrix} 0 & 0 \\ -\frac{k_3}{m_i} & -\frac{c_3}{m_i} \end{bmatrix}, \quad (2.33)$$

for $i \neq j$. Note that because the controllers are applied to the subsystems' centers of mass, this example is simplified by the fact that $B_{12} = B_{21} = 0$, which reduces the constraints (2.22a)-(2.22b) to the form of (2.23a)-(2.23b).

We now develop the decentralized RG scheme. In order to develop our RG scheme, we partition Y according to Proposition 2.5, choosing $Y^1 = 0.8Y$ and $Y^2 = 0.2Y$. We also choose $E_y^i = 0.05Y_i$ for $i = 1, 2$.

Taking advantage of the fact that A_{ii} are asymptotically stable, the sets E_i , $E_{(i)}$, are chosen by applying the disturbance invariant set algorithm from [5], which is applied iteratively until (2.21a)-(2.21c) are satisfied. Forces of equal magnitude but opposite direction are applied to each block and are set so that an equilibrium value of 0.032cm is achieved.

The results are presented in Figs. 2.8-2.9, where we compare the ordinary RG, which simultaneously governs the inputs for both masses, to the decentralized version. The results show that the algorithm is able to enforce the constraint in a decentralized manner. The response of the force applied to the first mass is slower to converge to the desired forced than that of the conventional RG. On the other

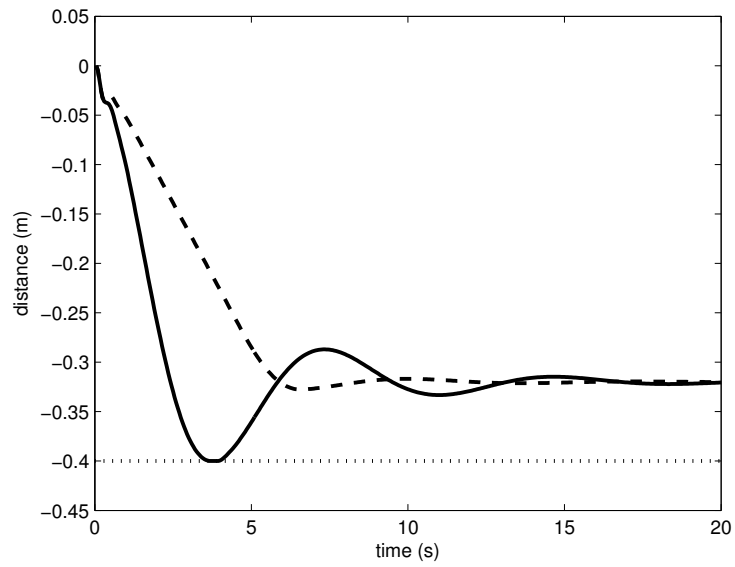


Figure 2.8: Distance between the two masses with ordinary (solid) and decentralized (dashed) RGs plotted against constraints (dotted)

hand, the force response of the second mass converges immediately; this is because the decentralization decouples the references and allows them to track their respective desired values independently of each other.

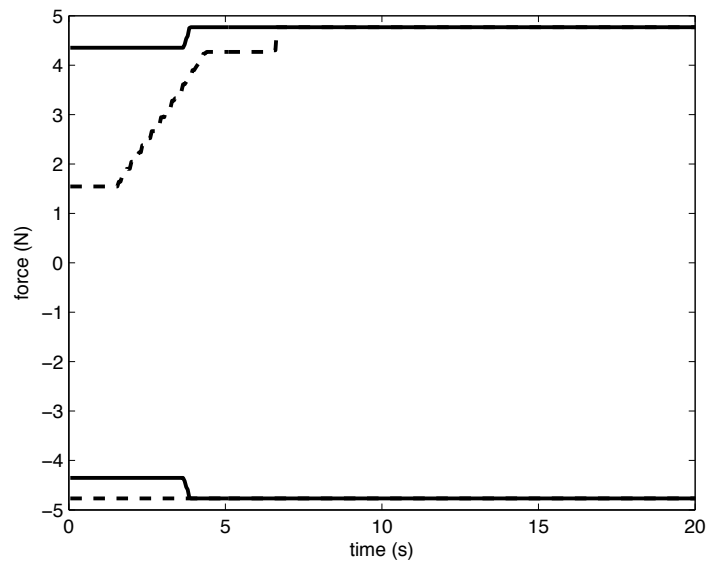


Figure 2.9: Force applied to each mass with ordinary (solid) and decentralized (dashed) RGs; the trajectory at the top corresponds to the force applied to the first mass and the bottom trajectory applies to the second

CHAPTER 3

Command governors for prioritized constraints and reference governors for prioritized references

3.1 Introduction

In this chapter, we consider the use of RGs and CGs as applied to prioritized constraint enforcement and prioritized reference tracking for disturbance-free systems. In the first case, CGs are applied to a set of “soft” constraints that have been prioritized through a penalty on a slack variable. In the second case, we consider the application of the RG to inputs $v(t)$, which are modified in order of priority.

The chapter is organized as follows. Section 3.2 presents the motivation for this problem and further outlines the contribution of the chapter. The next two sections present the two methods under consideration along with theoretical results and a numerical example: Section 3.3 introduces a method for prioritized constraint optimization using slack variables and Section 3.4 introduces the prioritized RG.

3.2 Problem motivation

Typical formulations of the reference governor are applied to systems with hard constraints, *i.e.*, systems where the constraint $y(t) \in Y$ for all $t \in \mathbb{Z}_+$ is strict. However, the case of soft constraints, where $y(t) \notin Y$ is undesirable but permitted under certain conditions, is also of interest. For instance, in some applications especially in MPC, output constraints are often treated as soft to ensure the solution can be computed even if constraint violation cannot be avoided [62]; in this situation, a control action which mitigates and reduces constraint violation is generated. In some other cases, it is allowed to trade-off constraint violation against the improvements in tracking performance [63].

To address this problem we will introduce an algorithmic method of relaxing constraints through the use of penalty functions on slack variables that weigh constraint infringement of Y against desired reference set-points in order to achieve a balance between tracking performance and constraint enforcement. We apply this cost function to the CG and illustrate the operation of the CG in the presence of prioritized constraints using a mass-spring-damper example that is subject to both hard and soft constraints in mass position. The hard constraint corresponds to a hard barrier which the mass must not hit and the soft constraint is imposed to limit the amount of overshoot.

As a related problem, we will also consider applying an RG to prioritized reference inputs. In this approach, we aim to achieve $v_i(t) = r_i(t)$ for higher priority individual inputs $v_i(t)$ before that of lower priority individual inputs. The example reported for this scheme is that of an F-16 aircraft for which the pitch attitude and flight path angle reference inputs are prioritized. Two simulations are performed corresponding to two different prioritizations: higher priority of the pitch attitude increases the aerial maneuverability of the aircraft, while higher priority of the flight path angle directly affects how quickly it tracks a desired trajectory.

3.3 Command governors for prioritized constraint sets

In this section we apply the CG to output constraints of the following form,

$$y(t) \in Y \cap Y_1 \cap \dots \cap Y_q, \quad (3.1)$$

where Y is a hard constraint set and Y_i is a soft constraint set for $1 \leq i \leq q$. That is, Y_i is a set for which $y(t) \in Y_i$ is not required as a strict inclusion but can be violated, incurring a penalty for doing so.

The penalty is introduced by way of a modifying the set Y_i . Specifically, we expand Y_i in all directions by a certain amount so that the output, $y(t)$, is contained in this modified set. To ease computational implementation, we assume Y_i is polyhedral and can be described as a set of n_c^i linear inequalities,

$$Y_i = \{y : P^i y \leq p^i\}, \quad (3.2)$$

where $P^i \in \mathbb{R}^{n_c^i \times n}$ and $p^i \in \mathbb{R}^{n_c^i}$. The matrix P^i is designed so that every row has

unit norm, *i.e.*,

$$\|P_j^i\|_2 = 1, \quad (3.3)$$

for all rows j . Note that if the constraints are not given in this form, then we can redefine, $p_j^i := p_j^i/\|P_j^i\|_2$ and $P_j^i := P_j^i/\|P_j^i\|_2$, without altering the structure of (3.2).

For each $1 \leq i \leq q$, we can define an expanded constraint set, Y_i^ε ,

$$Y_i^{\varepsilon_i} = \{(y, \varepsilon_i) : P^i y \leq p^i + \varepsilon_i \mathbf{1}_{n_c}\} = \{(y, \varepsilon_i) : \begin{bmatrix} P^i & -\mathbf{1}_{n_c} \end{bmatrix} \begin{bmatrix} y \\ \varepsilon \end{bmatrix} \leq p^i\}, \quad (3.4)$$

where $\varepsilon_i \geq 0$ is a scalar. $Y_i^{\varepsilon_i} \subset \mathbb{R}^p \times \mathbb{R}$ is the “relaxed” version of Y_i because it expands Y_i by an extra dimension, where $Y_i \times \{0\} \subset Y_i^{\varepsilon_i}$ and ε_i is the amount of relaxation. Because of condition (3.3), the polytope constraint $Y_i^{\varepsilon_i}$ retains the same shape as that of Y_i .

The projection of $Y_i^{\varepsilon_i}$ onto the y -axis is an expanded set that contains Y_i . In fact, $\text{Proj}_{\mathbb{R}^p} Y_i^{\varepsilon_i} \sim \mathcal{B}_{\varepsilon_i} = Y_i$. The proof of this follows from the requirement (3.3), since $\text{Proj}_{\mathbb{R}^p} Y_i^{\varepsilon_i} \sim \mathcal{B}_{\varepsilon_i} = \{z : P_j^i z \leq p_j^i + \varepsilon_i - h_{P_j^i}(\mathcal{B}_{\varepsilon_i}), 1 \leq j \leq n_c\} = \{z : P_j^i z \leq p_j^i, 1 \leq j \leq n_c\} = Y_i$.

We apply the ordinary CG to the set $Y_i^{\varepsilon_i}$, where each ε_i is treated as a control input and is constrained to be non-negative. This introduces a new input vector of slack variables,

$$\varepsilon(t) = (\varepsilon_1(t), \dots, \varepsilon_q(t)). \quad (3.5)$$

The system (0.1) can then be modified,

$$x(t+1) = Ax(t) + \begin{bmatrix} B & 0 \end{bmatrix} \begin{bmatrix} v(t) \\ \varepsilon(t) \end{bmatrix}, \quad (3.6a)$$

$$\hat{y}(t) = \begin{bmatrix} C \\ 0 \end{bmatrix} x(t) + \begin{bmatrix} D & 0 \\ 0 & I \end{bmatrix} \begin{bmatrix} v(t) \\ \varepsilon(t) \end{bmatrix} \in \hat{Y}, \quad (3.6b)$$

where $\hat{y}(t) = (y(t), \varepsilon(t))$ and,

$$\hat{Y} = \{(y, \varepsilon) : y \in Y, y \in Y_i^{\varepsilon_i}, 0 \leq \varepsilon_i \leq M, 1 \leq i \leq q\}, \quad (3.7)$$

is a hard constraint on $\hat{y}(t)$; the scalar term M is a very large number that is used to ensure \hat{Y} is compact. The rest of the development of the CG as applied to prioritized

constraints follows by noting that different sets Y_i may have different degrees of “softness”, *i.e.*, $y(t) \in Y_1$ may only admit a small violation, while $y(t) \in Y_q$, $q \neq 1$, being of secondary significance, may allow much larger constraint infringement. We treat this by weighing the elements of the input (both the reference and slack variables) in the same way as the ordinary CG, where the number of additional set-point commands is equal to the number of soft constraints.

This amounts to applying the CG to (3.6) and updating $(v(t), \varepsilon(t))$ using a modified version of the optimization (0.18). Specifically, we define a modified maximal admissible constraint set O_∞ for the expanded reference vector $(v(t), \varepsilon(t))$ and constraint set (3.6), which is denoted by $\hat{O}_\infty \subset \mathbb{R}^n \times \mathbb{R}^m \times \mathbb{R}^q$; we then introduce a diagonal positive penalty matrix Q_ε for use in solving for the reference $(v(t), \varepsilon(t))$ via the following optimization problem,

$$\min \|r(t) - v(t)\|_Q^2 + \|Q_\varepsilon \varepsilon\|_1, \quad (3.8a)$$

$$\text{sub. to } (x(t), v(t), \varepsilon(t)) \in \hat{O}_\infty. \quad (3.8b)$$

The penalty matrix serves to prioritize the constraints because a higher weight on ε_i amounts to a higher priority of the associated constraint Y_i .

Note that since \hat{Y} is the intersection of sets defined by linear inequalities, then \hat{Y} , and hence \hat{O}_∞ , can also be expressed as a set of linear inequalities.

The prioritization of constraints guarantees satisfaction of the hard constraint, Y , so as a design consideration, any constraints whose enforcement is required should be included in Y . The reason the penalty variables are not penalized using a 2-norm is because doing so may cause the CG to soften constraints even in case where the constraints are feasible [64, 65].

The approach to satisfying the constraints in a soft way is essentially a redefinition of the ordinary CG scheme, so the prioritized CG scheme shares many of the same properties with the ordinary CG; though all the properties apply to the output of expanded dimension, $\hat{y}(t)$, some properties, such as finite time convergence, are dimension-independent, as the sequel shows in further detail.

Remark 3.1. Other schemes may be defined that exploit \hat{O}_∞ . For instance, one may look for satisfying (3.8b) by progressively relaxing constraints, *i.e.*, initially with all ε_i set to zero, then with only one ε_i allowed to vary away from zero, and so on. The properties of these schemes are left to future work.

3.3.1 Theoretical results

The properties of CGs with prioritized constraints follow as an extension of the ordinary CG theory. All of the results of the CG theory apply when considering the dimensionally-expanded system (3.6). However, not all results apply to (0.1).

For example, a result from ordinary CG theory is convergence to the nearest feasible reference. The relaxed form of the CG exhibits another property, namely that if the steady-state response to the command is not inside the intersection of the soft constraints then, although the CG converges, it may not converge to the desired equilibrium. In order to demonstrate this, we first state the following. According to the conventional CG theory, when there exists an r_s such that for all $t \geq t_s$, $r(t) = r_s$, then there exists a t_f such that $v(t) = r_s^*$ and $\varepsilon(t) = \varepsilon^*$ for all $t \geq t_f$, where,

$$(r_s^*, \varepsilon^*) = \arg \min_{(r, \varepsilon) \in \hat{\Omega}} \|(r - r_s)\|_Q^2 + \|Q_\varepsilon \varepsilon\|_1, \quad (3.9)$$

$$\hat{\Omega} = \left\{ (r, \varepsilon) : \begin{bmatrix} (C\Gamma + D)r \\ \varepsilon \end{bmatrix} \in \hat{Y} \right\}, \quad (3.10)$$

where $\Gamma = (I_n - A)^{-1}B$.

Similarly, in the case of prioritized constraints, if the steady state response to r_s is not within Y_i for all $1 \leq i \leq q$, i.e., $(C\Gamma + D)r_s \notin Y_i$, then r_s^* may not coincide with r_s . We state the following proposition.

Proposition 3.2. $r_s^* = r_s$ if and only if $(C\Gamma + D)r_s \in Y_i$ for all $1 \leq i \leq q$.

Proof. Sufficiency. The hypothesis that $(C\Gamma + D)r_s \in Y_i$ for all $1 \leq i \leq q$ directly implies that $(r_s, 0) \in \hat{\Omega}$ by the definition in (3.10). Since $(r_s, 0)$ is the unique, unconstrained minimum of (3.9) and $(r_s, 0)$ is contained within constraints, then the solution to (3.9) is $(r_s^*, \varepsilon^*) = (r_s, 0)$.

Necessity. The assumption $r_s^* = r_s$ implies that the solution to (3.9) is (r_s, ε^*) . There are two possibilities: either $\varepsilon^* > 0$ or $\varepsilon^* = 0$. In the former case, because the lower bound on ε is 0, $(r_s, (1-c)\varepsilon^*)$ is constraint admissible for all $0 < c < 1$. Because $(C\Gamma + D)r_s \in \text{int } Y$, there exists $r'_s \neq r_s$ such that $\|(r'_s - r_s)\|_Q^2 < c' \|Q_\varepsilon \varepsilon\|_1$ for some $0 < c' < 1$, implying that $\|(r'_s - r_s)\|_Q^2 + (1-c') \|Q_\varepsilon \varepsilon\|_1 < \|Q_\varepsilon \varepsilon\|_1$. This contradicts the optimality of (r_s, ε^*) and the proof is complete. \square

3.3.2 Numerical example

This example considers a mass-spring-damper with equations of motion,

$$\begin{bmatrix} \dot{x}_1(t) \\ \dot{x}_2(t) \end{bmatrix} = \begin{bmatrix} 0 & 1 \\ -\frac{k}{m} & -\frac{c}{m} \end{bmatrix} \begin{bmatrix} x_1(t) \\ x_2(t) \end{bmatrix} + \begin{bmatrix} 0 \\ \frac{1}{m} \end{bmatrix} u(t), \quad (3.11)$$

where the parameters are taken from [29] as, $c = 0.6590\text{N}\cdot\text{s}/\text{m}$, $k = 38.94\text{N}/\text{m}$, $m = 1.54\text{kg}$, and,

$$u(t) = \begin{bmatrix} 0 & c_d \end{bmatrix} x(t) + kv(t), \quad (3.12)$$

and where $c_d = 4.0\text{N}\cdot\text{s}/\text{m}$ is a stabilizing feed-back gain and $v(t)$ is the steady-state set point for $x_1(t)$.

The system models the electromagnetically actuated mass-spring-damper from [29]. The control objective of the system is to bring the position of a small mass close to another object. Specifically, the second object is placed at 9mm and the mass must be brought to a position of 7.5mm. This leads to the introduction of two constraints. The first constraint is that of a hard barrier imposed as $x_1(t) \leq 0.009\text{m}$ in order to prevent a collision. Additionally, a soft constraint of $x_1(t) \leq 0.0075\text{m}$ is imposed to limit overshoot. Furthermore, the control input is soft-constrained to $0 \leq u(t) \leq 0.3$. We proceed by discretizing the continuous-time system using a zero-order hold with time step $T = 0.01$.

The modified output (3.6b) takes the following form,

$$\hat{y}(t) = \begin{bmatrix} 1 & 0 & 0 & 0 \\ 0 & c_d & 0 & 0 \\ 0 & 0 & 1 & 0 \\ 0 & 0 & 0 & 1 \end{bmatrix} \begin{bmatrix} x_1(t) \\ x_2(t) \\ \varepsilon_1(t) \\ \varepsilon_2(t) \end{bmatrix} + \begin{bmatrix} 0 \\ k \\ 0 \\ 0 \end{bmatrix} v(t) \in \hat{Y}, \quad (3.13)$$

where \hat{Y} is the expanded constraint (3.7) set and $\varepsilon_1(t), \varepsilon_2(t)$ are auxiliary reference inputs measuring soft-constraint adherence corresponding to the position constraint on $x_1(t)$ and control constraint on $u(t)$.

The simulations results are reported for a constant reference set-point, $r(t) \equiv 0.0075$ with initial condition set at the origin, $x(0) = 0$. The three different runs

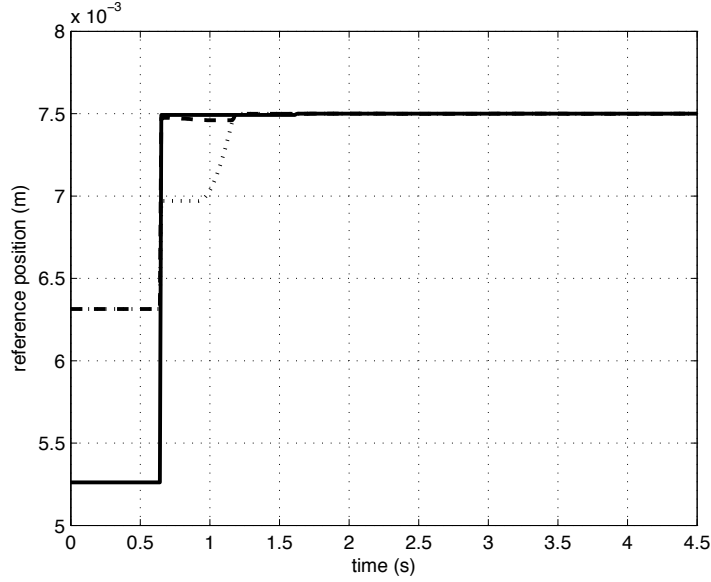


Figure 3.1: Time history of $v(t)$ for three different cases: $Q_{\epsilon,1}$ (solid), $Q_{\epsilon,2}$ (dotted), and $Q_{\epsilon,3}$ (dashed)

consist of three different weights for the optimization (3.8), $Q = 1$ and,

$$Q_{\epsilon,1} = \begin{bmatrix} 10^6 & 0 \\ 0 & 10^{-6} \end{bmatrix}, \quad Q_{\epsilon,2} = \begin{bmatrix} 10^{-6} & 0 \\ 0 & 10^6 \end{bmatrix}, \quad Q_{\epsilon,3} = \begin{bmatrix} 10^{-6} & 0 \\ 0 & 10^{-6} \end{bmatrix}.$$

The results are presented in Figs. 3.1-3.5 and show that prioritizing constraint adherence against set-point tracking can be used to manage overshoot of the output. Note that simulations using the ordinary CG, which has been designed under the assumption that all constraints are hard, are very similar to the case of $Q_{\epsilon,1}$ and thus have not been plotted. The similarity is explained by the fact that the constraint on the position is more stringent than the constraint on the control input.

Fig. 3.1 shows the three responses of the reference input $v(t)$. Fig. 3.2 shows the three responses of $x_1(t)$ with the soft and hard constraints plotted. None of the trajectories violate the hard constraint and we see that, as the weight on $\epsilon_1(t)$ increases, the amount of overshoot in the corresponding response is lessened. Fig. 3.3 shows the three responses of the control input $u(t)$. Figs. 3.4-3.5 show the slack variable responses and that lower weights correspond to higher amounts of slack.

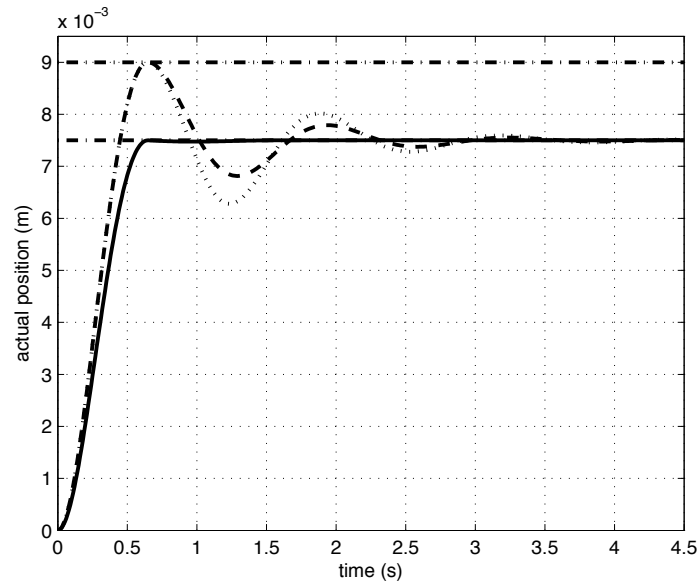


Figure 3.2: Time history of $x_1(t)$ for three different cases: $Q_{\epsilon,1}$ (solid), $Q_{\epsilon,2}$ (dotted), and $Q_{\epsilon,3}$ (dashed); the constraints are dot-dashed

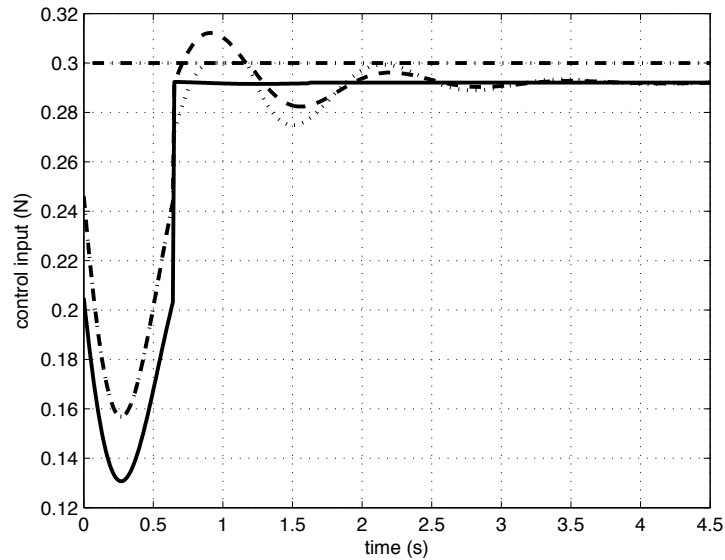


Figure 3.3: Time history of $u(t)$ for three different cases: $Q_{\epsilon,1}$ (solid), $Q_{\epsilon,2}$ (dotted), and $Q_{\epsilon,3}$ (dashed); the constraint is dot-dashed

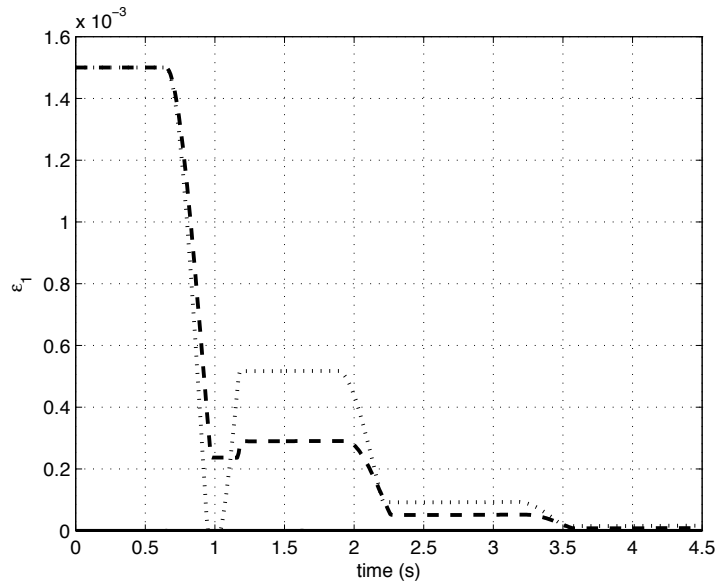


Figure 3.4: Time history of $\varepsilon_1(t)$ for two different cases: $Q_{\varepsilon,2}$ (dotted) and $Q_{\varepsilon,3}$ (dashed); note that in the case of $Q_{\varepsilon,1}$, $\varepsilon_1(t)$ is zero

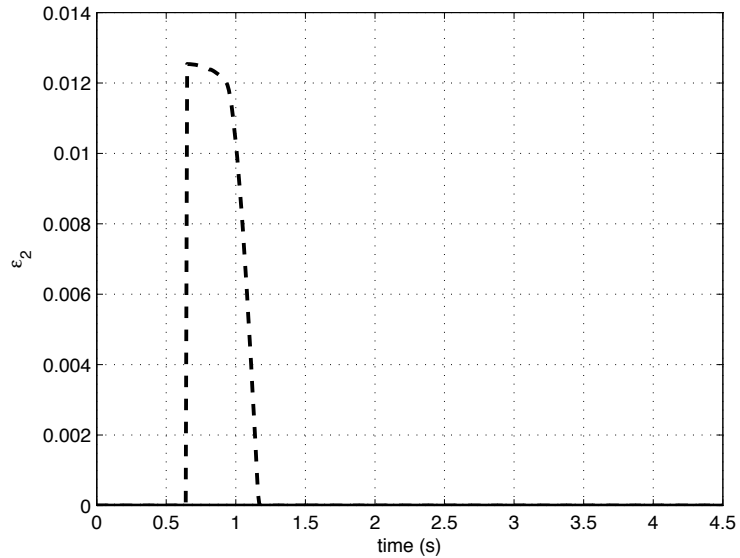


Figure 3.5: Time history of $\varepsilon_2(t)$ in the case of $Q_{\varepsilon,3}$ (dashed); note that in the cases of $Q_{\varepsilon,1}$ and $Q_{\varepsilon,2}$, $\varepsilon_2(t)$ is zero

3.4 Reference governors for prioritized references

Prioritized RGs (PRGs) operate by modifying a set of desired set-points in order of priority. With this approach, the higher priority commands are modified as little as possible and the closest feasible set-points are achieved for the highest priority commands.

In order to accomplish this, we order the elements of the vector, $v(t)$, in order of priority, such that $i < j$ implies that $v_i(t)$ has higher priority than $v_j(t)$. We then introduce *prioritized constraint sets*, which are slices of $\Pi(x(t))$ that depend on the desired reference $r(t)$,

$$\Pi_i(x, r) = \{v \in \Pi(x) : v_{i-1} = r_{i-1}, \dots, v_1 = r_1\}. \quad (3.14)$$

In this way $\Pi_i(x, r)$ is the set of feasible set-points for x when we set the first $i - 1$ set-points to their desired values. From the above definition, it follows that $\Pi_1(x, r) = \Pi(x)$ and $\Pi_i(x, r) \supset \Pi_{i+1}(x, r)$ for all $1 \leq i < m$. Note that the recoverable domain of initial states consists of all $x(0)$ for which $\Pi(x(0))$ is non-empty.

The prioritization scheme is developed by defining a diagonal matrix,

$$\mathbf{K}(t) = \begin{bmatrix} \kappa_1(t) & & \\ & \ddots & \\ & & \kappa_m(t) \end{bmatrix}, \quad (3.15)$$

with the requirement that $\kappa_i(t) \in [0, 1]$ for all $1 \leq i \leq m$. Subsequently, we implement the vector RG update policy from [13, 45], which is similar to the ordinary reference governor,

$$v(t) = v(t - 1) + \mathbf{K}(t)(r(t) - v(t - 1)). \quad (3.16)$$

The PRG online solution algorithm is different from that of the vector RG. It proceeds by finding the first set, $\Pi_i(x(t))$, such that there exists a feasible solution for $\kappa_i(t)$ and $\kappa_i(t) = 1$ is infeasible. Thus we choose the largest i such that $\Pi_i(x(t), r(t))$ is nonempty and set $\kappa_1(t) = \dots = \kappa_{i-1}(t) = 1$ to solve the following optimization problem,

$$\kappa_i(t) = \arg \max_{(\kappa_i, \dots, \kappa_m(t))} \kappa_i \in [0, 1], \quad (3.17a)$$

$$\text{sub. to } v(t - 1) + \mathbf{K}(t)(r(t) - v(t - 1)) \in \Pi_i(x(t), r(t)), \quad (3.17b)$$

The solution to (3.17) may not be unique. In order to ensure the uniqueness of $\kappa_i(t)$, and therefore $v_i(t)$, we may solve the optimization once again for $\kappa_{i+1}(t)$ using the new value of $\kappa_i(t)$ and the new constraint set $\Pi_{i+1}(x(t), r(t))$, repeating this until we obtain a unique solution to (3.17). The need for this sequential optimization of references can arise when direct constraints on the reference are present; *e.g.*, suppose $y(t) = v(t) \in Y$, where $Y = [-0.5, 0.5]^m$, $v(t-1) = 0$, and $r(t) = (1, 1)$. Then any $v(t) = (0.5, v_{cet})$, where $v_{cet} \in [0, 0.5]^{m-1}$ solves (3.17). In such a case, sequentially optimizing in the manner described above obtains a unique solution.

To summarize, we present the PRG in algorithmic form in Algorithm 1. The algorithm guarantees $\kappa_{1,\dots,i}(t) = 1$ for the largest possible $1 \leq i \leq m$, while the PRG satisfies imposed constraints with the rest of the available $m - i$ command inputs.

Algorithm 1: PRG algorithm

input : $x(t), r(t), v(t-1)$
output: $v(t)$

$i \leftarrow 1$;

solutionNotFound \leftarrow true;

while solutionNotFound **and** $i \leq m$ **do**

while $\Pi_i(x(t), r(t)) \neq \emptyset$ **do**

$\kappa_i(t) \leftarrow 1$;

$v_i(t) = r_i(t)$;

$i \leftarrow i + 1$;

 Solve (3.17) for $(\kappa_i(t), \dots, \kappa_m(t))$;

$v_i(t) = v_i(t-1) + \kappa_i(t)(r_i(t) - v_i(t-1))$;

$i \leftarrow i + 1$;

if $(\kappa_{i+1}(t), \dots, \kappa_m(t))$ are unique **then** solutionNotFound \leftarrow false;

 ;

while $i \leq m$ **do**

$v_i(t) = v_i(t-1) + \kappa_i(t)(r(t) - v(t-1))$;

$i \leftarrow i + 1$;

$v(t) = v(t-1) + \mathbf{K}(t)(r(t) - v(t-1))$;

3.4.1 Theoretical results

Under the condition that there exists an initial solution for $v(0)$, *i.e.*, $\Pi(x(0)) \neq \emptyset$, the PRG, like the RG, guarantees constraint admissibility for all future time. We summarize this in the following proposition.

Proposition 3.3. *If $\Pi(x(0)) \neq \emptyset$ then there exists a sequence of admissible references*

$v(t)$ computed via Algorithm 1, such that $y(t) \in Y$ for all $t \in \mathbb{Z}_+$.

Proof. Assume that for $t \geq 0$, $y(t+1) \in Y$ and $v(t) \in \Pi(x(t+1))$. Then for some i , $v(t+1) \in \Pi_i(x(t+1)) \subset \Pi(x(t+1))$, which implies that $(x(t+1), v(t+1)) \in O_\infty$.

By assumption, there exists a $v(0) \in \Pi(x(0))$. This implies that $(x(0), v(0)) \in O_\infty$ and $(x(1), v(0)) \in O_\infty$, implying that $y(1) \in Y$ and $v(0) \in \Pi(x(1))$.

The proof follows by induction. By the definition of $\Pi(x(t))$, since there always exists an i such that $v(t) \in \Pi_i(x(t)) \subset \Pi(x(t))$, then $(x(t), v(t)) \in O_\infty$. \square

3.4.2 Numerical example

We apply the PRG to a linear model of an F-16 aircraft. The linear equations of motion are taken from [66],

$$\dot{x}(t) = Ax(t) + Bu(t), \tag{3.18a}$$

$$u(t) = -KCx(t) + Gv(t), \tag{3.18b}$$

$$y(t) = Hx(t), \tag{3.18c}$$

where the state, $x(t) = (\gamma(t), q(t), \alpha(t), \delta_e(t), \delta_f(t))$, consists of the flight path angle, pitch rate, angle of attack, elevator deflection, and flaperon deflection, respectively; the controls in $u(t) = (\delta_{ec}(t), \delta_{fc}(t))$ are commanded elevator and flaperon deflections; the output is $y(t) = (\theta(t), \gamma(t))$, where $\theta(t) = \gamma(t) + \alpha(t)$ is the pitch attitude; the reference input is $v(t) = (\theta_c(t), \gamma_c(t))$, where $\theta_c(t)$ is the commanded pitch attitude

and $\gamma_c(t)$ is the commanded flight path angle. The system matrices are given by,

$$\begin{aligned}
 A &= \begin{bmatrix} 0 & 0.0067 & 1.3410 & 0.1689 & 0.2518 \\ 0 & -0.8693 & 43.2230 & -17.2510 & -1.5766 \\ 0 & 0.9933 & -1.3410 & -0.1689 & -0.2518 \\ 0 & 0 & 0 & -20 & 0 \\ 0 & 0 & 0 & 0 & -20 \end{bmatrix}, \\
 K &= \begin{bmatrix} -0.931 & -0.149 & -3.25 & -0.153 & 0.747 \\ 0.954 & 0.210 & 6.10 & 0.537 & -1.04 \end{bmatrix}, \\
 C &= \begin{bmatrix} 0 & 1 & 0 & 0 & 0 \\ 0 & -0.268 & 47.76 & -4.56 & 4.45 \\ 1 & 0 & 0 & 0 & 0 \\ 0 & 0 & 0 & 1 & 0 \\ 0 & 0 & 0 & 0 & 1 \end{bmatrix}, \\
 B &= \begin{bmatrix} 0 & 0 \\ 0 & 0 \\ 0 & 0 \\ 20 & 0 \\ 0 & 20 \end{bmatrix}, \quad G = \begin{bmatrix} -2.88 & -0.367 \\ 2.02 & 4.08 \end{bmatrix}, \quad H = \begin{bmatrix} 1 & 0 & 1 & 0 & 0 \\ 1 & 0 & 0 & 0 & 0 \end{bmatrix}.
 \end{aligned}$$

The system is subject to constraints on the elevator and flaperon deflections where, in degrees,

$$-25 \leq \delta_e \leq 25, \quad (3.19a)$$

$$-20 \leq \delta_f \leq 20. \quad (3.19b)$$

If the controller signals violate these limits, the closed-loop system can easily become unstable as the open-loop system is unstable and the inputs will saturate. Since the closed-loop system is stable, the RG may be used in order to enforce these constraints.

We discretize the system using a zero-order hold with time-step $T = 0.01$. We perform two simulations starting from a zero initial condition $x(0) = 0$, with the desired reference values set constant at $(\theta_c(t), \gamma_c(t)) \equiv (11^\circ, 13.65^\circ)$. The simulations are performed corresponding to two different prioritizations.

The first simulation is done by ordering the vector $r(t) = (\theta_c(t), \gamma_c(t))$ so that the pitch attitude is given higher priority than flight path angle. The second simulation is done *vice versa*, with $r(t) = (\gamma_c(t), \theta_c(t))$. The results are presented in Figs. 3.6-3.8

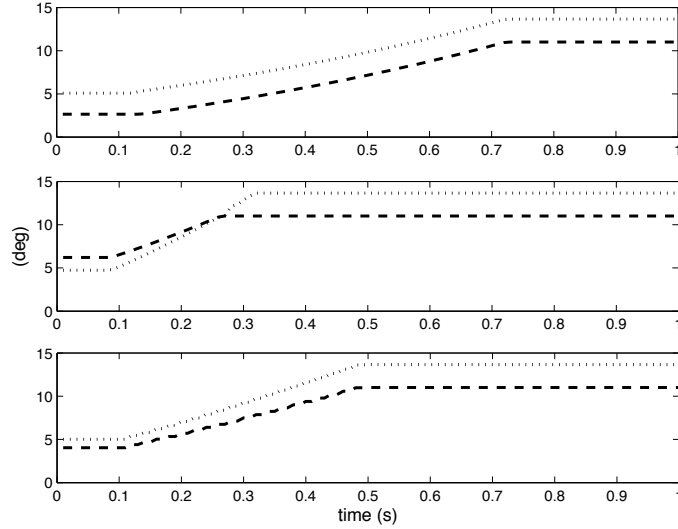


Figure 3.6: Top: First order of priority; Middle: Second order of priority; Bottom: Ordinary RG; the responses are $\theta_c(t)$ (dashed) and $\gamma_c(t)$ (dotted)

along with a plot of the ordinary RG response.

The effect of prioritization is seen in Fig. 3.6. The figure first shows that, when $\gamma_c(t)$ is prioritized, the initial value for $\gamma_c(t)$ is slightly higher than for the second prioritization. The same is true for $\theta_c(t)$ with the second prioritization. Fig. 3.6 also suggests that both references converge faster when $\theta_c(t)$ is prioritized, with only a modest reduction in the initial value of $\gamma_c(t)$. The response of the ordinary RG is between that of the other two subplots, since the ordinary RG gives equal priority to both inputs.

Figs. 3.7-3.8 show the responses of $\delta_e(t)$ and $\delta_f(t)$ with respect to the two prioritizations. It is shown that the RG keeps the elevator and flaperon responses within system constraints; the results also show that only the flaperon constraint becomes active for both orders of priority, with slightly faster convergence rate when $\theta_c(t)$ is prioritized.

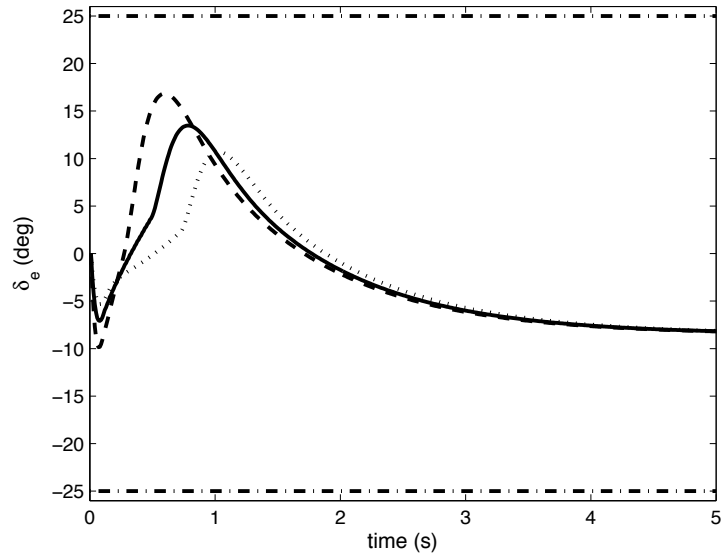


Figure 3.7: Responses of $\delta_e(t)$ corresponding to the first (dashed) and second (dotted) orders of priority plotted against the ordinary RG (solid) and constraints (dot-dashed)

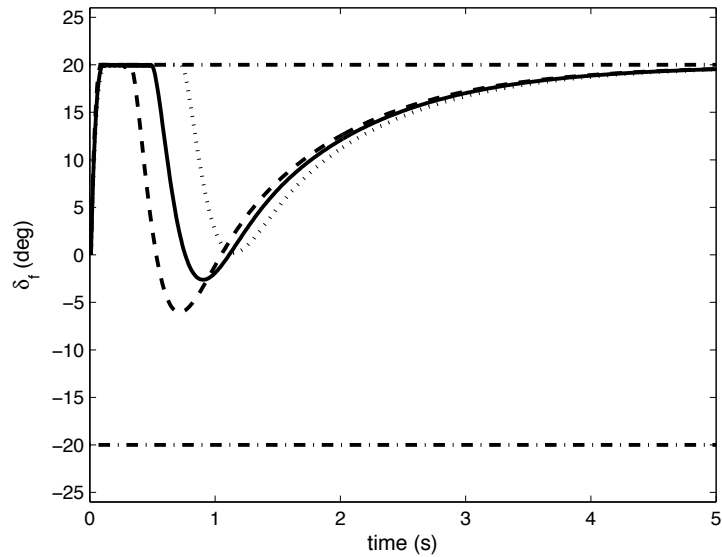


Figure 3.8: Responses of $\delta_f(t)$ corresponding to the first (dashed) and second (dotted) orders of priority plotted against the ordinary RG (solid) and constraints (dot-dashed)

CHAPTER 4

Reference governors for linear systems subject to nonlinear constraints

4.1 Introduction

In this chapter, we consider the case where the system dynamics are *linear* but the output constraints are specified by requiring that a set of *nonlinear* functional inequalities be satisfied.

To motivate the consideration of this problem, we note that control constraints may impede effective implementation of controllers based on feedback linearization, where nonlinear dynamics are rendered linear by a coordinate transformation and an appropriately defined feedback law [67]. After the transformation of the dynamics into linear form, the control input becomes a function of the state, and control constraints may become nonlinear state constraints.

The main developments relate to computing the parameter $\kappa(t) \in [0, 1]$ in (0.11a). We show that, in the case of *convex* constraints, a typical situation is when the constraint-admissible values of $\kappa(t)$ form a proper interval $[0, \kappa_{\max}(t)] \subset [0, 1]$. The value of $\kappa_{\max}(t)$ can then be computed using bisections or other root finding procedures. In the case when the constraints are convex and quadratic, κ_{\max} can be computed by solving simple quadratic equations. A similar approach of characterizing the constraint-admissible values of $\kappa(t)$ and showing that they form a proper interval is then applied in the case of mixed logical-dynamic (MLD) constraints of *if-then* type. Finally, concave nonlinear constraints are considered by approximating them with dynamically reconfigurable linear constraints.

Furthermore, we consider two applications. An application to a spacecraft rendezvous and proximity maneuvering problem is considered first, in which the model for the relative spacecraft motion in this problem is linear, and the constraints on

thrust magnitude, line-of-sight (LOS) cone positioning, and velocity of approach are of quadratic and of *if-then* type. The RG algorithm developed based on the results in this paper is shown to successfully guide the rendezvous maneuver for docking with another spacecraft moving around the Earth in a circular orbit. Then an application to an electromagnetically actuated mass-spring-damper system is considered. The constraint on the maximum force applied by the electromagnet is shown to be concave and is handled using approximations with dynamically reconfigurable linear constraints.

This chapter is organized as follows. Section 4.2 considers various cases of nonlinear constraints. Section 4.3 presents the spacecraft rendezvous example. Section 4.4 presents the mass-spring-damper example.

4.2 Reference governors for nonlinear constraints

We consider an application of RGs to disturbance-free, *i.e.*, $W = 0$, linear systems (0.1) where we relax the specification that Y be polyhedral. Specifically, we consider the case when Y is specified by nonlinear functional inequalities,

$$Y = \{y : h_i(y) \leq 0, i = 1, \dots, r\}, \quad (4.1)$$

where h_i are continuous functions. We note that the existing theoretical results in [15, 7] for treating the constrained problem for system (0.1) with constraints (4.1) apply as long as Y is compact, convex, and $0 \in \text{int} Y$. Hence we focus on the computational treatment of different classes of nonlinear constraints.

When Y is not polyhedral, it can be approximated by a polyhedron; however such approximations may not be easy to obtain or accurate, especially when Y has multiple dimensions, and it can lead to many linear inequalities and significant on-line computational effort. Our approach is to use the linear model (0.1) to predict the output response but treat the nonlinear functions $h_i(y)$ directly and without modification, thereby avoiding the need for approximation by polyhedral constraints.

Results in [2] apply to the case of linear systems with nonlinear constraints and can be used to guarantee finite time convergence of $v(t)$ to $r(t)$ for several classes of $r(t)$. This is a desirable property indicating that after transients caused by large changes in $r(t)$, the RG becomes inactive and nominal closed-loop system performance is recovered. In this chapter, we therefore focus on issues pertinent to the RG implementation for several different classes of nonlinear constraints.

4.2.1 Output prediction

The state and output response of (0.1) at the time instant $t + k$ can be easily predicted, given the state $x(t)$ at time instant t , and assuming a constant $v(t + k) = v(t)$ for $k \geq 0$. We define,

$$\begin{aligned}\Psi_x^k &= CA^k, \\ \Psi_v^k &= (C - \Psi_x^k)\Gamma + D,\end{aligned}$$

where $\Gamma = (I_n - A)^{-1}B$ is defined as in the introduction. Then the predicted output k steps ahead of the current time instant t can be expressed using the state transition formula for linear discrete-time systems as,

$$y(t + k|t) = \Psi_x^k x(t) + \Psi_v^k v(t). \quad (4.2)$$

With (0.2), it follows that,

$$\begin{aligned}y(t + k|t) &= \Psi_x^k x(t) + \Psi_v^k (v(t - 1) + \kappa(t)(r(t) - v(t - 1))), \\ &= \Psi_x^k x(t) + \Psi_v^k v(t - 1) + \kappa(t)\Psi_v^k (r(t) - v(t - 1)).\end{aligned} \quad (4.3)$$

4.2.2 Convex constraints

Suppose that h_i , $i = 1, \dots, r$, in (4.1) are convex functions satisfying,

$$\begin{aligned}h_i(\alpha y_1 + (1 - \alpha)y_2) &\leq \alpha h_i(y_1) + (1 - \alpha)h_i(y_2), \\ \forall i = 1, \dots, r, \forall y_1, y_2 \in \mathbb{R}^p, 0 \leq \alpha \leq 1.\end{aligned} \quad (4.4)$$

Consider now the values of $\kappa(t)$ in (4.3) such that $h_i(y(t + k|t)) \leq 0$. By convexity of h_i and linearity of $y(t + k|t)$ in $\kappa(t)$, it follows that $h_i(y(t + k|t))$ with $y(t + k|t)$ given by (4.3) is a convex function of $\kappa(t) \in [0, 1]$. This in turn shows that the set of allowed values for $\kappa(t)$ is either empty or is a connected interval. In what follows, let the set be denoted by

$$K_i^k = [\kappa_{i,\min}^k, \kappa_{i,\max}^k] \subset [0, 1]. \quad (4.5)$$

By intersecting the intervals K_i^k for all $k = 0, \dots, t^*$, and $i = 1, \dots, r$, we obtain an admissible interval for the values of $\kappa(t)$, which is denoted by $K(t) = [\kappa_{\min}(t), \kappa_{\max}(t)]$. Here t^* is the length of time which guarantees that if the constraints are satisfied for $t \leq t^*$, then the constraints will be satisfied for all future t . See [12, 2] for details.

The RG guarantees that the output response with $v(t+k) = v(t)$ satisfies the imposed constraints, and hence it guarantees the recursive feasibility of $\kappa(t) = 0$, *i.e.*, if $v(-1)$ can be chosen for the given $x(0)$, so that $\kappa(0) = 0$ at the time instant 0, then there exist a feasible choice for $\kappa(t)$, namely $\kappa(t) = 0$ for $t \geq 0$. This leads to the following result.

Proposition 4.1. *If h_i , $i = 1, \dots, r$, are convex and $\kappa(0) = 0$ is feasible at the initial time 0, then an admissible interval for the values of $\kappa(t)$ is of the form $K(t) = [0, \kappa_{max}(t)]$, and the RG sets $\kappa(t) = \kappa_{max}(t)$, where $0 \leq \kappa_{max}(t) \leq 1$.*

Proposition 4.1 leads to an easily implementable Algorithm 2 to determine $\kappa(t)$. The algorithm performs a bisection search whenever the value of $\kappa(t)$ under consideration does not satisfy the constraints. The “tol” variable is a small tolerance that is used to facilitate the bisection search. Typically, only a few bisections need to be performed. Re-ordering the $r \times t^*$ constraints to firstly evaluate the ones active at the previous time instant can practically speed up the computations.

Algorithm 2: RG algorithm for convex constraints

input : $x(t)$, $r(t)$, $v(t-1)$, tol

output: $v(t)$

$\alpha \leftarrow 1$;

for $i \leftarrow 1$ **to** r **do**

for $k \leftarrow 0$ **to** t^* **do**

if $h_i(\Psi_x^k x(t) + \Psi_v^k v(t-1) + \alpha \Psi_v^k (r(t) - v(t-1))) > 0$ **then**

$\alpha^+ \leftarrow \alpha$;

$\alpha^- \leftarrow 0$;

while $\alpha^+ - \alpha^- > \text{tol}$ **do**

$\alpha_m = \frac{\alpha^+ + \alpha^-}{2}$;

if $h_i(\Psi_x^k x(t) + \Psi_v^k v(t-1) + \alpha_m \Psi_v^k (r(t) - v(t-1))) > 0$ **then**

$\alpha^+ = \alpha_m$;

 ;

else $\alpha^- = \alpha_m$;

 ;

$\alpha = \alpha^-$;

$v(t) = v(t-1) + \alpha(r(t) - v(t-1))$;

4.2.3 Quadratic constraints

Further simplifications in calculating K_i^k occur if h_i are convex, quadratic constraints of the form,

$$y^T \tilde{Q}y + \tilde{S}y + \tilde{C} \leq 0, \quad (4.6)$$

where $\tilde{Q} = \tilde{Q}^T \succeq 0$. Note that we focus on the case where $\tilde{Q} \neq 0$, because the case where $\tilde{Q} = 0$ reduces to the ordinary RG.

When constraints are of the form in (4.6), the algorithm for determining K_i^k reduces to a simple and explicit formula which is derived from the solution of the quadratic equation.

Suppressing the use of the independent variable t , along with sub- and super-scripts, k and i , we define,

$$\begin{aligned} \bar{Q}_k &= \begin{bmatrix} \Psi_x^{kT} \tilde{Q} \Psi_x^k & \Psi_x^{kT} \tilde{Q} \Psi_v^k \\ \Psi_v^{kT} \tilde{Q} \Psi_x^k & \Psi_v^{kT} \tilde{Q} \Psi_v^k \end{bmatrix}, \\ \bar{S}_k &= \begin{bmatrix} \tilde{S} \Psi_x^k & \tilde{S} \Psi_v^k \end{bmatrix}. \end{aligned}$$

In determining feasible values of $\kappa = \kappa(t)$, *i.e.*, the interval $K = K(t)$, we set the left hand side of (4.6) to zero,

$$y^T \tilde{Q}y + \tilde{S}y + \tilde{C} = 0, \quad (4.7)$$

which becomes,

$$\begin{bmatrix} x^T & v^T + \kappa(r - v)^T \end{bmatrix} \bar{Q}_k \begin{bmatrix} x \\ v + \kappa(r - v) \end{bmatrix} + \bar{S}_k \begin{bmatrix} x \\ v + \kappa(r - v) \end{bmatrix} + \tilde{C} = 0. \quad (4.8)$$

Expanding and collecting, this results in a quadratic equation in κ . Specifically, define,

$$\begin{aligned} \tilde{q}_k &= \begin{bmatrix} 0 & (r - v)^T \end{bmatrix} \bar{Q}_k \begin{bmatrix} 0 \\ r - v \end{bmatrix}, \\ \tilde{s}_k &= \left(2 \begin{bmatrix} x^T & v^T \end{bmatrix} \bar{Q}_k + \bar{S}_k \right) \begin{bmatrix} 0 \\ r - v \end{bmatrix}, \\ \tilde{c}_k &= \begin{bmatrix} x^T & v^T \end{bmatrix} \bar{Q}_k \begin{bmatrix} x \\ v \end{bmatrix} + \bar{S}_k \begin{bmatrix} x \\ v \end{bmatrix} + \tilde{C}, \end{aligned}$$

we obtain the quadratic equations,

$$\kappa^2 \tilde{q}_k + \kappa \tilde{s}_k + \tilde{c}_k = 0. \quad (4.9)$$

If $\tilde{q}_k \neq 0$, the solution to (4.9) is,

$$K = \left[\frac{-\sqrt{\tilde{s}_k^2 - 4\tilde{q}_k\tilde{c}_k} - \tilde{s}_k}{2\tilde{q}_k}, \frac{\sqrt{\tilde{s}_k^2 - 4\tilde{q}_k\tilde{c}_k} - \tilde{s}_k}{2\tilde{q}_k} \right] \cap [0, 1], \quad (4.10)$$

and otherwise, if $\tilde{s}_k \neq 0$, the solution is,

$$K = \left(-\infty, -\frac{\tilde{c}_k}{\tilde{s}_k} \right] \cap [0, 1] \text{ or } \left[-\frac{\tilde{c}_k}{\tilde{s}_k}, \infty \right) \cap [0, 1]. \quad (4.11)$$

Otherwise, $K = \emptyset$ or $[0, 1]$.

4.2.4 Mixed logical-dynamic constraints

We now consider a set of constraints of *if-then* type,

$$g_i(y) > 0 \rightarrow h_i(y) \leq 0, \quad i = 1, \dots, r, \quad (4.12)$$

where g_i and h_i are convex functions. Consistently with [68], we refer to the constraint (4.12) as an MLD constraint, since this constraint depends on the output variables that change dynamically.

The treatment of (4.12) relies on the observation that the set of $\kappa(t) \in [0, 1]$ for which $g_i(y(t+k|t)) \leq 0$ where $y(t+k|t)$ is given by (4.3) is an interval $\hat{K}_i^k \subseteq [0, 1]$, which may be possibly empty, and the set of $\kappa(t) \in [0, 1]$ for which $h_i(y(t+k|t)) \leq 0$ is another interval $K_i^k \subseteq [0, 1]$, which may also be possibly empty. Then the set of $\kappa(t)$ for which (4.12) is satisfied with $y = y(t+k|t)$ given by (4.3) is also an interval, $\tilde{K}_i^k = [\kappa_{i,\min}^k, \kappa_{i,\max}^k]$,

$$\tilde{K}_i^k = [0, 1] \cap \left(\hat{K}_i^k \cup \left((\hat{K}_i^k)^C \cap K_i^k \right) \right) = [0, 1] \cap \hat{K}_i^k \cap K_i^k, \quad (4.13)$$

where $(\hat{K}_i^k)^C$ is the complement of \hat{K}_i^k . Assuming that the recursive feasibility of $\kappa(t) = 0$ is preserved by the RG, it follows that $\kappa_{i,\min}^k = 0$,

$$\kappa(t) = \min_{k=0,\dots,t^*, i=1,\dots,r} \kappa_{i,\max}^k. \quad (4.14)$$

The confinement of the values of $\kappa(t)$ to a single connected interval considerably simplifies computations and, while it is of interest to handle other classes of MLD constraints, this appears to be a special property of *if-then* constraints and *and*-type constraints. For instance, handling *or*-type constraints, that can be quite useful in non-convex obstacle avoidance problems, appears to be significantly more involved.

Remark 4.2. The ability to treat *if-then* constraints significantly enlarges the class of nonlinear constraints that can be handled. For instance, nonlinear constraints approximated by piecewise affine or piecewise quadratic functions can be treated following this approach.

4.2.5 Concave constraints

Suppose that the constraint set Y is of the form (4.1), where h_i are *concave* functions. In this case, we approximate the constraints $y(t+k|t) \in Y$ by the *affine*, and therefore convex, constraints,

$$y(t+k|t) \in Y_c(t), \quad (4.15)$$

where,

$$Y_c(t) = \{y : h_i(y_{i,*}(t)) + h'_i(y_{i,*}(t))(y - y_{i,*}(t)) \leq 0\}, \quad i = 1, \dots, r. \quad (4.16)$$

Note that $y_{i,*}(t)$ can depend on t or $x(t)$ so that the linear constraints in (4.16) are dynamically reconfigurable online. Since h_i are concave functions, it follows that if $y(t+k|t) \in Y_c(t)$ then $y(t+k|t) \in Y$ so $Y_c(t) \subset Y$. Compared to the previous development, in addition to computing $\kappa(t)$, we now also need to compute $y_{i,*}(t)$. We now note that this approach guarantees the recursive feasibility; however, while the constraints can be satisfied using the RG, the conditions guaranteeing the convergence of $v(t)$ to $r(t)$ to a constant $r(t)$ appear to be considerably more involved.

Proposition 4.3. *If $y_{i,*}(0)$, $i = 1, \dots, r$ exist such that $\kappa(0) = 0$ is feasible, then $\kappa(t) = 0$ and $y_{i,*}(t) = y_{i,*}(t-1)$ are feasible for $t > 0$.*

Numerical examples are now presented that illustrate the above approaches to the handling of constraints.

4.3 Example 1: Satellite rendezvous and proximity maneuvering

We use an example of spacecraft rendezvous and proximity maneuvering to illustrate the RG capability to handle nonlinear convex quadratic constraints and constraints of MLD type. While the constraints are nonlinear, the use of a linear model to represent the spacecraft relative motion dynamics at small relative distance and velocity is standard [69]. References [70, 71, 72] reported applications of MPC to spacecraft rendezvous and docking problems. In [71], various approximations had to be employed to deal with the same constraints as in this paper, while using computationally effective linear quadratic MPC solutions. The need to make these approximations is avoided altogether with the RG, while the nominal unconstrained control strategy need not be replaced by a new controller.

4.3.1 Problem formulation

Let there be two spacecraft, a Chief and a Deputy. The Deputy performs a rendezvous with the Chief, while the Chief orbits around the Earth along a circular orbit. In this problem, we attach the non-inertial Hill frame to the Chief, in which the 1-2-3 axes point respectively in the radial direction away from earth, the along-track direction towards the Chief's motion, and in the cross-track direction towards the Chief's angular momentum. Linearizing and neglecting perturbation effects during the short maneuver time period, the discrete Hill-Clohessy-Wiltshire (HCW) equations,

$$x(t+1) = A_{\text{HCW}}x(t) + B_{\text{HCW}}u(t), \quad (4.17)$$

describe the motion of the Deputy in the Hill frame [73], where,

$$x(t) = \begin{bmatrix} x_1 \\ x_2 \\ x_3 \\ \dot{x}_1 \\ \dot{x}_2 \\ \dot{x}_3 \end{bmatrix},$$

is the state vector of the Deputy's positions and velocities in the 3 axes, and,

$$u(t) = \begin{bmatrix} F_1 \\ F_2 \\ F_3 \end{bmatrix},$$

is the vector of thrust forces with entries corresponding to the axes. The A_{HCW} and B_{HCW} matrices of the discrete version of the HCW equations for the sampling period h are,

$$A_{\text{HCW}} = \begin{bmatrix} 4 - 3 \cos \omega h & 0 & 0 & \frac{1}{\omega} \sin \omega h & \frac{2}{\omega} (1 - \cos \omega h) & 0 \\ 6(\sin \omega h - \omega h) & 1 & 0 & -\frac{2}{\omega} (1 - \cos \omega h) & \frac{4}{\omega} \sin \omega h - 3h & 0 \\ 0 & 0 & \cos \omega h & 0 & 0 & \frac{1}{\omega} \sin \omega h \\ 3\omega \sin \omega h & 0 & 0 & \cos \omega h & 2 \sin \omega h & 0 \\ 6\omega(\cos \omega h - 1) & 0 & 0 & -2 \sin \omega h & 4 \cos \omega h - 3 & 0 \\ 0 & 0 & -\omega \sin \omega h & 0 & 0 & \cos \omega h \end{bmatrix}$$

$$B_{\text{HCW}} = \begin{bmatrix} \frac{1}{m\omega^2} (1 - \cos \omega h) & \frac{2}{m\omega^2} (\omega h - \sin \omega h) & 0 \\ -\frac{2}{m\omega^2} (\omega h - \sin \omega h) & \frac{4}{m\omega^2} (1 - \cos \omega h) - \frac{3h^2}{2m} & 0 \\ 0 & 0 & \frac{1}{m\omega^2} (1 - \cos \omega h) \\ \frac{1}{m\omega} \sin \omega h & \frac{2}{m\omega} (1 - \cos \omega h) & 0 \\ -\frac{2}{m\omega} (1 - \cos \omega h) & \frac{4}{m\omega} \sin \omega h - 3h & 0 \\ 0 & 0 & \frac{1}{m\omega} \sin \omega h \end{bmatrix},$$

where $\omega = \sqrt{\mu/r_O}$, and μ and r_O are the Earth's gravitational constant and the radius of the Chief's orbit, respectively, and m is the mass of the Deputy. The first three states are the positions of the Deputy in the x-y-z-axes of the Hill frame, the last three are the velocities, and the three inputs are the forces in the three directions.

We first design a feedback linear-quadratic regulator (LQR) control gain K_{HCW} , to control the Deputy in the Hill frame. For our solution, we choose our Q and R cost matrices to be $Q = \text{diag}(100, 1, 100, 0, 0, 0)$ and $R = I$, penalizing the 1- and 3-directions more than the 2-direction, in which the Deputy approaches the Chief's dock. We further introduce a feedforward gain G_{HCW} , so that $v(t) \in \mathbb{R}^3$ becomes the reference position of the Deputy, with $u(t) = G_{\text{HCW}}v(t)$. The closed loop dynamics are,

$$x(t+1) = (A_{\text{HCW}} + BK_{\text{HCW}})x(t) + B_{\text{HCW}}G_{\text{HCW}}v(t) = \hat{A}x(t) + \hat{B}v(t). \quad (4.18)$$

Furthermore, we define the C and D matrices such that the output consists of all the states and reference inputs,

$$y(t) = Cx(t) + Dv(t) = \begin{bmatrix} I \\ 0 \end{bmatrix} x(t) + \begin{bmatrix} 0 \\ I \end{bmatrix} v(t). \quad (4.19)$$

We use the theory developed in this chapter to satisfy constraints related to the problem. The first is the LOS constraint or the requirement that the Deputy stay within a half-cone in the along-track direction so that the Chief can visually detect it. This is described as a half-cone with its center 1m behind the docking point, with a 15° half-angle. In convex quadratic form, this is written,

$$\begin{aligned} h_1(y) &= x_1^2 + x_3^2 - \tan^2 15^\circ (x_2 + 1)^2, \\ &= x_1^2 - (7 - 4\sqrt{3})x_2^2 + x_3^2 - 2(7 - 4\sqrt{3})x_2 - (7 - 4\sqrt{3}) \leq 0. \end{aligned} \quad (4.20)$$

The second constraint is that the Deputy always stay in front of the docking point in the along-track direction,

$$h_2(y) = -x_2 \leq 0. \quad (4.21)$$

The third constraint is that of thrust limitation; the maximum force allowed is 4N,

$$h_3(y) = u^T u - 4^2, \quad (4.22)$$

$$= (K_{\text{HCW}}x + G_{\text{HCW}}v)^T (K_{\text{HCW}}x + G_{\text{HCW}}v) - 4^2, \quad (4.23)$$

$$= \begin{bmatrix} x^T & v^T \end{bmatrix} \begin{bmatrix} K_{\text{HCW}}^T K_{\text{HCW}} & K_{\text{HCW}}^T G_{\text{HCW}} \\ G_{\text{HCW}}^T K_{\text{HCW}} & G_{\text{HCW}}^T G_{\text{HCW}} \end{bmatrix} \begin{bmatrix} x \\ v \end{bmatrix} - 4^2 \leq 0. \quad (4.24)$$

We assume that the spacecraft is reoriented instantaneously to provide the thrust vector. The thrust magnitude is realized through the modulation of thruster on/off times [74].

The final constraint is MLD of *if-then* type. If the spacecraft approaches to within 1m of the dock in the along-track direction, then its speed must be less than 0.1m/s.

$$g_4(y) = -x_2 + 1 > 0 \rightarrow h_4(y) = \dot{x}_1^2 + \dot{x}_2^2 + \dot{x}_3^2 - 0.1^2 \leq 0. \quad (4.25)$$

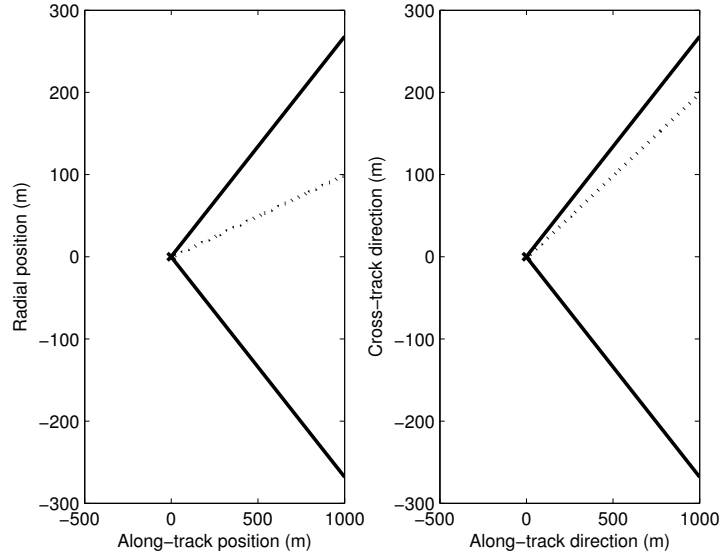


Figure 4.1: Trajectories (dotted) of the Deputy in the 1-2 and 2-3 planes of the Hill frame, respectively, with constraint boundaries (solid) and docking point (\times)

4.3.2 Simulation results

Using a sampling period of $h = 0.1s$, the constraint-admissible initial conditions for the Deputy are chosen to be, in meters and seconds,

$$x(0) = \begin{bmatrix} 100 \\ 1000 \\ 200 \\ 0 \\ 0 \\ 0 \end{bmatrix}, \quad (4.26)$$

implying that,

$$u(0) = \begin{bmatrix} 100 \\ 1000 \\ 200 \end{bmatrix}. \quad (4.27)$$

We set a constant reference $r(t) \equiv 0$.

The resulting trajectory is shown in Fig. 4.1, showing the Deputy staying within the LOS-cone as it approaches the Chief. Fig. 4.2 shows the trajectory close up, with the additional constraint that the Deputy stay in the positive half-plane in the

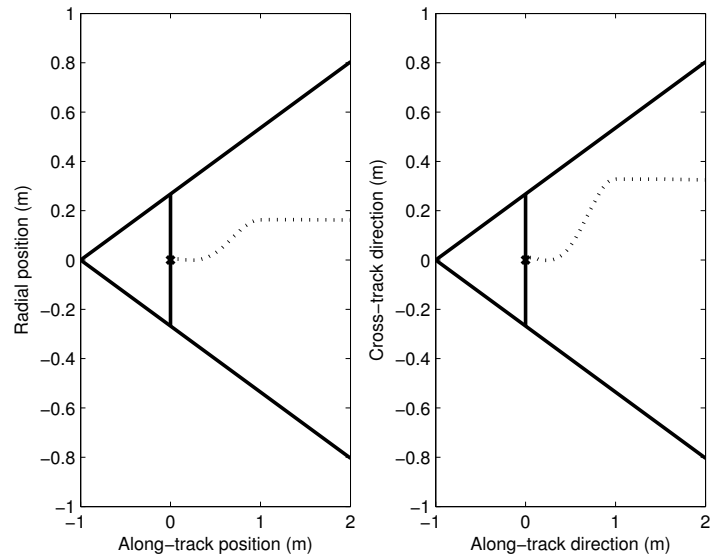


Figure 4.2: Close-up views of the trajectories (dotted) of the Deputy in the 1-2 and 2-3 planes of the Hill frame, respectively, with constraint boundaries (solid) and docking point (\times)

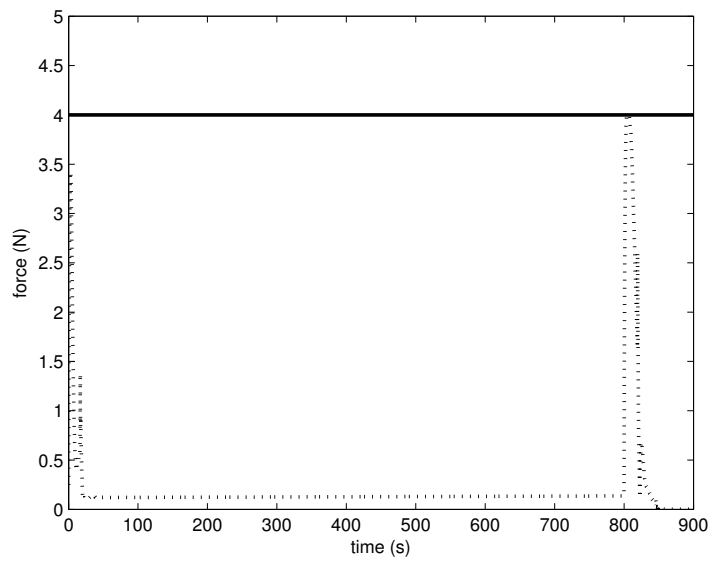


Figure 4.3: Thrust force (dotted) plotted against the thrust constraint (solid)

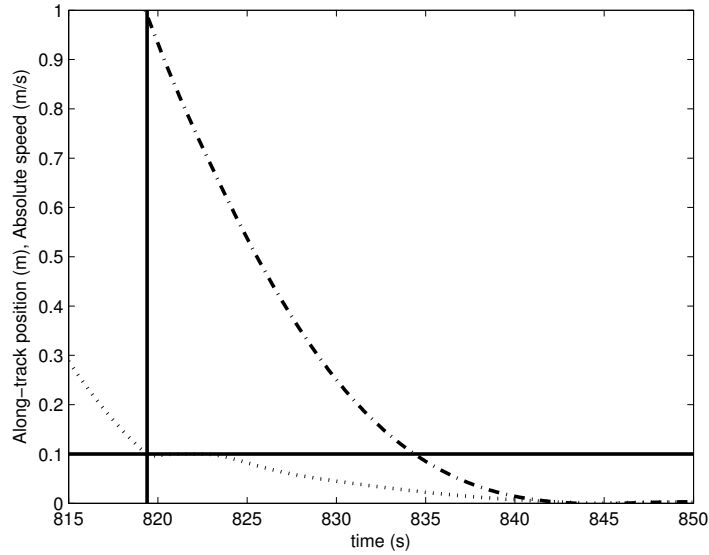


Figure 4.4: Along-track position (dot-dashed) and the relative velocity (dotted) in the Hill frame plotted with soft-docking constraint boundaries (solid)

along-track direction. As it comes close to the Chief, the Deputy moves to the side in order to stay within the LOS-cone and to perpendicularly dock with the Chief.

The other two constraints are also satisfied, as shown in Figs. 4.3 and 4.4. In Fig. 4.3, the thrust force magnitude never exceeds 4N and in Fig. 4.4, when the along-track position is less than 1m (after the 189.4s mark), the Deputy is guaranteed to have a relative velocity of at most 0.1m/s.

4.4 Example 2: Electromagnetically actuated mass-spring-damper system

In this section, we apply the RG to the same electromagnetically actuated mass-spring damper system as considered in Section 3.4. This example was also considered in [75] and a nonlinear RG was applied to this example in [2]. Here we demonstrate an alternative treatment of this example using the linear system model and a nonlinear constraint model.

4.4.1 Problem formulation

In continuous-time, the nonlinear system dynamics are given by,

$$\begin{bmatrix} \dot{x}_1 \\ \dot{x}_2 \end{bmatrix} = \begin{bmatrix} 0 & 1 \\ -k/m & -c/m \end{bmatrix} \begin{bmatrix} x_1 \\ x_2 \end{bmatrix} + \begin{bmatrix} 0 \\ 1/m \end{bmatrix} u, \quad (4.28)$$

$$u = \frac{\alpha i^\mu}{(d_0 - x_1)^\gamma}, \quad (4.29)$$

where x_1 , x_2 , and i are the position and velocity of the mass and the applied current, respectively. The rest are parameters with values as in [2]. As in Section 3.4, we choose feedback and feedforward gains, $K = [0 - c_d]$ and $G = k$, where $c_d = 4.0$, so that the system is in the form (4.18) and $u = kv - c_d x_2$. We delay the choice of the C and D matrices until formulating the constraints.

The first constraint is that the position of the mass not be too close to the actuator,

$$h_1(y) = x_1 - 0.008 \leq 0. \quad (4.30)$$

The other two constraints are related to actuator limitations,

$$0 \leq u \leq \frac{\alpha i_{\max}^\mu}{(d_0 - x_1)^\gamma}, \quad (4.31)$$

where i_{\max} is the maximum current available in the electromagnet. The left-hand side of the constraint is a simple linear constraint,

$$h_2(y) = -u = c_d x_2 - kv \leq 0. \quad (4.32)$$

The right-hand side of (4.31) is nonlinear in x_1 . To handle this nonlinear constraint, we linearize the constraint about (\bar{x}_1, \bar{u}) at which the constraint is active so that,

$$0 \geq (u - \bar{u}) - \frac{\alpha \gamma i_{\max}^\mu}{(d_0 - \bar{x}_1)^{\gamma+1}} (x_1 - \bar{x}_1) = u - \frac{\alpha i_{\max}^\mu}{(d_0 - \bar{x}_1)^\gamma} - \frac{\alpha \gamma i_{\max}^\mu}{(d_0 - \bar{x}_1)^{\gamma+1}} (x_1 - \bar{x}_1). \quad (4.33)$$

This approach is visualized in Fig. 4.5 and satisfies the requirement for Proposition 4.3 to apply. To deal with this constraint, we define two new variables,

$$\xi_0 = \frac{\alpha i_{\max}^\mu}{(d_0 - \bar{x}_1)^\gamma}, \quad \xi_1 = \frac{\alpha \gamma i_{\max}^\mu}{(d_0 - \bar{x}_1)^{\gamma+1}}. \quad (4.34)$$

If these variables, along with \bar{x}_1 , are treated as constant state variables, then this

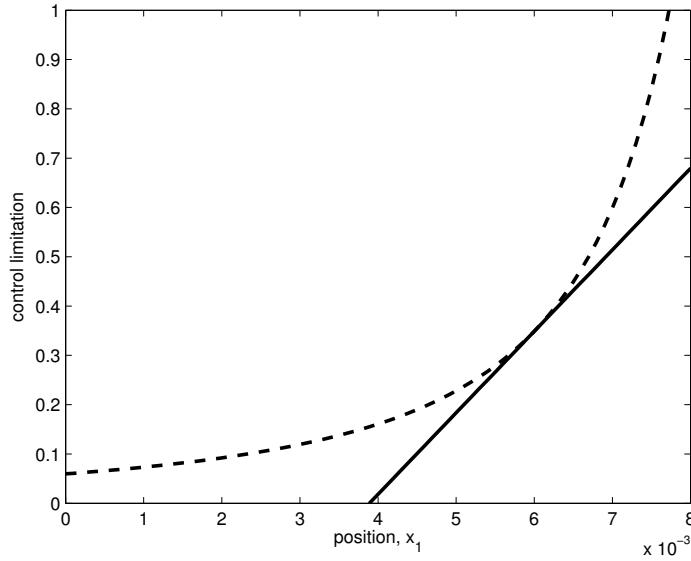


Figure 4.5: The upper limit on the control $u(t)$, with the nonlinear limit (dashed) and the linearized limit (solid) about the equilibrium $\bar{x}_1 = 0.006\text{m}$

creates a constraint that is linear with respect to the non-constant states,

$$h_3(y) = -x_1\xi_1 + \bar{x}_1\xi_1 - c_d x_2 - \xi_0 + kv. \quad (4.35)$$

4.4.2 Simulation results

Following the example in [2], we choose initial conditions, $x_1(0) = 0$ and $x_2(0) = 0.012$ and a time-step of 0.01s. We then run two simulations, with $i_{\max} = 0.5342$ and with $i_{\max} = 0.365$. The former limit corresponds to that in [2], but the latter is close to the minimum limit that is needed to achieve any equilibrium position within the commanded range in steady-state [29]. The simulations for the two situations, along with the unconstrained case, are presented in Figs. 4.6-4.8.

In Figs. 4.6 and 4.7, we see that the RG takes two different approaches depending on the current limitation. For the larger limit, it acts similarly to the unconstrained case, the reason for which can be seen in Fig. 4.8, where $u_{\max}(t)$, the maximum allowed value of the control at time t , is plotted alongside $u(t)$. In this case, the actuator limits in the latter simulation are imposed for a longer period of time since there is not much difference between the available current and the maximum equilibrium current. Furthermore, Fig. 4.8 shows a separation between the control limit and the governed input; this is due to sequential linearizations and suggests that decreasing

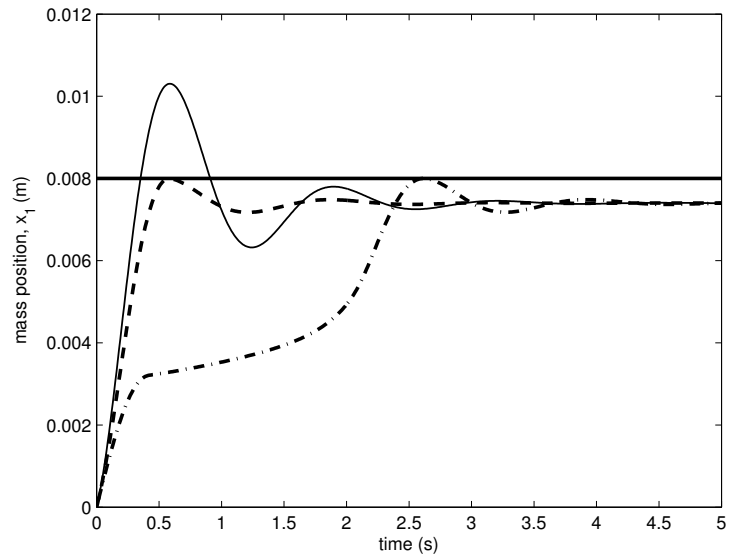


Figure 4.6: Mass position responses for the three cases: unconstrained (solid), $i_{\max} = 0.5342$ (dashed), and $i_{\max} = 0.365$ (dot-dashed), with constraint shown by a horizontal line

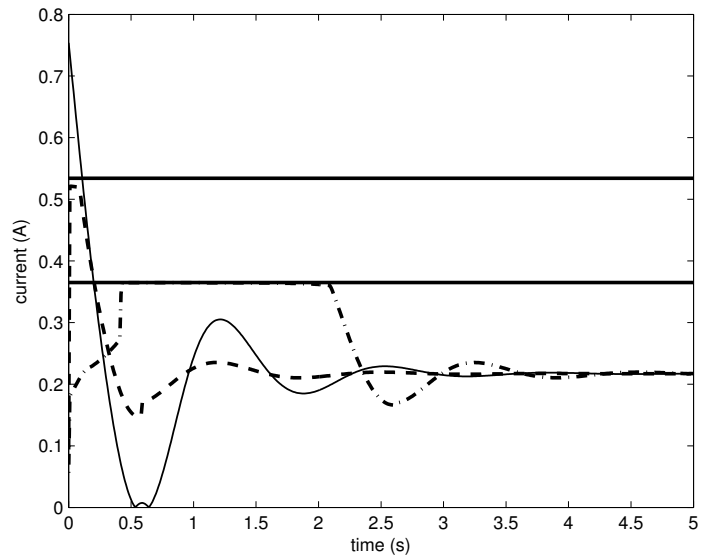


Figure 4.7: Current responses for the three cases: unconstrained (solid), $i_{\max} = 0.5342$ (dashed), and $i_{\max} = 0.365$ (dot-dashed), with constraints shown by horizontal lines

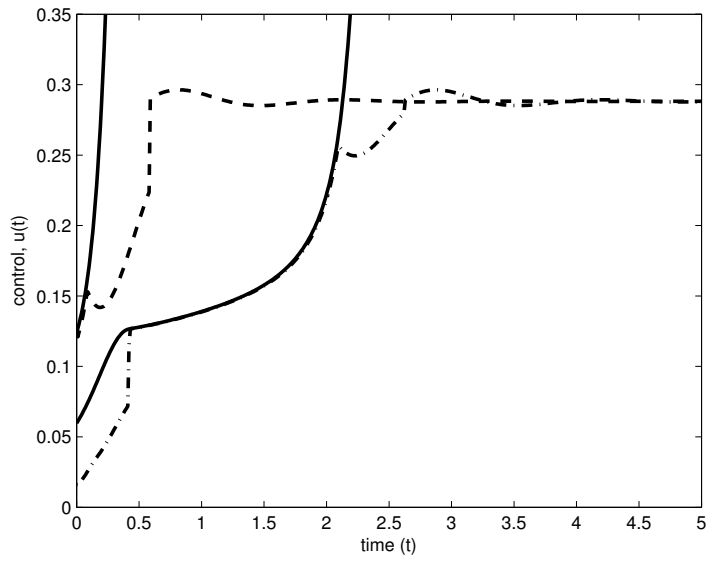


Figure 4.8: Control responses for two cases: $i_{\max} = 0.5342$ (dashed) and $i_{\max} = 0.365$ (dot-dashed), plotted against respective constraints u_{\max} (solid)

the time-step and therefore more frequent approximations would result in a better response.

CHAPTER 5

Reference and command governors for systems with slowly time-varying references and time-dependent constraints

5.1 Introduction

In this chapter, we replace the use of O_∞ with sets that, in addition to being invariant, are also contractive in cross-sections by $v(t)$. Specifically, this new set, which we denote by O_∞^λ , has cross-sections $O_\infty^\lambda(v)$ such that if $x(t) \in O_\infty^\lambda(v(t))$, then $x(t+1) \in \lambda O_\infty^\lambda(v(t))$ for some $0 < \lambda < 1$.

The use of λ -contractive sets in RG and CG design enables us to handle slowly time-varying references and constraints. In particular, we show that because the parameter λ is strictly less than 1, we can determine a neighborhood of admissible references v_0 around $v(t)$, guaranteeing that the pair $(x(t+1), v_0)$ will be contained in O_∞^λ . We exploit this property of O_∞^λ to show that if the rate of change in $r(t)$ is bounded by a set that depends on λ , then $v(t)$ converges to $r(t)$ in finite time. We also consider the case of constraints that vary in time and show that if they vary slowly enough, we are able to guarantee constraint adherence.

These results are important because of their potential use in applications. In particular, the finite-time convergence results of RGs and CGs are extended to the case of ramp or other slowly-varying command tracking. The time-varying constraints emerge in many practical situations, including when one desires to avoid moving obstacles. We consider two examples. In the first example, we consider an F-16 aircraft with a time-varying pitch and flight path angle commands and in the second example, we consider a mass-spring-damper system with a time-varying overshoot constraint.

This chapter is organized as follows. Section 5.2 introduces robustly λ -contractive sets. Section 5.3 reports results for the case of time-varying references and Section 5.4 reports results for the case of time-varying constraints. Sections 5.5 and 5.6 are the examples.

5.2 Robustly λ -contractive sets

Consider the linear discrete-time system (0.1) without control input, *i.e.*, $v(t) \equiv 0$,

$$\bar{x}(t+1) = A\bar{x}(t) + B_w w(t), \quad (5.1a)$$

$$\bar{y}(t) = C\bar{x}(t) + D_w w(t) \in Y. \quad (5.1b)$$

As before, we assume $w(t) \in W$, where W is compact with $0 \in W$, A is Schur and (C, A) is observable. The maximal output admissible set \bar{O}_∞ for (5.1) is defined by,

$$\bar{O}_\infty = \{\bar{x} : \bar{x}(0) = \bar{x}, (5.1) \text{ is satisfied for all } \{w(t)\} \in W, t \in \mathbb{Z}_+\}. \quad (5.2)$$

It follows that \bar{O}_∞ is a disturbance invariant set, *i.e.*,

$$A\bar{O}_\infty \oplus B_w W \subset \bar{O}_\infty. \quad (5.3)$$

We now turn our attention to λ -contractive sets, which satisfy the following definition.

Definition 5.1. For a linear system (5.1), a set $H \subset \mathbb{R}^n$ is λ -contractive [76] if it satisfies the Minkowski assumptions, *i.e.*, H is compact, convex, and contains 0 in its interior, along with,

$$AH \oplus B_w W \subset \lambda H, \quad (5.4)$$

for some scalar $0 < \lambda < 1$.

A method of computing the maximal λ -contractive set for (5.1) is to consider the state update equation,

$$\bar{x}(t+1) = \frac{1}{\lambda} A\bar{x}(t) + \frac{1}{\lambda} B_w w(t), \quad (5.5a)$$

with output (5.1b) and compute its maximal output admissible set \bar{O}_∞ , which we

denote by \bar{O}_∞^λ . It is necessary that,

$$|\rho(A)| < \lambda < 1, \quad (5.6)$$

be satisfied because otherwise \bar{O}_∞^λ will either have empty interior¹ or will not necessarily be contractive². Note that, depending on the size of W , λ may need be substantially larger than $|\rho(A)|$, and if $W = \{0\}$, then (5.6) becomes a sufficient condition. It remains to show that \bar{O}_∞^λ is indeed λ -contractive and this is done in the following.

Proposition 5.2. \bar{O}_∞^λ is λ -contractive for (5.1).

Proof. By the definition and invariance properties of \bar{O}_∞^λ , it follows that $\frac{1}{\lambda}(A\bar{O}_\infty^\lambda \oplus B_w W) \subset \bar{O}_\infty^\lambda$. Multiplying both sides by λ , we obtain $A\bar{O}_\infty^\lambda \oplus B_w W \subset \lambda\bar{O}_\infty^\lambda$. \square

The set \bar{O}_∞^λ is maximal because any λ -contractive set for (5.1) is an invariant set for (5.5a). \bar{O}_∞^λ satisfies the following sequence of subset inclusions,

$$A\bar{O}_\infty^\lambda \oplus B_w W \subset \lambda\bar{O}_\infty^\lambda \subset \bar{O}_\infty^\lambda \subset \bar{O}_\infty. \quad (5.7)$$

An illustration of the sets above is shown in Fig. 5.1 for a two-dimensional system with eigenvalues 0.8 and 0.6 where,

$$A = \begin{bmatrix} 0 & 1 \\ -0.8 \cdot 0.6 & 0.8 + 0.6 \end{bmatrix}, \quad \lambda = 0.81, \quad B_w = I_2, \quad W = [-10^{-3}, 10^{-3}]^2.$$

5.3 Slowly-varying references

In the RG and CG, the reference is kept constant over the prediction horizon, so we can treat it as a dynamic variable with a simple eigenvalue at 1 as in [15, 7]. A method of constructing O_∞ is to introduce the dynamics $v(t+1) = v(t)$ for the admissible reference so that the state update equation (5.1a) becomes,

$$x(t+1) = Ax(t) + Bv(t) + B_w w(t), \quad (5.8aa)$$

$$v(t+1) = v(t). \quad (5.8ab)$$

¹If $\lambda \leq |\rho(A)|$, (5.5a) is unstable.

²If $\lambda \geq 1$, \bar{O}_∞^λ is not necessarily contractive.

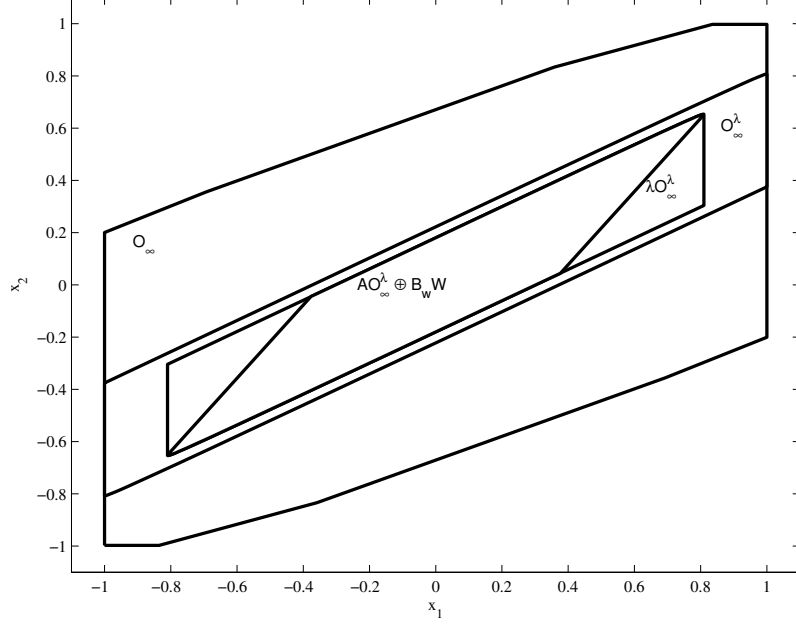


Figure 5.1: An illustration of the set inclusions in (5.7) generated using [77]

We then compute the maximal output admissible set for these dynamics, using the sets Ω and Ω_d from (0.6) to ensure finite determination.

Now consider the system above with the state update equation for $x(t)$ replaced with,

$$x(t+1) = \frac{1}{\lambda}(Ax(t) + Bv(t) + B_w w(t)), \quad (5.9aa)$$

with $|\rho(A)| < \lambda < 1$. Denote the maximal output admissible set for the system (5.9aa), (5.8ab), (0.1b) as O_∞^λ . This new set has two properties that will be useful and are stated in the following.

Proposition 5.3. *Let $O_\infty^\lambda(v) = \{x : (x, v) \in O_\infty^\lambda\}$ be the cross section of O_∞^λ at v . Then (i) $O_\infty^\lambda(v)$ is λ -contractive for the dynamics (5.9aa), (5.8ab) and (ii) O_∞^λ is λ -contractive if the reference dynamics in (5.8ab) are replaced with,*

$$v(t+1) = \lambda v(t). \quad (5.9ab)$$

Proof. By the definition of O_∞^λ , $(x(t), v) \in O_\infty^\lambda \implies (\frac{1}{\lambda}(Ax(t) + Bv + B_w w(t)), v) \in O_\infty^\lambda \implies \frac{1}{\lambda}(Ax(t) + Bv + B_w w(t)) \in O_\infty^\lambda(v) \implies x(t+1) = Ax(t) + Bv + B_w w(t) \in \lambda O_\infty^\lambda(v)$, proving part (i). Part (ii) is a direct consequence of $\frac{1}{\lambda}\lambda = 1$ and Proposition 5.2. \square

Because $O_\infty^\lambda(v_0)$ is λ -contractive for all v_0 for which $O_\infty^\lambda(v_0)$ is neither empty nor

a singleton, it follows that there exists a neighborhood around v_0 such that for all v in this neighborhood, $(Ax(t) + Bv + B_w w(t), v) \in O_\infty^\lambda$. Define,

$$E = C\Gamma + D. \quad (5.10)$$

$E : \mathbb{R}^m \rightarrow \mathbb{R}^p$ is the matrix map from the constant v to the steady-state solution $y(t)$ for (0.1b). For v_0 such that $O_\infty^\lambda(v_0) \neq \emptyset$, the size of the neighborhood or admissible references around v_0 can be determined with the help of the following result.

Proposition 5.4. *Let $\Omega^\lambda = \{v : (\Gamma v, v) \in O_\infty^\lambda\}$ be the set of all feasible admissible references in steady-state and let $v_0 \in \Omega^\lambda$. Then $\lambda O_\infty^\lambda(v_0) \subset O_\infty^\lambda(v)$ for all $v \in (1 - \lambda)(\Omega^\lambda \sim \{v_0\}) \oplus \{v_0\}$.*

Proof. For $r \in \Omega^\lambda$, apply the affine transformations $x_r(t) := x(t) - \Gamma r$ and $v_r(t) := v(t) - r$. Then the dynamics in (5.8a), (0.1b) become,

$$\begin{bmatrix} x_r(t+1) \\ v_r(t+1) \end{bmatrix} = \begin{bmatrix} A & B \\ 0 & I_m \end{bmatrix} \begin{bmatrix} x_r(t) \\ v_r(t) \end{bmatrix} + \begin{bmatrix} B_w \\ 0 \end{bmatrix} w(t), \quad (5.11a)$$

$$y(t) = \begin{bmatrix} C & D \end{bmatrix} \begin{bmatrix} x_r(t) \\ v_r(t) \end{bmatrix} + D_w w(t) \in Y \sim \{Er\}. \quad (5.11b)$$

The maximal λ -contractive output admissible set for this system is $O_\infty^\lambda \sim \{(\Gamma r, r)\}$. Applying Proposition 5.3(ii), we obtain that $O_\infty^\lambda \sim \{(\Gamma r, r)\}$ and therefore $\Omega^\lambda \sim \{r\}$ are λ -contractive for the dynamics (5.11a) with I_m replaced by λI_m . This implies that $\lambda O_\infty^\lambda(v_0) \subset O_\infty^\lambda(\lambda(v_0 - r) + r) = O_\infty^\lambda((1 - \lambda)(r - v_0) + v_0)$ for all $r \in \Omega^\lambda$. To complete the proof, let $v = (1 - \lambda)(r - v_0) + v_0$. \square

From the proposition, given a $v_0 \in \Omega^\lambda$, the references in $(1 - \lambda)(\Omega^\lambda \sim \{v_0\})$ are admissible provided $O_\infty^\lambda(v_0)$ is not a singleton.

Corollary 5.5. *Let $r \in \Omega^\lambda$, where Ω^λ is defined as in Proposition 5.4. Let \mathcal{P} be a set satisfying the Minkowski assumptions and inclusion $\mathcal{P} \subset (1 - \lambda)(\Omega^\lambda \sim \{v_0\})$ for all $v_0 \in \Omega^\lambda$. Assume the desired reference varies within the neighborhood \mathcal{P} of r , i.e., $\{r(t)\} \in \{r\} \oplus \mathcal{P}$. Further assume that $v(t)$ is computed according to (0.11) where O_∞ is replaced by O_∞^λ in the definition of the set $\Pi(x)$ in (0.12). Then there exists a finite time $t_f \in \mathbb{Z}_+$ such that $v(t) = r(t)$ for all $t \geq t_f$.*

Proof. The proof is similar to the proof of Theorem 4.2 in [7] and is based on the compactness of Ω^λ along with the fact that $(1 - \lambda)(\Omega^\lambda \sim \{r\})$ has non-empty interior for all $r \in \Omega^\lambda$. \square

The following result is a sufficient condition on how quickly the desired reference $r(t)$ can vary so that $v(t)$ will converge to $r(t)$ in finite time for the case of the CG.

Proposition 5.6. *Let Ω^λ be defined as in Proposition 5.4. Assume the desired reference $\{r(t)\} \in \Omega^\lambda$ varies such that $r(t+1) - r(t) \in (1-\lambda)(\Omega^\lambda \sim \{r(t)\})$ for all $t \in \mathbb{Z}_+$. Then for any $v(0) \in \Omega^\lambda$, if $v(t)$ is determined according to (0.18) where O_∞ is replaced by O_∞^λ in the definition of the set $\Pi(x)$ in (0.12), there exists a time $t^* \in \mathbb{Z}_+$ such that $v(t) = r(t)$ for all $t \geq t^*$.*

Proof. Represent $r(t), v(t), r(t+1), v(t+1)$ by r, v, r^+, v^+ , respectively. Note that the constraint $r^+ - r \in (1-\lambda)(\Omega^\lambda \sim \{r\})$ can be rewritten as $r^+ - \lambda r \in (1-\lambda)\Omega^\lambda$. Also, the result in Proposition 5.4 implies that $v^+ = v'$ is feasible if $v' - \lambda v \in (1-\lambda)\Omega^\lambda \subset (1-\lambda)\Omega^\lambda$. Therefore $v^+ = r^+ - \lambda r + \lambda v$ is feasible and by optimality, $\|r^+ - v^+\| \leq \|r^+ - (r^+ - \lambda r + \lambda v)\| = \|\lambda(r - v)\| = \lambda\|r - v\|$ where $\lambda < 1$. Therefore $\|r(t) - v(t)\| \rightarrow 0$ as $t \rightarrow \infty$. By compactness of Ω^λ and similar arguments as in [7], the convergence occurs in finite time. \square

5.4 Slowly-varying constraints

We now consider the case of time-varying constraints, *i.e.*, the case where the set Y in (0.1b) depends on t ,

$$Y = Y_t.$$

We also assume that the constrained output has no feed-forward term, *i.e.*, $D = 0$. As a consequence of Proposition 5.6, if the desired reference varies slowly enough, then we are able to ensure constraint satisfaction with the use of maximal λ -contractive admissible sets. Alternatively, in some applications the constraints vary while the desired reference stays constant. In this case, because Proposition 5.4 guarantees that admissible references exist within a neighborhood of the presently admissible reference, if the constraints vary slowly enough and our present reference is constraint admissible, we are able to enforce constraint adherence for all future time. The result relies on the following.

Proposition 5.7. *Let $Y_t \subset \mathbb{R}^p$ be a set and let $O_{\infty,t}^\lambda$ be the maximal λ -contractive constraint admissible set corresponding to Y_t . Let Ω_t^λ be the time-varying set Ω^λ corresponding to Y_t defined as in Proposition 5.4, *i.e.*, $\Omega_t^\lambda = \{v : (\Gamma v, v) \in O_{\infty,t}^\lambda\}$. Assume that $Y_{t+1} \supset \lambda(Y_t \sim \{Ev_0\}) \oplus \{Ev_0\}$ for some $v_0 \in \Omega_t^\lambda$.*

If $(x(t), v(t-1)) \in O_{\infty,t}^\lambda$, then $(Ax(t) + Bv_1 + B_w w(t), v_1) \in O_{\infty,t+1}^\lambda$ for all $\{w(t)\} \in W$ where $v_1 = \lambda(v(t-1) - v_0) + v_0$.

Proof. $O_{\infty,t}^\lambda \sim \{(\Gamma v_0, v_0)\}$ is the maximal λ -contractive constraint admissible set corresponding to $Y_t \sim \{Ev_0\}$. Due to λ -contractivity, since $x(t) \in O_{\infty,t}^\lambda$, then $(Ax(t) + Bv_1 + B_w w(t), v_1) \in \lambda(O_{\infty,t}^\lambda \sim \{(\Gamma v_0, v_0)\}) \oplus \{(\Gamma v_0, v_0)\}$. Therefore, $Y_{t+1} \supset \lambda(Y_t \sim \{Ev_0\}) \oplus \{Ev_0\}$ implies that $\lambda(O_{\infty,t}^\lambda \sim \{(\Gamma v_0, v_0)\}) \oplus \{(\Gamma v_0, v_0)\} \subset O_{\infty,t+1}^\lambda$. \square

Remark 5.8. When using the RG to enforce time-varying constraints, the RG update equation (0.2) for $v(t)$ must be modified to,

$$v(t) = v_1 + \kappa(t)(r(t) - v_1), \quad (5.12)$$

where $v_1 = \lambda(v(t-1) - v_0) + v_0$, and $v_0 \in \Omega_t^\lambda$ at time t but is otherwise arbitrary. The RG solves an optimization problem similar to (0.11),

$$\max \kappa(t) \in [0, 1], \quad (5.13a)$$

$$\text{sub. to } (x(t), v_1 + \kappa(t)(r(t) - v_1)) \in O_{\infty,t}^\lambda. \quad (5.13b)$$

This way, $v(t)$ is varied along the line segment connecting v_1 and $r(t)$ instead of $v(t-1)$ and $r(t)$. The modification is done so that constraints that decay at a rate slower than or equal to λ are enforceable while ensuring that the solution v_1 corresponding to $\kappa(t) = 0$ is feasible. It is not necessary to modify the CG algorithm (0.18) because it considers all inputs as solution candidates.

Remark 5.9. According to the proposition above, the constraint at the next time instant, *i.e.*, $y(t+1) \in Y_{t+1}$, is enforced at time t . The constraint $(Ax(t) + Bv(t) + B_w w(t), v(t)) \in O_{\infty,t+1}^\lambda$ does not take into account the present-time constraint $y(t) = Cx(t) + Dv(t) \in Y_t$. For this reason, we require $D = 0$.

5.5 Example 1: Slowly-varying reference

Here we apply the results presented above to a linear simulation of an F-16 aircraft. This example is considered as an application of the prioritized RG in Section 3.4 where the linear model is taken from [66]. Applying Design No. 2 in [66], $x(t) = (\gamma(t), q(t), \alpha(t), \delta_e(t), \delta_f(t))$ is the state vector of flight path angle, pitch rate, angle of attack, elevator deflection, and flaperon deflection, $v(t) = (\theta_c(t), \gamma_c(t))$ is the input vector of commanded pitch attitude and commanded flight path angle, and $y(t) = (\delta_e(t), \delta_f(t), \dot{\delta}_e(t), \dot{\delta}_f(t))$ is the output vector. The pitch attitude $\theta(t)$ is related to the flight path angle and angle of attack by $\theta(t) = \gamma(t) + \alpha(t)$. The system is discretized

using a zero-order hold with time-step $T = 0.02$ sec. The constraint set is,

$$Y = [-25, 25] \times [-20, 20] \times [-42, 42] \times [-56, 56]. \quad (5.14)$$

The magnitudes of the discrete-time eigenvalues range between 0.678 and 0.980. Because there are no disturbances affecting the system, we choose $\lambda = 0.99$, which is greater than 0.980, and compute O_∞^λ .

In this example, we apply a CG (0.18) with $Q = I_2$ for the calculation of $v(t)$. The simulation time is 12 sec and the reference input is given by,

$$r(t+T) = \begin{cases} r(t), & t < 6 \text{ sec}, \\ \lambda r(t) + (1-\lambda)p_s, & 6 \text{ sec} \leq t \leq 12 \text{ sec}, \end{cases}$$

where $r(0) = p_s = (9, 6.5)$ is the initial value of the reference that stays constant for 6 sec. By choosing the decay rate of $r(t)$ after 6 sec to be λ , we satisfy the assumption of Proposition 5.6. The results are presented in Figs. 5.2-5.4.

Fig. 5.2 shows the only constraints to become active and we can see that the reference $v(t)$ plotted in Figs. 5.3-5.4 converges to $r(t)$ after 6 sec. Before 6 sec, even though the output $y(t)$ is in the interior of the constraint set, as we can see in Fig. 5.2, $v(t)$ converges to a value that does not equal $r(t)$. This is because O_∞^λ is smaller than O_∞ and steady-state values that satisfy constraints may not be in the λ -contractive set. To show that this is indeed the case, we run another simulation with the same parameters with the exception that we now use O_∞ as the CG constraint set. The results are plotted in Fig. 5.5, where in the second subplot we see circled that there is a small difference between the desired and commanded $\theta(t)$. This confirms that the rate of decay λ is too fast for the command governor to guarantee $v(t) = r(t)$.

5.6 Example 2: Slowly-varying constraint

In this section, we consider a mass-spring-damper system with a slowly-varying constraint representing a moving obstacle. The goal is to bring the mass to a desired reference $r(t) \equiv 1$ without violating the moving constraint.

The parameters of the system are the spring constant $k = 10\text{N/m}$, the damping coefficient $c = 1\text{N}\cdot\text{s/m}$, and the mass $m = 0.5\text{kg}$. The continuous-time system

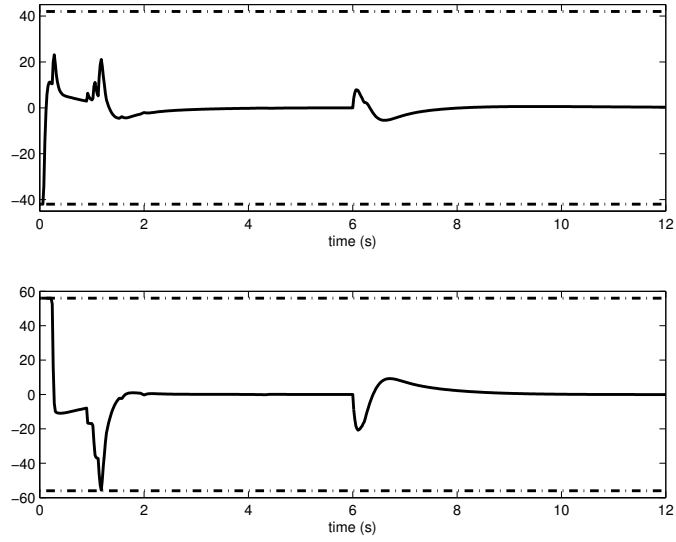


Figure 5.2: $\dot{\delta}_e(t)$ (top) and $\dot{\delta}_f(t)$ (bottom) responses with constraints (dot-dashed) and CG based on O_∞^λ

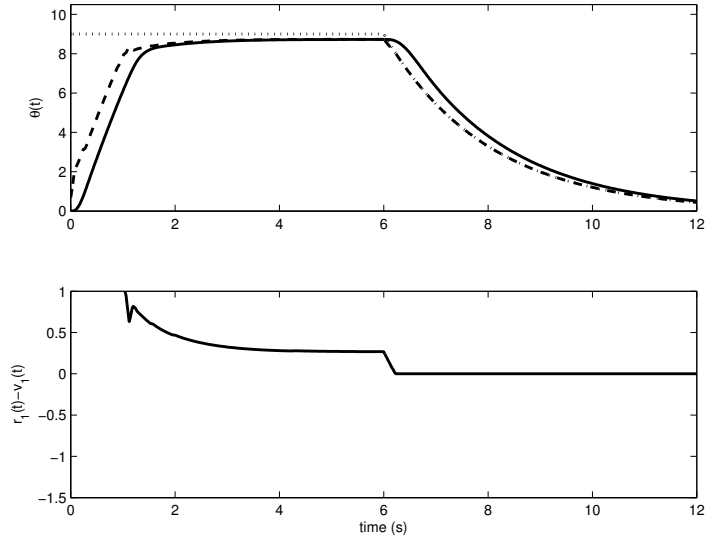


Figure 5.3: Top: Desired (dotted), commanded (dashed), and actual (solid) $\theta(t)$ responses with CG based on O_∞^λ ; Bottom: Difference between desired and commanded

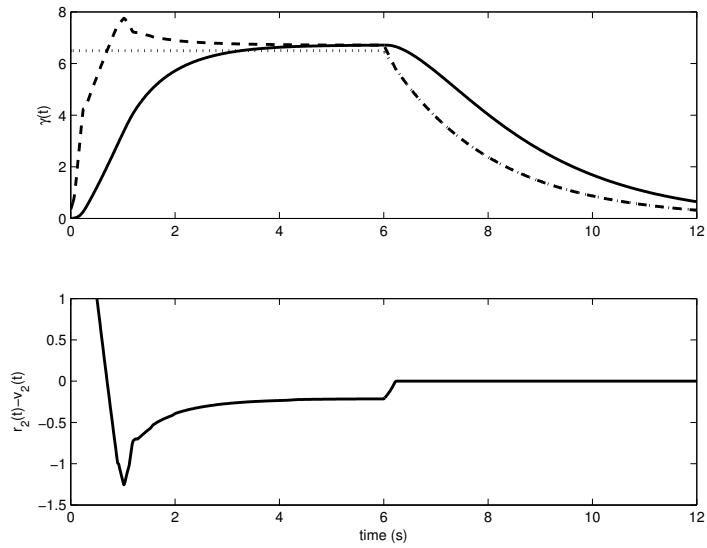


Figure 5.4: Top: Desired (dotted), commanded (dashed), and actual (solid) $\gamma(t)$ responses with CG based on O_∞^λ ; Bottom: Difference between desired and commanded

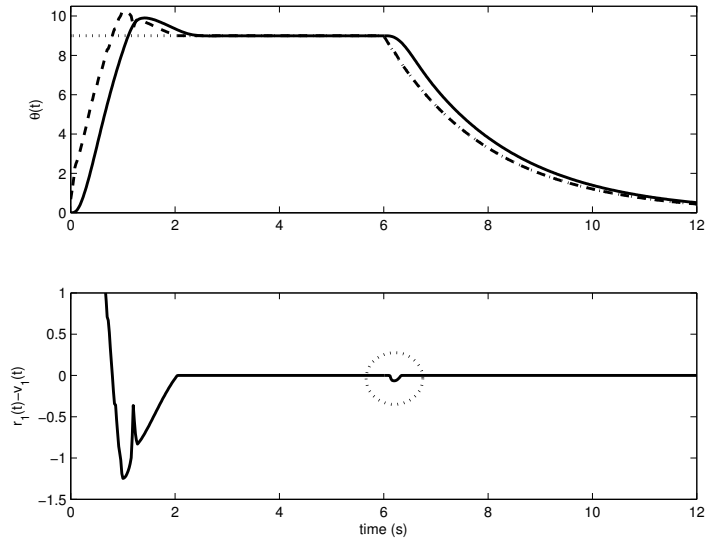


Figure 5.5: Top: Desired (dotted), commanded (dashed), and actual (solid) $\theta(t)$ responses with CG based on O_∞ ; Bottom: Difference between desired and commanded

dynamics are,

$$\dot{x}(t) = \begin{bmatrix} 0 & 1 \\ -\frac{k}{m} & -\frac{c}{m} \end{bmatrix} x(t) + \begin{bmatrix} 0 \\ \frac{1}{m} \end{bmatrix} u(t), \quad (5.15a)$$

$$y(t) = \begin{bmatrix} 1 \\ 0 \end{bmatrix} x(t) \in Y_t, \quad (5.15b)$$

where $Y_t = [-1, a(t)]$ and $a(t) = 1 + A_0 \sin(\omega_0 \pi t)$. The parameter $A_0 = 0.05$ and ω_0 will vary in the subsequent analysis. We now discretize the system with time-step $T = 0.01$ s so that $|\rho(A)| = 0.99$ and we let $u(t) = kv(t)$ so that the output steady-state map is $E = 1$. Because the constraint $y(t) \geq -1$ will never be active, we redefine the constraint set to be $\bar{Y}_t = [-a(t), a(t)]$ so that we may use the theory from Section 5.4. Finally, we choose $\lambda = 0.999$ and compute $v(t)$ using the update equation (5.12) with $v_0 = 0$.

Because of our choice of $v_0 = 0$, according to Propostion 5.7, we require $\bar{Y}_{t+1} \supset \lambda \bar{Y}_t$ for all time. The constraint set evolves according to $\bar{Y}_{t+1} = \frac{a(t+T)}{a(t)} \bar{Y}_t$ for all $t \in \mathbb{Z}_+$ and the minimum of $\frac{a(t+T)}{a(t)}$ occurs when $t = \frac{1}{\omega_0} - \frac{1}{2}T$. Define,

$$\lambda^* = \frac{1 - \frac{1}{2}A_0\omega_0\pi T}{1 + \frac{1}{2}A_0\omega_0\pi T} < \frac{1 + A_0 \sin(\omega_0\pi(\frac{1}{\omega_0} + \frac{1}{2}T))}{1 + A_0 \sin(\omega_0\pi(\frac{1}{\omega_0} - \frac{1}{2}T))} = \frac{a(1/\omega_0 + T/2)}{a(1/\omega_0 - T/2)}.$$

The above implies that if $\omega_0 \leq \frac{2}{\pi T} \frac{1-\lambda}{1+\lambda}$, then $\lambda \leq \lambda^*$ and $\bar{Y}_{t+1} \supset \lambda^* \bar{Y}_t \supset \lambda \bar{Y}_t$ for all $t \in \mathbb{Z}_+$.

The analysis is performed for fixed $A_0 = 0.05$ and three different choices of ω_0 , which are tabulated in Table 5.1 along with corresponding values of λ^* . The results are presented in Figs. 5.6-5.8.

ω (rad/s)	λ^*
0.350	0.9995
0.637	λ
0.800	0.9987

Table 5.1: Table of parameters for the function $a(t)$

The results show that the constraints are enforceable in the first two cases but are violated in the third. However, because the CG is more flexible, it is possible that we can use it to achieve constraint enforcement for the case where $\lambda^* < \lambda$. We perform a second simulation, using the CG instead of the RG, to modify the reference. The results are presented in Fig. 5.9 and show that it is possible to achieve constraint

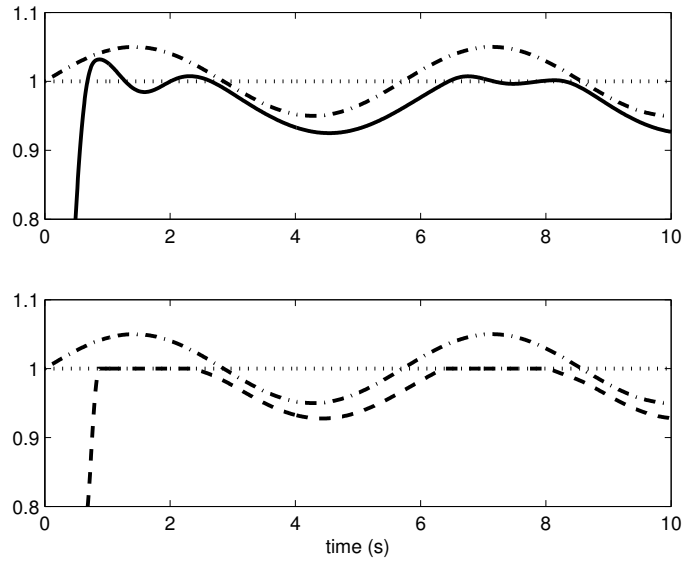


Figure 5.6: $r(t)$ (dotted), $v(t)$ (dashed), and $y(t)$ (solid) responses corresponding to moving constraint $a(t)$ with $\omega = 0.350\text{rad/s}$

adherence with the use of the CG, but the CG must be much more aggressive in order to enforce constraints.

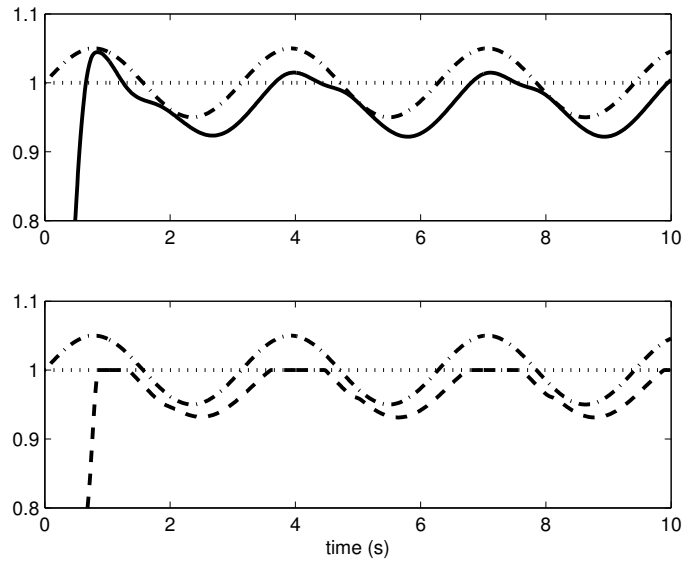


Figure 5.7: $r(t)$ (dotted), $v(t)$ (dashed), and $y(t)$ (solid) responses corresponding to moving constraint $a(t)$ with $\omega = 0.637\text{rad/s}$

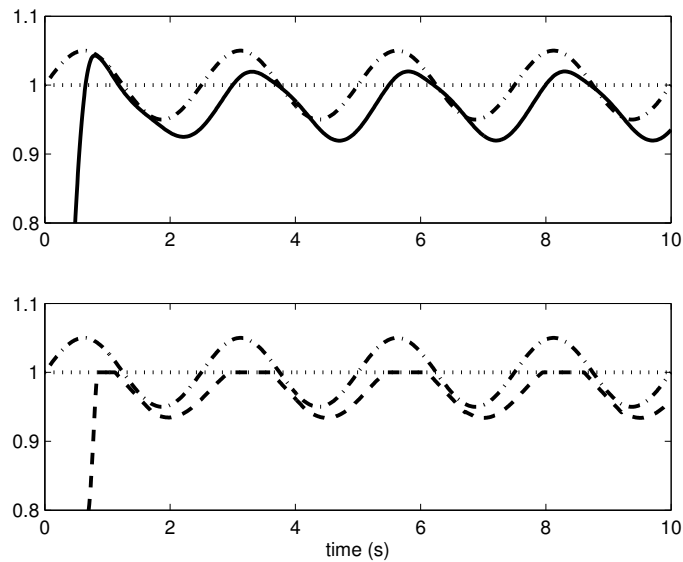


Figure 5.8: $r(t)$ (dotted), $v(t)$ (dashed), and $y(t)$ (solid) responses corresponding to moving constraint $a(t)$ with $\omega = 0.800\text{rad/s}$

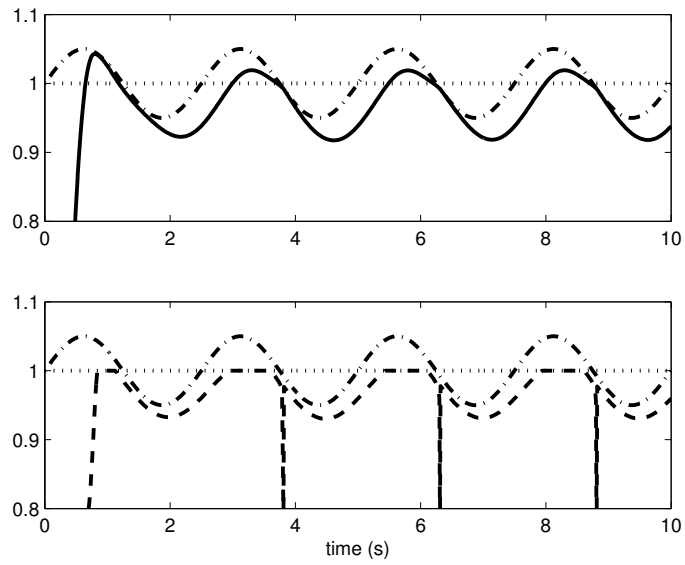


Figure 5.9: $r(t)$ (dotted), $v(t)$ (dashed), and $y(t)$ (solid) responses corresponding to moving constraint $a(t)$ with $\omega_0 = 0.800\text{rad/s}$ and use of the CG

Part II

Practical applications of reference governors

CHAPTER 6

Reference governors for the enforcement of compressor surge constraints

6.1 Introduction

In this chapter, we consider an approach for enforcing compressor surge constraints in turbocharged gasoline engines using the RG. Compressor surge is an unstable flow process that is characterized by oscillations in the compressor flow and pressure ratio [78] which lead to noise and driveability concerns. Surge typically occurs during rapid reductions in throttle angle that happen, for example, when the driver tips out of the accelerator pedal. We utilize the RG to minimally limit the air demand or the throttle actuator command to avoid compressor surge during such tip-outs. This approach does not rely on the compressor bypass valve (CBV), which is an extra component conventionally used to prevent tip-out surge. The successful application of the RG to the surge constraint suggests that the CBV can be eliminated in some engine designs, thereby providing a cost save.

The RG provides a computationally simple and minimally intrusive mechanism to enforce constraints. Its use to enforce surge constraints in turbocharged engines is considered in Section 1.5, where the RG was applied to modify the throttle command. In this chapter, we refer to the placement of the RG ahead of the throttle as the inner-loop RG because of its placement inside the control loop. This placement was

considered initially as it can be easily integrated into the existing control strategy and software. This placement of the RG gives rise to a number of interesting theoretical issues in terms of ensuring that interactions of RG with upstream subsystems are well-behaved; these are further addressed in our recent work [79] but are not included as a part of this thesis. Apart from this, we develop a new outer-loop RG, which governs the desired air flow command, and compare the two RG designs in vehicle experiments. We demonstrate that unlike the inner-loop design, the outer-loop design can be based on a single linear model for prediction and does not require scheduling based on engine speed.

The chapter is organized as follows. Section 6.2 formulates the surge constraint enforcement problem. Section 6.3 describes the engine model. Sections 6.4 and 6.5 present the development and analysis of the inner- and outer-loop RGs along with vehicle results. Section 6.6 presents a discussion comparing the two RG approaches.

6.2 Surge constraint

Compressor surge is an unstable flow process that is characterized by oscillations in the compressor flow and pressure ratio [78, 80, 81, 82]. In the worst of cases, these oscillations can lead to compressor damage but more often lead to noise and vibration and driveability concerns. The area of stable compressor operation is typically provided by the manufacturer in terms of a compressor map, like one shown in Fig. 6.1.

The compressor map is a chart of the region of allowable compressor operation plotted on the plane of corrected compressor flow and pressure ratio. Corrected compressor flow $W_{c,corr}(t)$ is the flow through the compressor at ambient temperature and pressure conditions and is given by the formula,

$$W_{c,corr}(t) = W_c(t) \frac{\sqrt{T_{c,in}(t)/T_{ref}}}{p_{c,in}(t)/p_{ref}}, \quad (6.1)$$

where $W_c(t)$ is the flow through the compressor, $T_{c,in}(t)$ is the temperature at the compressor inlet, $p_{c,in}(t)$ is the pressure, at the compressor inlet and T_{ref} and p_{ref} are the temperature and pressure at which the compressor map was constructed by the manufacturer.

In Fig. 6.1, the left-hand boundary of the compressor map is called the surge line and the onset of surge may occur when the compressor operates past the boundary. We thus wish to operate to the right of the surge line and whenever possible avoid

the surge region to the left.

A surge frequently occurs very quickly during a tip-out, *i.e.*, a closing of the throttle [80]. When the throttle closes rapidly, flow through the compressor decreases faster than compressor exit pressure, which decreases relatively slowly. This can force compressor operation to the left of the surge line for an extended period of time. An illustration of this is provided in Fig. 6.1, which shows a typical tip-in/tip-out trajectory using vehicle data plotted on the compressor map.

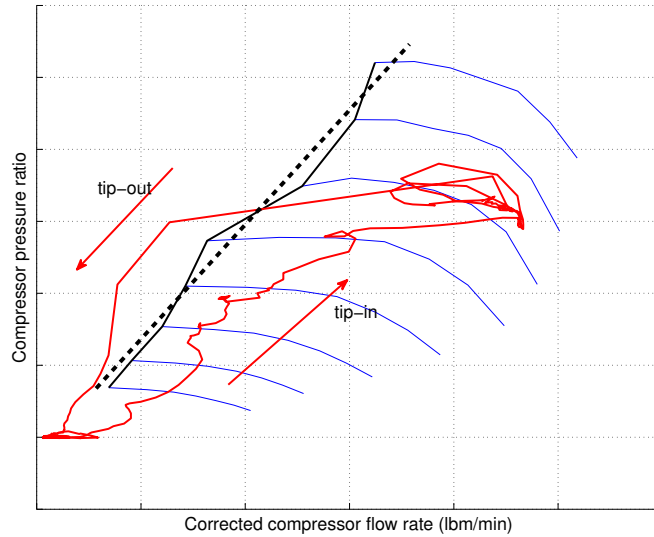


Figure 6.1: Typical tip-in/tip-out trajectory (red) with manufacturer’s surge constraint (solid) and approximate linearized constraint (dashed); the bottom arrow shows the direction of the tip-in and the top arrow shows the direction of the tip-out

In this chapter, we apply the RG to enforce the surge constraint. Applications of the RG to the enforcement of surge constraints in fuel cell compressors have been considered in [33, 34] but no experimental results were presented.

Typical RG computational procedures require that the constraint set be a polytope. The true surge line in Fig. 6.1 is jagged but can be closely approximated by a single line segment so we choose a single line to be our constraint boundary on the compressor map, *i.e.*, the dashed line in Fig. 6.1. With the assumption that the correction factor in (6.1) is approximately equal to 1, we choose the linear constraint

to be similar to that in [45],

$$\frac{p_b(t)}{p_{ref}} - 30.62W_c(t) \leq 1.15, \quad (6.2)$$

where $p_b(t)$ is the boost pressure in kPa, and W_c is the compressor flow in kg/s.

The approach is generalized to an arbitrary choice of linearization point. Linearizing about an equilibrium output y_{op} , the S and s matrices in (0.7) become,

$$S = \begin{bmatrix} 0.01 & -30.62 \end{bmatrix}, \quad s = 1.15 - Sy_{op}, \quad (6.3)$$

where $y(t) = (p_b(t), W_c(t))$ is the system output and y_{op} is the output at equilibrium.

6.3 Engine model

A schematic of the engine system is shown in Fig. 6.2. The locations of sensors used by the PCM and additional instrumentation installed for testing are shown in the figure. Measurements available for use by the PCM are:

- boost pressure, $p_b(t)$,
- intake manifold pressure, $p_i(t)$,
- mass air flow to both compressors, $W_{2c}(t)$,
- and engine speed, $N_e(t)$.

Additional instrumentation on the test vehicle measures the compressor inlet temperature, $T_{c,in}$.

A Simulink model of the engine, which is developed based on physical principles [81, 82, 83], has been calibrated to reflect the engine used in our test vehicle. The state variables of the model are the intake manifold pressure $p_i(t)$, the boost pressure or the pressure at the throttle inlet $p_b(t)$, the exhaust manifold pressure $p_e(t)$, the turbocharger shaft speed $N_{tc}(t)$, and the wastegate canister pressure $p_{can}(t)$. The actuation variables are throttle angle command $\theta(t)$, the wastegate duty cycle command $u_{wg}(t)$, and the CBV command $u_{cbv}(t)$. Engine speed $N_e(t)$ is considered as a disturbance input and the input to the control strategy is the desired cylinder flow $W_{cyl,d}(t)$ which is computed from the desired engine torque assuming stoichiometric air-to-fuel ratio. The output of the model is,

$$y(t) = (p_b(t), W_c(t)), \quad (6.4)$$

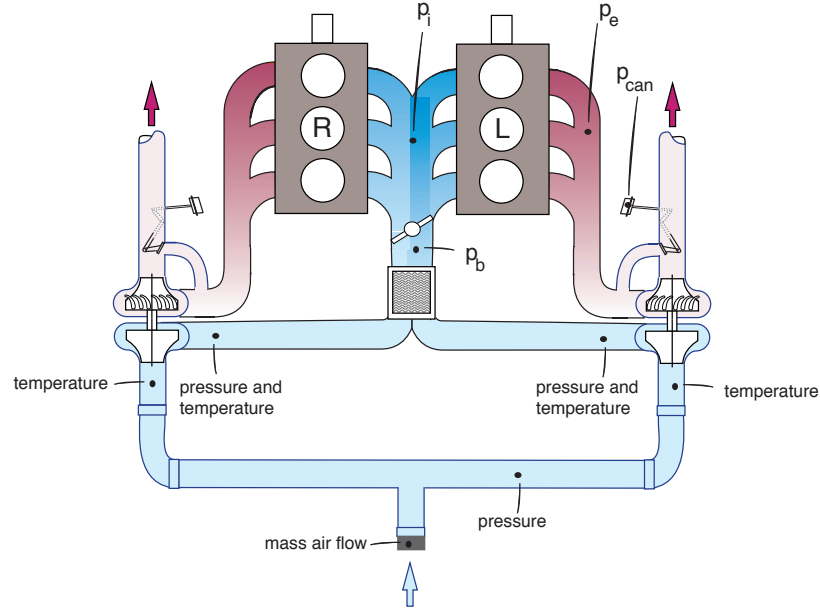


Figure 6.2: Engine schematic

where we set $W_c(t) = W_{2c}(t)/2$, *i.e.*, half of the flow through both compressors.

The model is validated by comparing simulation results with data collected from the test vehicle. An example showing four successive tip-in/tip-out maneuvers is given in Figs. 6.3-6.4. The actuator commands from the vehicle, shown in Fig. 6.3, are inputs to the Simulink model, which produces the results of Fig. 6.4. The model captures the system response to the aggressive inputs reasonably well.

6.4 Inner-loop reference governor

We begin by considering an inner-loop RG design in which the RG is placed downstream of the vehicle control strategy in order to govern the throttle input $\theta(t)$. From a software implementation perspective, this design is minimally invasive and easy to integrate with the rest of the control strategy. The model we consider is of the form,

$$\dot{x}(t) = f_{in}(x(t), \theta(t), p(t)), \quad (6.5a)$$

$$y(t) = h_{in}(x(t), \theta(t), p(t)), \quad (6.5b)$$

where $x(t)$ is the vector of model states and $p(t)$ is the vector of ungoverned variables.

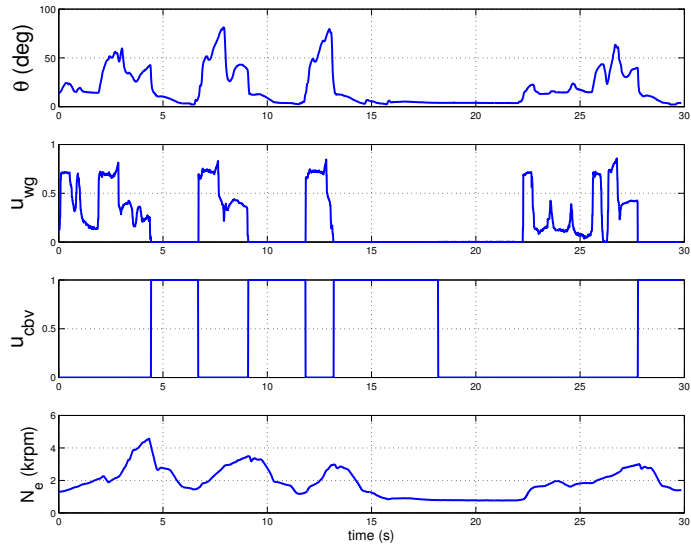


Figure 6.3: Input commands

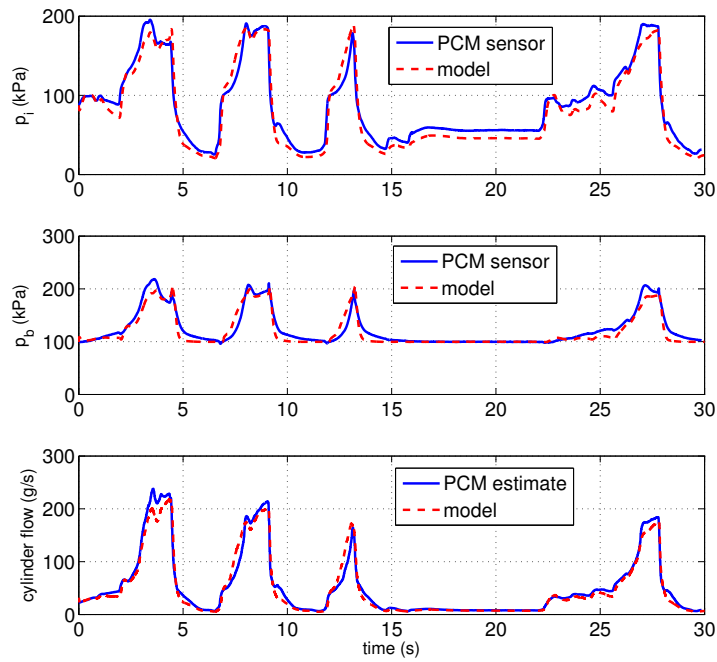


Figure 6.4: Comparison of vehicle (solid) and model (dashed) responses

6.4.1 Linear control development

We derive a linearization of the system (6.5) in order to apply the RG.

$$\delta x(t) = x(t) - x_{op},$$

$$\delta \theta(t) = \theta(t) - \theta_{op},$$

$$\delta p(t) = p(t) - p_{op},$$

$$\delta y(t) = y(t) - y_{op},$$

where the subscript op refers to a value of the variable at an operating point. Note that the values x_{op} and y_{op} are steady-state values that depend on the inputs θ_{op} and p_{op} .

The linear model is computed through numerical linearization of the nonlinear model (6.5); the Jacobian matrices are computed by numerical differentiation, resulting in a linear system of the form,

$$\delta \dot{x}(t) = \left[\frac{\partial f_{in}}{\partial x} \right]_{op} \delta x(t) + \left[\frac{\partial f_{in}}{\partial \theta} \right]_{op} \delta \theta(t), \quad (6.6a)$$

$$\delta y(t) = \left[\frac{\partial h_{in}}{\partial x} \right]_{op} \delta x(t) + \left[\frac{\partial h_{in}}{\partial \theta} \right]_{op} \delta \theta(t). \quad (6.6b)$$

The inner-loop RG is designed based on the dynamics of (6.6). Note that in the linear model (6.6) used by the RG for prediction of constraint violation, the vector of ungoverned inputs is assumed to stay constant at the nominal operating point value, *i.e.* $\delta p(t) \equiv 0$.

After choosing inputs θ_{op} and p_{op} , we compute the steady-state variables x_{op} and the corresponding continuous-time linear system matrices and upon discretization we have a linear dynamic model of the form (0.1). The discretization time-step is equal to the rate at which the ECU executes software commands to update the control inputs.

6.4.2 Nonlinear control development and analysis

6.4.2.1 Surge Margin Offset

We apply the linear RG with full state-measurement to the nonlinear model (6.5). Applying step changes in the desired throttle angle, as shown in Fig. 6.5, the governed throttle command gets stuck after the first tip-out because the linear RG predicts constraint infeasibility for all future time and sets $\kappa(t) \equiv 0$. To address this problem,

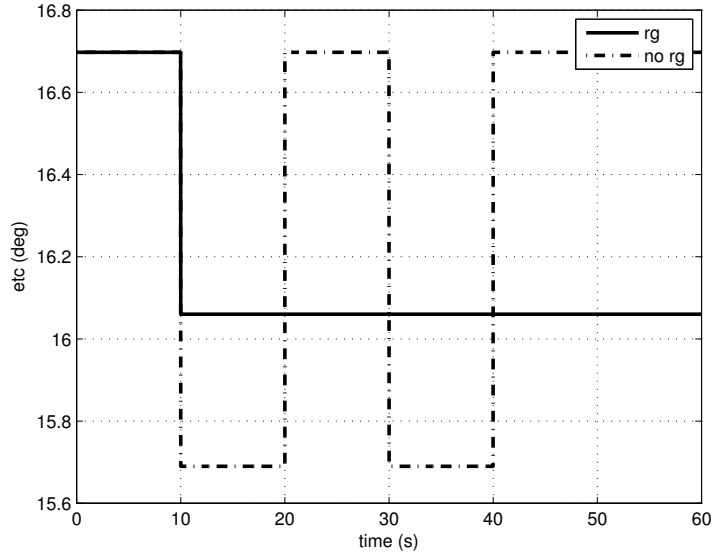


Figure 6.5: Reference and governed throttle commands based on nonlinear model simulation

we apply an offset that is equal to the difference in the predicted and measured surge margins, *i.e.* the difference in the distances from the surge line that are predicted by the linear model and measured through the nonlinear model.

The basic approach to compensate for the differences between linear prediction model and nonlinear plant is based on [34]. In it, we replace O_∞ in the development of the RG by,

$$O_\infty^{off}(t) = \{(x_0, r') : H_x x_0 + H_r r' \leq h + s_{off}(t) \mathbf{1}_{n_c}\}, \quad (6.7)$$

where $s_{off}(t) = \max(S(y(t) - (\delta y(t) + y_{op})), 0)$. The constraint $O_\infty^{off}(t)$ is time-varying and corresponds to replacing Y by the time varying constraint set,

$$Y_{off}(t) = \{y' : y' - (y(t) - (\delta y(t) + y_{op})) \in Y\}. \quad (6.8)$$

Note that if the linear model over-predicts the surge margin, the constraints are tightened, however the constraints are not relaxed in case of under-prediction.

The governed throttle command using this approach and the response trajectories are shown Figs. 6.6-6.7. The arrows in Fig. 6.7 represent the direction of the trajectory in time. The governed throttle command behaves as it did in the linear analysis and the surge constraint is not violated.

We further evaluate our design in a more realistic scenario by obtaining a set

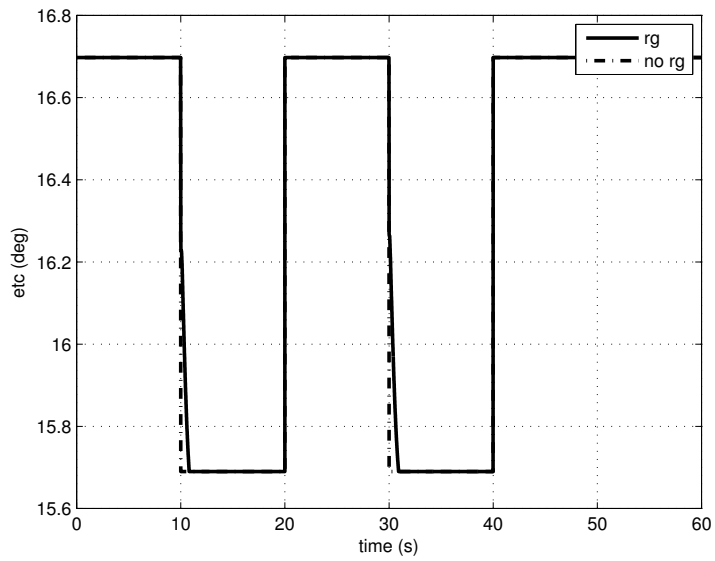


Figure 6.6: Reference and governed throttle commands with surge margin offset based on nonlinear model simulation

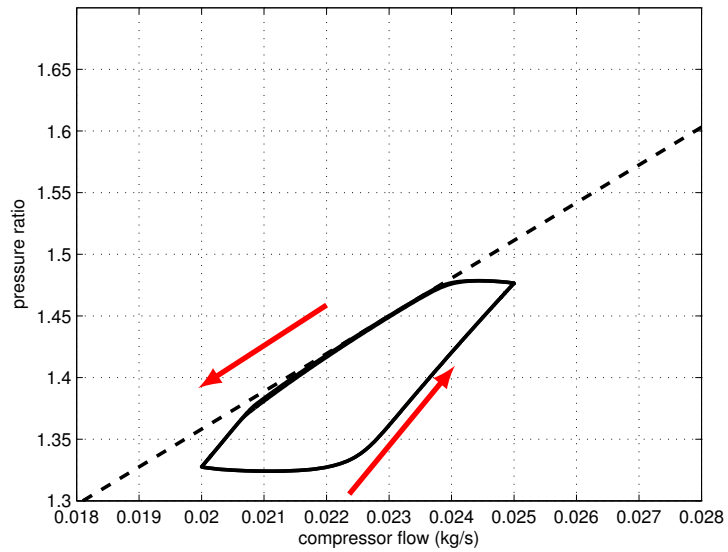


Figure 6.7: Response trajectory with surge margin offset based on nonlinear model simulation

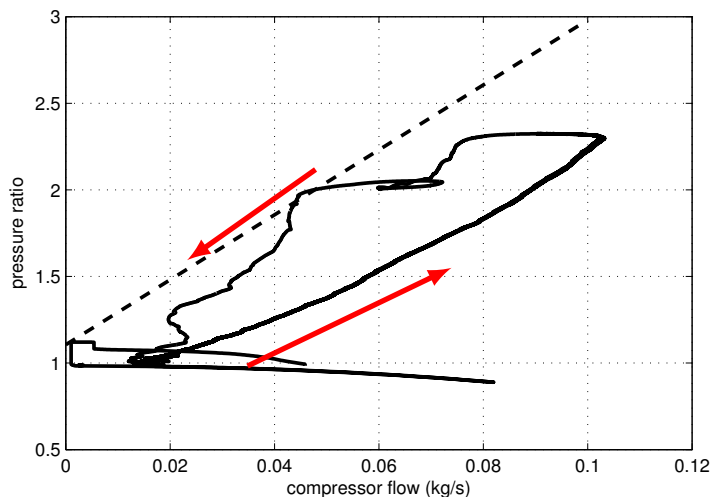


Figure 6.8: Tip-in/tip-out response on a compressor map using a high-flow OP

of inputs from a vehicle run and applying them to the model. Specifically, we use measured values of $\theta(t)$, $u_{wg}(t)$, $u_{cbv}(t)$, and $N_e(t)$ as inputs to the nonlinear model in the simulations.

Figs. 6.8-6.9 show the nonlinear model’s response to these inputs. The excursion to the left of the surge line is small and brief. However, the throttle does not return to the reference after the tip-out. Also, the response is quite conservative, in that it is relatively far away from the surge line for most of the maneuver.

Therefore we consider an alternate calibration. Specifically, we choose an operating point corresponding to a lower turbocharger speed line on the compressor map and define a linear model based on this point. This results in an operating point that is lower on the compressor map (see Fig. 6.1). The results are shown in Figs. 6.10-6.11 where we observe that the response is less conservative but violates the constraint because the true dynamics higher on the compressor map are faster than the predicted dynamics.

The two approaches are complementary; the more aggressive calibration performs well at higher points on the compressor map, whereas the less aggressive calibration on lower ones. This motivates us to use a scheduled RG approach.

6.4.2.2 Scheduled RG

To retain the performance of the RG design based on the high-speed operating point while still allowing the throttle to settle after tip-out, we design an algorithm that is scheduled on engine speed. We use the high-speed linearization when the

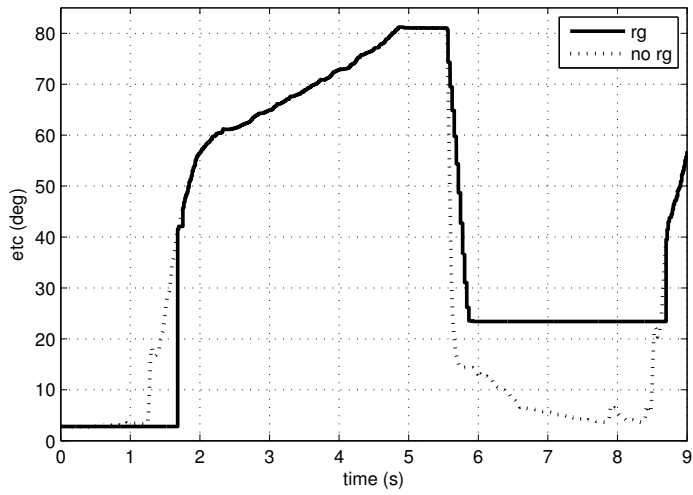


Figure 6.9: Governed (solid) and reference (dashed) throttle inputs using a high-flow OP

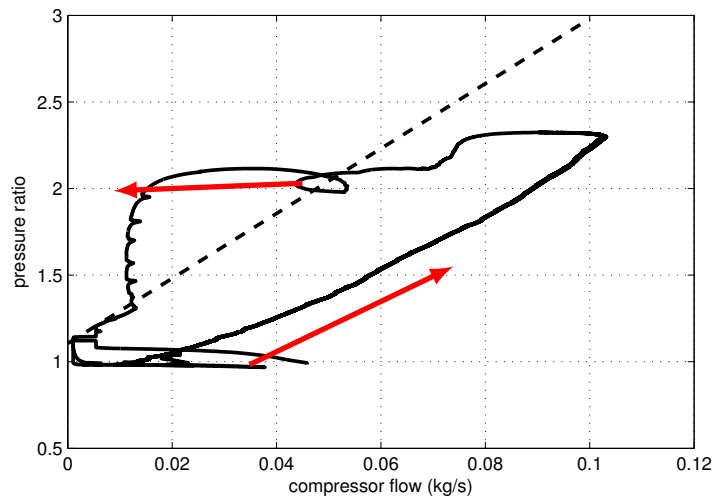


Figure 6.10: Tip-in/tip-out response on a compressor map using a low-flow OP

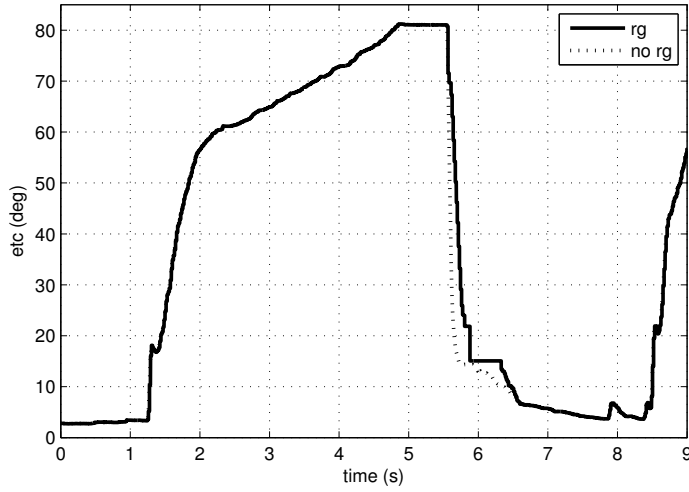


Figure 6.11: Governed (solid) and reference (dashed) throttle inputs using a low-flow OP

engine speed is over 2000 rpm and the low-speed linearization otherwise. The corresponding results are shown in Figs. 6.12-6.13. The response is not as conservative and the surge constraint is mostly enforced.

6.4.2.3 Linear state observer

We obtain our state estimates from an observer that takes advantage of available measurements. Specifically, we subsequently employ a constant gain Luenberger observer to obtain the estimated state $\delta\hat{x}(t)$, which is the input to the RG.

With the addition of an observer matrix gain L , we obtain a linear observer,

$$\delta\dot{\hat{x}}(t) = \left[\frac{\partial f_{in}}{\partial x} \right]_{op} \delta\hat{x}(t) + \left[\frac{\partial f_{in}}{\partial \theta} \right]_{op} \delta\theta(t) \quad (6.9a)$$

$$+ L(y(t) - (\delta\hat{y}(t) + y_{op})),$$

$$\delta\hat{y}(t) = \left[\frac{\partial h_{in}}{\partial x} \right]_{op} \delta\hat{x}(t) + \left[\frac{\partial h_{in}}{\partial \theta} \right]_{op} \delta\theta(t), \quad (6.9b)$$

where $\delta\hat{y}(t)$ is the estimated linear model output.

6.4.2.4 Nonlinear inner-loop RG scheme

We summarize the developments above into a block diagram in Fig. 6.14. This diagram shows the interconnection of all components within the closed-loop control system.

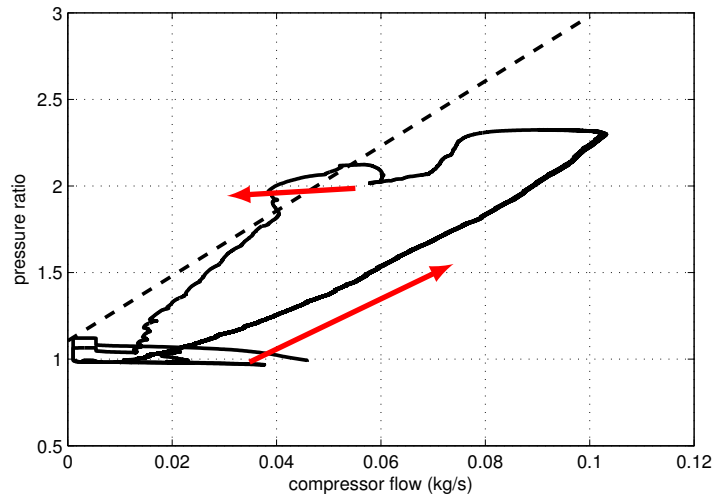


Figure 6.12: Tip-in/tip-out response on a compressor map using scheduled RGs

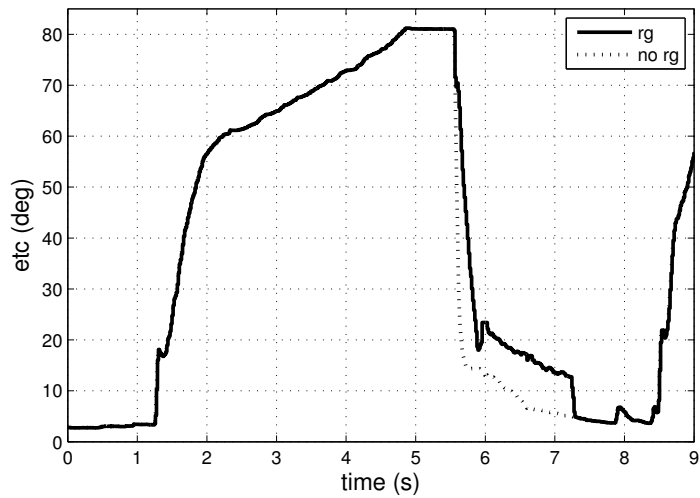


Figure 6.13: Governed (solid) and reference (dashed) throttle inputs using scheduled RGs

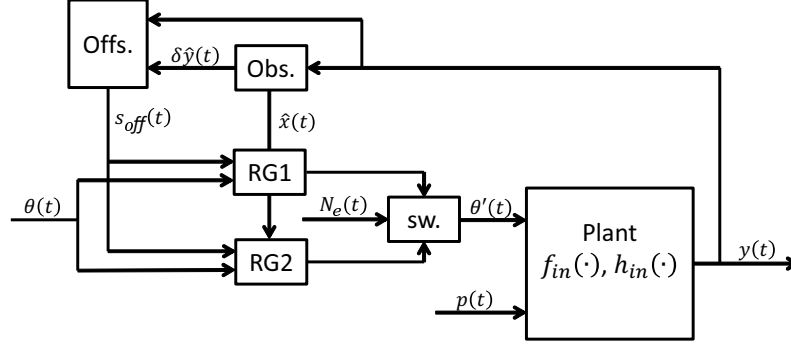


Figure 6.14: Inner-loop RG schematic

6.4.3 Vehicle implementation and experimental results

We present the results of vehicle testing on the vehicle test-bed using the modified inner-loop RG algorithm described above. In order to make sure that the effects of surge avoidance are due to the RG, the testing was done with a manually closed CBV. Two sets of tests were performed: a test of the inner-loop RG, and a baseline test using the conventional vehicle strategy for comparison. The tests were performed in Dearborn, Michigan, on a Ford test vehicle. In order to test the RG, the baseline strategy was modified and the ECU was flashed with this new version of software. Although the implementation of the RG required a significant portion of ROM capacity, the additional computations involved in executing the RG strategy did not impose a burden on the ECU, as it was able to execute the modified strategy at the update rate of the baseline strategy.

The results are plotted in Figs. 6.15-6.19. Fig. 6.15 shows a tip-in/tip-out trajectory plotted on a compressor map, Fig. 6.16 shows the corrected compressor flow response, Fig. 6.17 shows the boost pressure response. Fig. 6.18 shows the cylinder flow response as compared to the requested cylinder flow. Note that these plots superimpose the results of two representative runs with RG on and RG off at similar tip-outs and are consistent with results observed for other tests. The reason that the ungoverned trajectory begins at 2 sec is that the trajectories have been aligned to tip out at the same time.

The results show that the reference governor has reduced the incursion into the surge region along with compressor flow oscillations. This can be seen in Fig. 6.15, where the governed trajectory does not overshoot the constraint boundary as much as the ungoverned. Furthermore, the results in Fig. 6.16 show that the flow oscillations are lessened with the use of the RG. The cylinder flow response, plotted in Fig. 6.18, is different from the nominal controller in the case of RG operation which affects engine

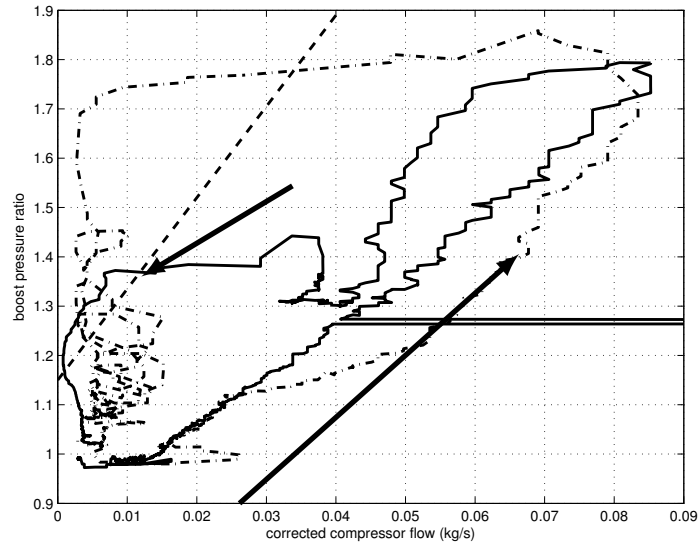


Figure 6.15: Vehicle data: Ungoverned (dash-dotted) and governed (solid) tip-in/tip-out responses on a compressor map using the inner-loop RG

torque response. Fig. 6.19 shows the engine speed response, from which we can see that the switch from the high-flow to the low-flow calibrated RG occurs shortly after the 6 sec mark.

6.5 Outer-loop reference governor

The inner-loop RG is an RG placed downstream of the control strategy in order to govern the throttle input $\theta(t)$. This placement governs only the throttle input and does not directly affect the performance of other actuators in the system. Since the engine dynamics are nonlinear, to implement the inner-loop RG we resorted to the use of multiple linear models and scheduling based on engine speed. This requires more ROM because we need to generate a new linearization and constraint set O_∞ with the addition of every operating point.

An outer-loop RG, placed before the closed-loop and governing a reference input may avoid the need for scheduling. Specifically in our outer-loop RG design, we choose to govern the desired cylinder flow $W_{cyl,d}(t)$, using the RG and then compute the corresponding throttle command $\theta(t)$, while using the ungoverned reference input $W_{cyl,d}(t)$ where required in the rest of the strategy.

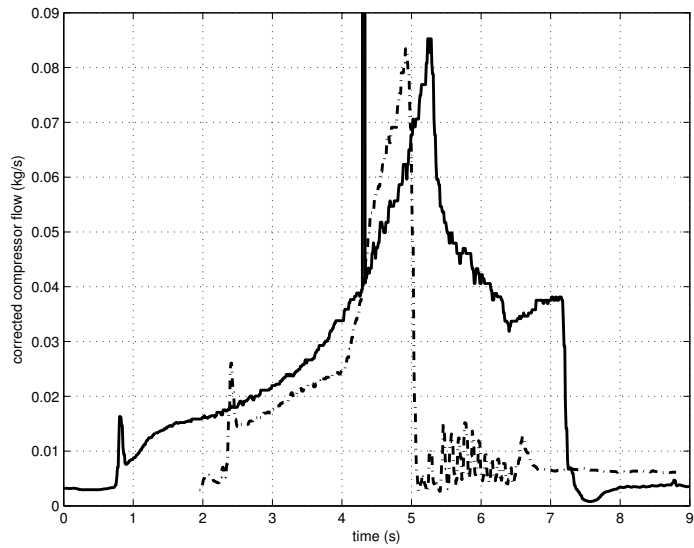


Figure 6.16: Vehicle data: Ungoverned (dash-dotted) and governed (solid) compressor flow responses using the inner-loop RG

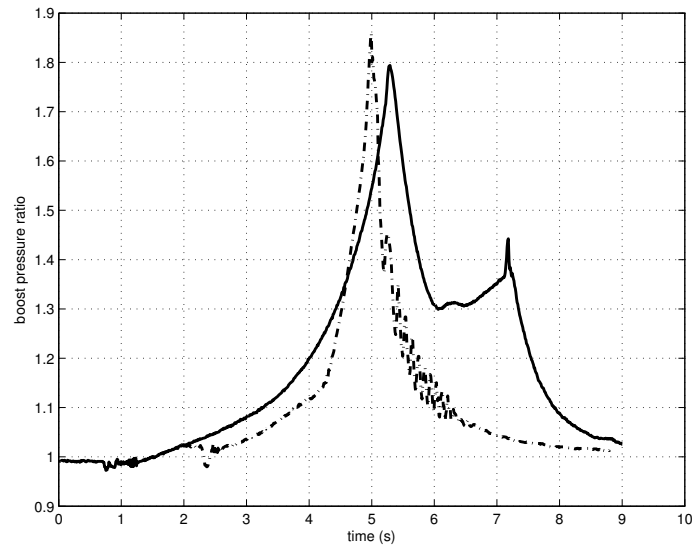


Figure 6.17: Vehicle data: Ungoverned (dash-dotted) and governed (solid) boost pressure responses using the inner-loop RG

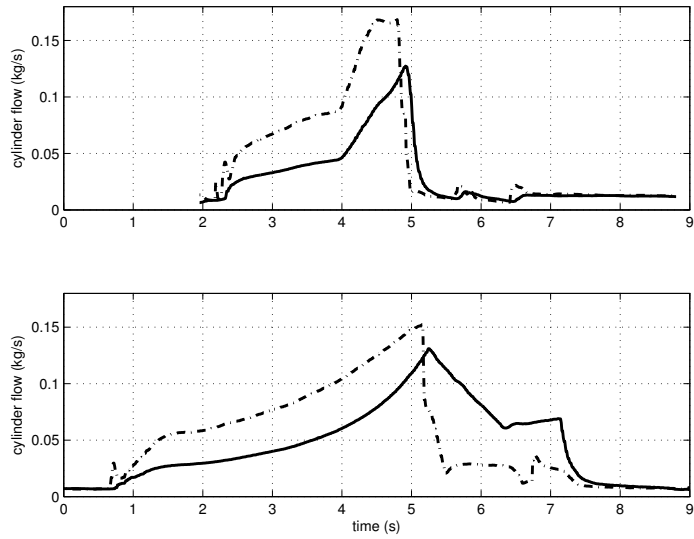


Figure 6.18: Vehicle data: Ungoverned (top) and governed (bottom) desired (dash-dotted) and actual (solid) cylinder flow responses using the inner-loop RG

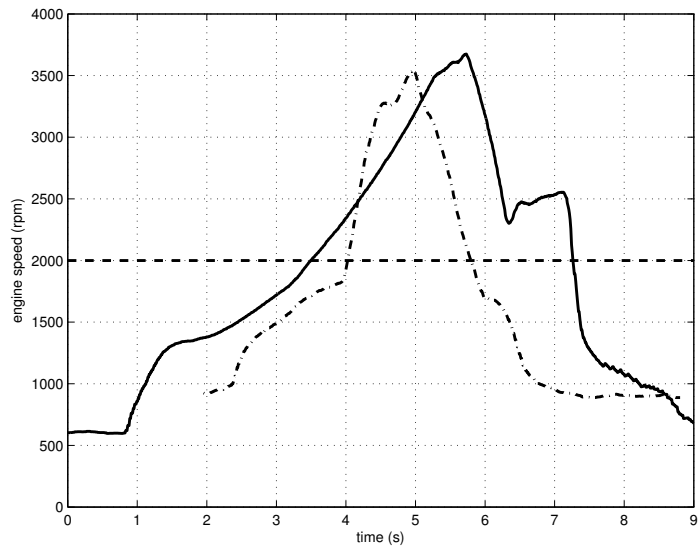


Figure 6.19: Vehicle data: Ungoverned (dash-dotted) and governed (solid) engine speed responses using the inner-loop RG with the 2000 rpm switching line (dashed)

The model dynamics are now of the form,

$$\dot{x}(t) = f_{out}(x(t), W_{cyl,d}(t), p(t)), \quad (6.10a)$$

$$y(t) = h_{out}(x(t), W_{cyl,d}(t), p(t)), \quad (6.10b)$$

where $p(t)$ is a vector of ungoverned parameters. The outer-loop RG scheme is designed in the same way as the inner-loop RG scheme with the exception of scheduling (compare the schematic in Fig. 6.20 to the schematic in Fig. 6.14), which we have found to be unnecessary.

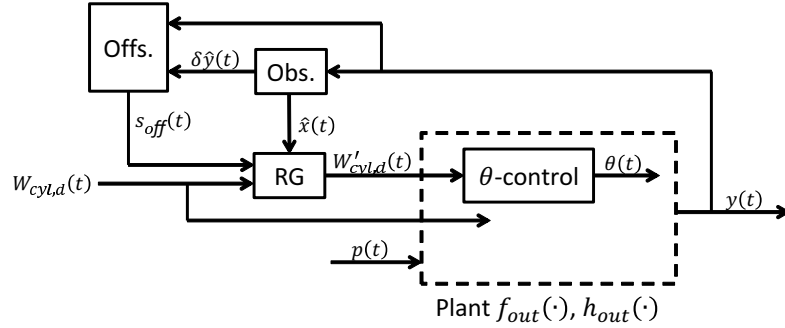


Figure 6.20: Outer-loop RG schematic

6.5.1 Vehicle implementation and experimental results

In this section, we present results of vehicle tests of the outer-loop RG strategy. Testing was performed in the same vehicle and under similar conditions as the tests of the inner-loop RG.

The results from two representative tip-in/tip-out sequences with RG turned on and off are plotted in Figs. 6.21-6.24. Fig. 6.21 shows a tip-in/tip-out trajectory plotted on a compressor map, Fig. 6.22 shows the corrected compressor flow response, Fig. 6.23 shows the boost pressure ratio response, and Fig. 6.24 shows the cylinder flow response as compared to the requested cylinder flow. From Fig. 6.21, we can see that the outer-loop RG is able to reduce the incursion into the surge region without scheduling. Furthermore, a comparison of Fig. 6.22 with Fig. 6.16 also shows that during the tip-in, the flow response tracks the flow request much more closely in the case of the outer-loop RG.

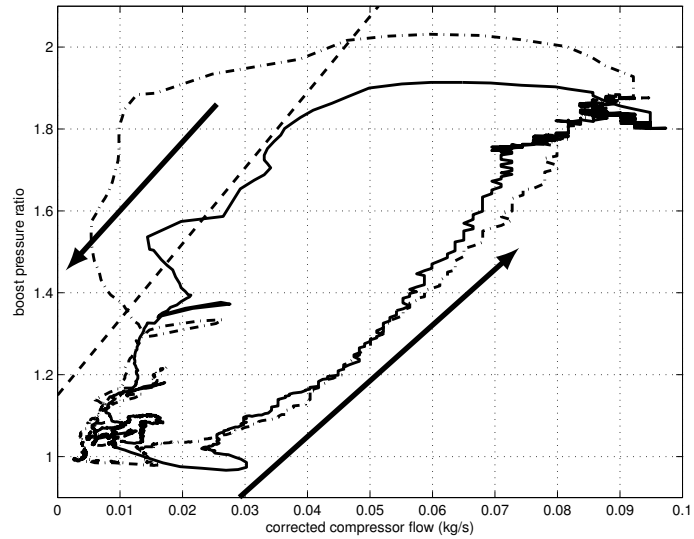


Figure 6.21: Vehicle data: Ungoverned (dash-dotted) and governed (solid) tip-in/tip-out response on a compressor map using the outer-loop RG

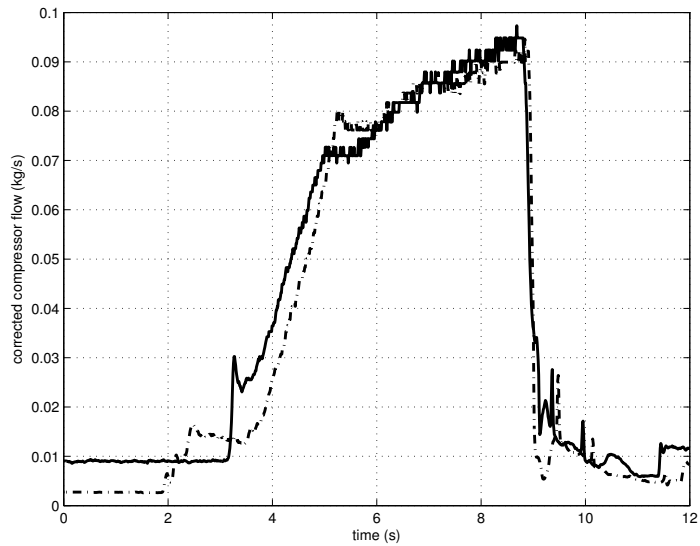


Figure 6.22: Vehicle data: Ungoverned (dash-dotted) and governed (solid) compressor flow response using the outer-loop RG

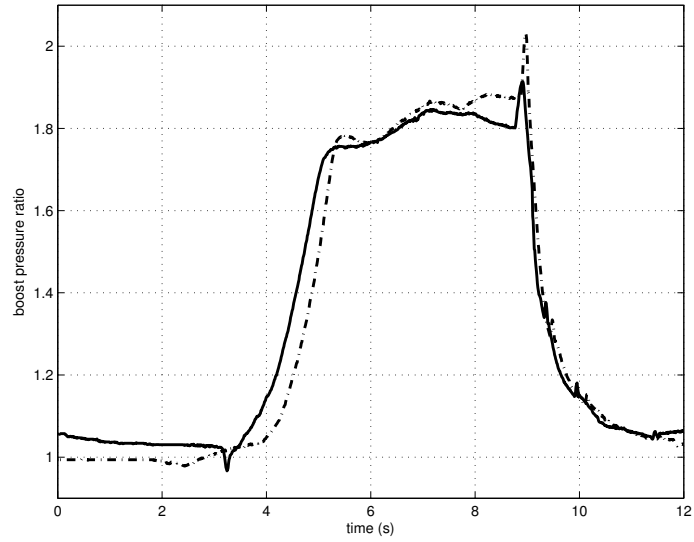


Figure 6.23: Vehicle data: Ungoverned (dash-dotted) and governed (solid) boost pressure response using the outer-loop RG

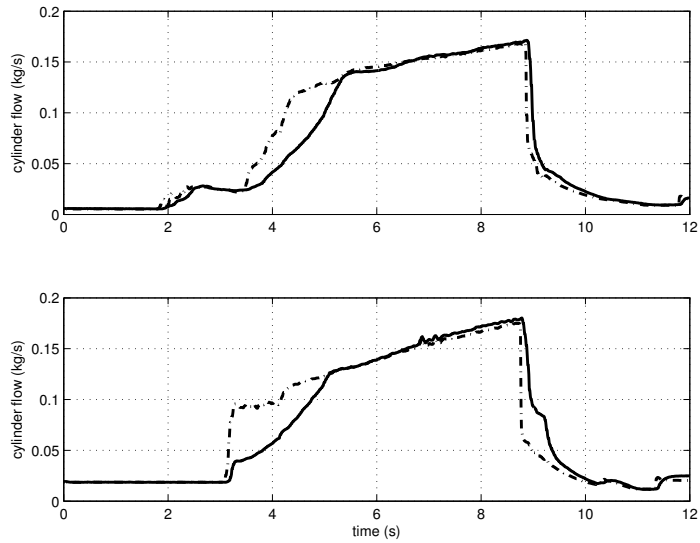


Figure 6.24: Vehicle data: Ungoverned (top) and governed (bottom) desired (dash-dotted) and actual (solid) cylinder flow response using the outer-loop RG

6.6 Discussion

In this chapter, we presented two RG designs for the enforcement of the compressor surge constraint. The first design is an inner-loop RG that governs the throttle actuator command. The second design is an outer-loop RG that governs the desired cylinder flow command.

Vehicle tests verify that both designs are able of enforcing the surge constraint, with the inner-loop reference governor requiring a modification using scheduling on engine speed in order to do so.

Both RG designs effectively reduce excursions into the surge region and the oscillations observed in the vehicle during tip-outs is reduced. Based on our simulations and experiments, the outer-loop RG design, which modifies the desired air flow demand, is preferred over the inner-loop design that directly modifies the throttle command. In particular, the outer-loop RG does not require scheduling of multiple linear models at different operating points. Therefore it has a smaller computational footprint; specifically it has half the memory requirement. The placement of the outer-loop RG is also more consistent with the existing theoretical results in which the RG is normally applied to the set-points. Further theoretical analysis of inner-loop RGs is considered in recent work [79].

The RG approach changes the response of cylinder flow to a driver tip-out request. Since cylinder flow is closely linked to engine torque in a gasoline engine, driveability may be affected.

CHAPTER 7

Reference governors for airborne wind energy systems

7.1 Introduction

Wind represents a substantial source of new renewable energy installations. Limitations on ground-level wind speeds and large tower installation costs have motivated the study of tethered, high-altitude airborne wind energy systems, described in [84, 85, 86, 87, 88, 89, 90, 91, 92, 93]. Based on studies presented in [94, 95], wind at 600m altitude carries upwards of 5 times the power density of ground level wind in many locations. Furthermore, tethered systems offer the advantage of rapid deployability, which makes them an attractive alternative to diesel generators for off-grid and short-term applications, including oil and gas exploration, military bases, and disaster relief.

This chapter considers the application of the RG to the Altaeros system, shown in Fig. 7.1, which uses a buoyant shroud to elevate a horizontal axis turbine to altitudes of up to 600m. The full Altaeros system consists of a rotating base station which houses winches that regulate the release of tethers leading to the shroud.

Although, under normal atmospheric conditions, Altaeros's Helium shroud provides constant buoyancy approximately equal to 120 percent of the shroud's weight, it is nevertheless essential that the system maintains non-negative aerodynamic lift in high wind speeds through an acceptable angle of attack. Furthermore, it is important that the tethers remain in an acceptable tension range where they neither become slack, resulting in a loss of controllability, nor exceed structural limitations.

Several control strategies have been proposed in an effort to track setpoints while satisfying the aforementioned constraints. In [92], a heuristically-designed hierarchical control system was proposed, wherein a static outer loop controller maps setpoints



Figure 7.1: Photograph of Altaeros’s proof-of-concept system, which was flown at Loring Air Force Base during the winter of 2012 [46]

to a steady-state flying envelope, and an inner loop controller performs setpoint tracking. This strategy was successfully flight-tested in winter, 2012; however, the proposed control strategy provided no guarantee of constraint satisfaction. In order to provide guaranteed transient constraint enforcement, an MPC strategy was proposed in [93], which does guarantee transient constraint satisfaction but is computationally burdensome.

This chapter presents an alternative, computationally simpler, RG approach for guaranteeing transient constraint satisfaction. The approach adjusts altitude and pitch angle setpoints in order to satisfy pointwise-in-time state and control input constraints, including constraints on altitude, angle of attack and tether tensions. The RG serves as an add-on to a closed-form base controller, which is designed using LQ techniques in this paper. Under realistic bounds on the wind speed disturbance, the approach guarantees that the system constraints are satisfied during both transient and steady-state operation. Ultimately, this RG-based approach accomplishes

Table 7.1: Key shroud model variables

Component	Variable	Description
Shroud	x_g, z_g	ground-fixed c.m. pos.
States	u, w	body-fixed c.m. velocity
	θ	pitch angle
	q	pitch rate
	Winch	l_i
States	\bar{v}_i	tether i release speed
Tether	T_i	tether i tension
Control	\bar{u}_i	winch speed command
Disturbances	u_{wind}	horizontal wind speed
	w_{wind}	vertical wind speed

constraint enforcement under a fraction of the computational load that is required by the MPC algorithm of [93]. In this paper, we apply the RG to the longitudinal system dynamics, which dominate the motion of the system once it has been stabilized to a downwind condition [92].

The chapter is organized as follows. Section 7.2 provides the details of the longitudinal dynamic model, and Section 7.3 describes the constrained control design. Section 7.4 provides simulation results on the linearized model, and Section 7.5 provides simulation results on the nonlinear model. These results demonstrate that the RG does an effective job of ensuring that critical state constraints are enforced.

7.2 Longitudinal dynamic model

The longitudinal dynamic model of the shroud is based on the model introduced in [92] and is briefly discussed in this section. The model components and variables are summarized in Table 7.1. Because this chapter focuses on the treatment of the system longitudinal dynamics, the model of [92] is reduced to the 10 states that are relevant when the dynamic behavior is restricted to the vertical x - z plane. Furthermore, this work on the longitudinal system assumes synchronized port and starboard tether motions, and therefore the control space is limited to 2 control variables. The subscript i (used with control inputs, tether tensions, and unstretched lengths) denotes a particular tether set, where $i = 1$ represents the forward tether set and $i = 2$ represents the aft tether set.

Nonlinear shroud dynamics

The shroud dynamics follow a standard 3-degree-of-freedom model in which the body-fixed x and z axes are in the direction of the aft and top of the shroud, respectively. The rotational equations of motion are given by,

$$\dot{\theta} = q, \quad (7.1a)$$

$$\dot{q} = \frac{1}{I_{yy}}(M_y^{aero} + M_y^{tether} + M_y^b), \quad (7.1b)$$

where I_{yy} represents the pitch moment of inertia and M_y^{aero} , M_y^{tether} , and M_y^b respectively represent the total aerodynamic, tether-generated, and buoyancy-generated moments about the y -axis.

The translational equations of motion are given by,

$$\dot{u} = -wq + \frac{1}{m}(F_x^{eb} + F_x^{aero} + F_x^{tether}), \quad (7.2a)$$

$$\dot{w} = uq + \frac{1}{m}(F_z^{eb} + F_z^{aero} + F_z^{tether}), \quad (7.2b)$$

where m represents the shroud mass and $F_{x,z}^{eb}$, $F_{x,z}^{aero}$, and $F_{x,z}^{tether}$ respectively represent the excess buoyant (buoyant force minus gravitational force), aerodynamic, and tether forces along both axes. Using the rotation matrix associated with θ , the body-frame velocities are easily converted to ground-fixed frame, and x_g and z_g are readily calculated using integration.

Winch and tether spooling dynamics

The winches comprise AC motors that drive a drum and regulate the unstretched line length of each of the control tethers. They are governed by the following equations.

$$\dot{l}_i = \bar{v}_i, \quad (7.3a)$$

$$\dot{\bar{v}}_i = \frac{1}{\tau_{winches}}(\bar{u}_i - \bar{v}_i). \quad (7.3b)$$

Here, $\tau_{winches}$ represents the approximate actuator time constant associated with the winches, which is taken as 0.1 sec for this work.

Table 7.2: Nominal Operating Point for Linearized Model

System parameters	Nominal values
$u_{wind,0}$	20
$w_{wind,0}$ (m/s)	0
$l_{i,0}^{unstretched}$ (m)	595
$x_{g,0}$ (m)	258
$z_{g,0}$ (m)	543
α_0 ($^\circ$)	10.8
$T_{1,0}$ (N)	10852
$T_{2,0}$ (N)	8113
$\bar{u}_{i,0}$ (m/s)	0

Tether tension calculation

The tethers are modeled, as in [96, 97], as spring-dampers that can assume only positive tension. Specifically, the tether tension is given by,

$$T_i = \max\left(0, k_{tethers}(\|\mathbf{r}_i^{shroud} - \mathbf{r}_i^{bs}\| - l_{i,0}^{unstretched}) + b_{tethers} \frac{d}{dt} \|\mathbf{r}_i^{shroud} - \mathbf{r}_i^{bs}\|\right), \quad (7.4)$$

where $\mathbf{r}_i^{shroud,bs}$ represents the two-dimensional position vector of the attachment point of tether i relative to the base station, $k_{tethers}$ represents the tether stiffness, and $b_{tethers}$ represents the tether damping. Stiffness and damping terms are the for the forward and aft tethers. Note also that in the longitudinal model we lump two forward tethers into a single equivalent tether and the two aft tethers into a single equivalent tether.

Linearized system dynamics

The RG design for the Altaeros system is based on linear models. In this chapter, we consider the linearizations of the longitudinal dynamics of the system about a representative operating condition summarized in Table 7.2.

The continuous-time linear model of the system has the following form,

$$\dot{x}(t) = A_c x(t) + B_c \bar{u}(t) + B_{c,w} \bar{w}(t), \quad (7.5a)$$

$$y(t) = C x(t) + D \bar{u}(t) + D_w \bar{w}(t). \quad (7.5b)$$

The components of the output vector $y(t)$ are the variables to be constrained. These are deviations in the altitude $\delta z_g(t)$, front tether tension $\delta T_1(t)$, aft tether tension $\delta T_2(t)$, angle of attack $\delta \alpha(t)$, front tether rate $\delta \bar{u}_1(t)$, and aft tether rate $\delta \bar{u}_2(t)$ from

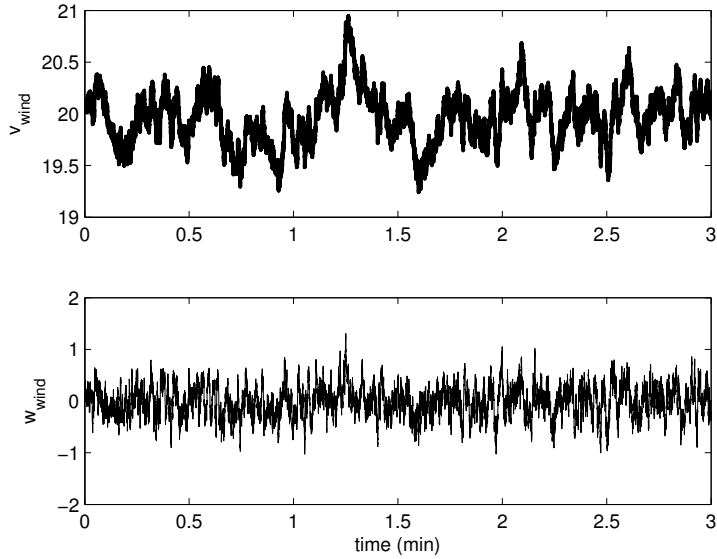


Figure 7.2: Horizontal (top) and vertical (bottom) wind speeds

the nominal conditions. The components of the input vector $\bar{u}(t)$ for the linear model are the commanded front tether rate $\bar{u}_1(t)$ and the aft tether rate $\bar{u}_2(t)$. As with the disturbance $\bar{w}(t)$, the upper bar notation is used in $\bar{u}(t)$ in order to distinguish the control input vector from the body-fixed x velocity, denoted by u . The 10 states in (7.5) are denoted by $x(t)$. The components of the disturbance vector $\bar{w}(t)$ are the deviations of the base wind speed $\delta u_{wind}(t)$ and the vertical wind speed $\delta w_{wind}(t)$ from the nominal wind speeds, about which the linearization was taken.

In the simulations, the wind speed disturbances are modeled using a Dryden turbulence model [98], which characterizes the spectral properties of turbulence as a function of altitude and base wind speed. This is incorporated into the model by passing band-limited white noise through a coloring filter whose parameters are directly related to turbulence intensity, scale length, and base wind speed. Fig. 7.2 shows the wind speed disturbance inputs.

System constraints

A summary of the system constraints follows. The altitude is constrained to a limit of 609m, arising from an FAA limit of 2000ft above ground level for moored balloons. The angle of attack is constrained to between 0° and 20° , where the limits correspond to insufficient lift and stall, respectively. The tether tensions T_i , are constrained to between 100N and 20kN, where the lower limit prevents slack tethers,

with a margin for robustness, and the upper limit arises from material limitations. Finally, the control inputs \bar{u}_i are constrained to between $\pm 1\text{m/s}$ in order to account for saturation limits.

The constraint set Y is given as, $Y = \{y(t) : 0 \leq z_{g,0} + \delta z_g \leq 609, 0 \leq \alpha_0 + \delta \alpha \leq 20, 100 \leq T_{i,0} + \delta T_i \leq 20000, -1 \leq \bar{u}_{i,0} + \delta \bar{u}_{i,0} \leq 1, i = 1, 2\}$. Note that Y is polyhedral.

7.3 Baseline controller design

To begin the controller design, the system (7.5) is discretized using a zero-order hold using a sampling time of $T_s = 0.1\text{s}$.

The base controller is designed to track set-points for altitude and pitch commands. Define the constraint-admissible and reference command, respectively,

$$v(t) = \begin{bmatrix} \delta z_{g,gov}(t) \\ \delta \theta_{gov}(t) \end{bmatrix}, \quad r(t) = \begin{bmatrix} \delta z_{g,d}(t) \\ \delta \theta_d(t) \end{bmatrix}. \quad (7.6)$$

Let C_r be such that $C_r x(t) = (\delta z_g(t), \delta \theta(t))$. Since $\bar{u}(t)$ are rate inputs, we design the tracking controller so that $C_r x(t) \rightarrow r(t)$ while $\bar{u}(t) \rightarrow 0$. This proceeds by defining error dynamics, $e(t+1) = e(t) + C_r x(t) - r(t)$, and coupling them with (7.5a) to obtain,

$$\begin{bmatrix} e(t+1) \\ x(t+1) \end{bmatrix} = \begin{bmatrix} I & C_r \\ 0 & A \end{bmatrix} \begin{bmatrix} e(t) \\ x(t) \end{bmatrix} + \begin{bmatrix} 0 \\ B \end{bmatrix} \bar{u}(t) - \begin{bmatrix} I \\ 0 \end{bmatrix} r(t). \quad (7.7)$$

The nominal controller is a linear quadratic regulator to minimize,

$$J = \frac{1}{2} \sum_{t=0}^{\infty} (e^T(t) Q_\epsilon e(t) + x^T(t) Q x(t) + \bar{u}^T(t) R \bar{u}(t)) dt, \quad (7.8)$$

for $r(t) \equiv 0$, where Q_ϵ and Q are positive semi-definite, and R is positive definite, so that the control is of the following form,

$$\bar{u}(t) = -K_\epsilon e(t) - K x(t). \quad (7.9)$$

Note that this controller achieves zero tracking error for constant commands $r(t)$, due to the fact that the plant contains an integrator.

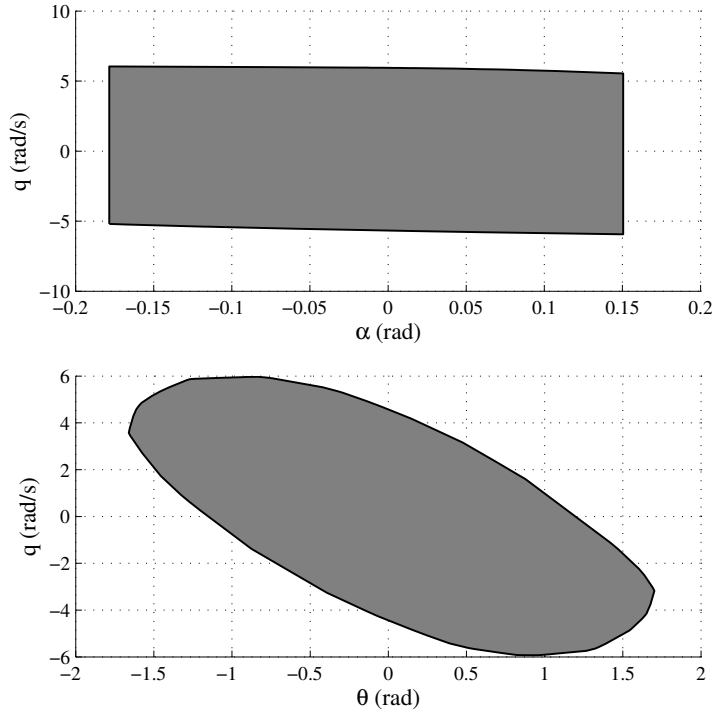


Figure 7.3: Projections of O_∞ onto the α - q (top) and θ - q (bottom) planes

7.4 Linear model simulation

The following results correspond to a 3 minute simulation with reference inputs $r(t)$ given in Fig. 7.4 and disturbances $\bar{w}(t)$ given in Fig. 7.2. Practical considerations have governed the selection of the disturbance set as $W = [-0.2, 0.2]^2$ and two projections of the resulting O_∞ corresponding to the linear system are provided in Fig. 7.3. To avoid conservatism in the RG response and recognizing that wind velocity does not change instantaneously between extreme values as assumed in the theory of the RG, the choice of length of W is set slightly larger than the rms of the expected disturbance (corresponding to one standard deviation), which is approximately 0.13. This size of W provides adequate protection against simulated wind disturbances.

The results are given in Figs. 7.4-7.8. Fig. 7.4 shows the constraint-admissible reference $v(t)$ as computed by the RG.

Overall, this set of simulations demonstrates that the RG keeps the system responses within acceptable bounds over the course of setpoint changes superimposed on top of realistic wind disturbance scenarios. On the other hand, the ungoverned system exhibits a variety of constraint violation at some point. Fig. 7.5 shows improved tracking and constraint satisfaction with the RG, whereas the ungoverned

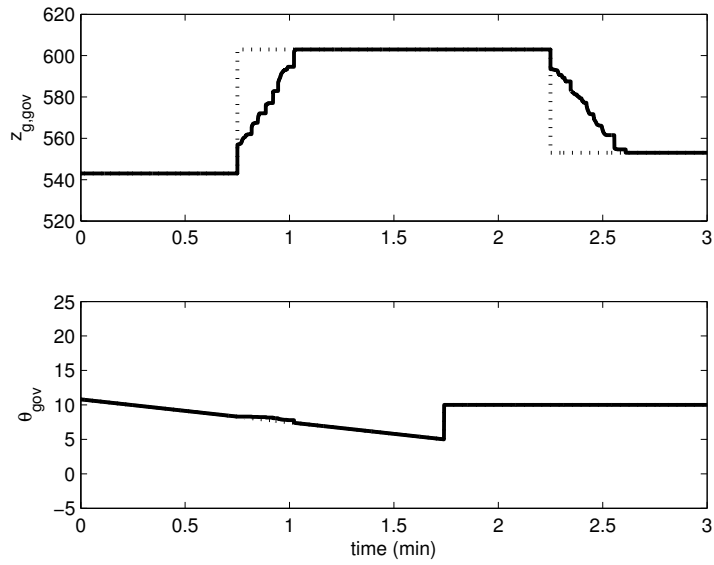


Figure 7.4: Desired (dotted) and governed (solid) reference inputs for $z_{g,d}(t)$ (top) and $\theta_d(t)$ (bottom)

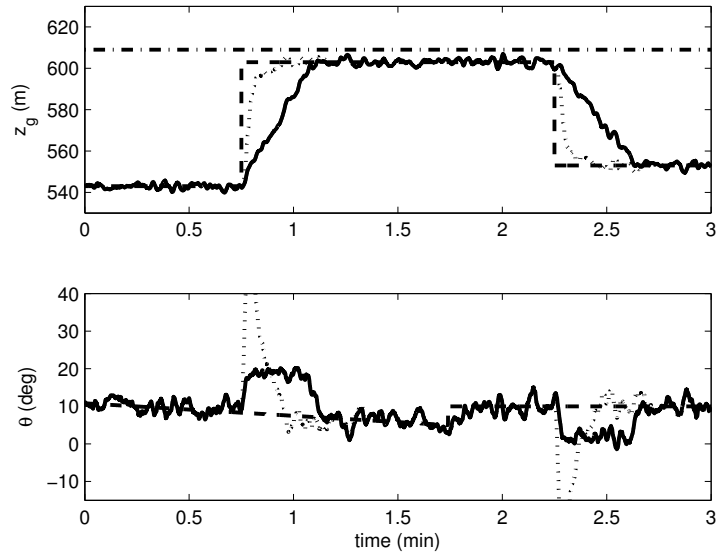


Figure 7.5: z_g and θ ungoverned (dotted) and governed (solid) responses plotted against desired set-point $r(t)$ (dashed) and the altitude constraint (dot-dashed)

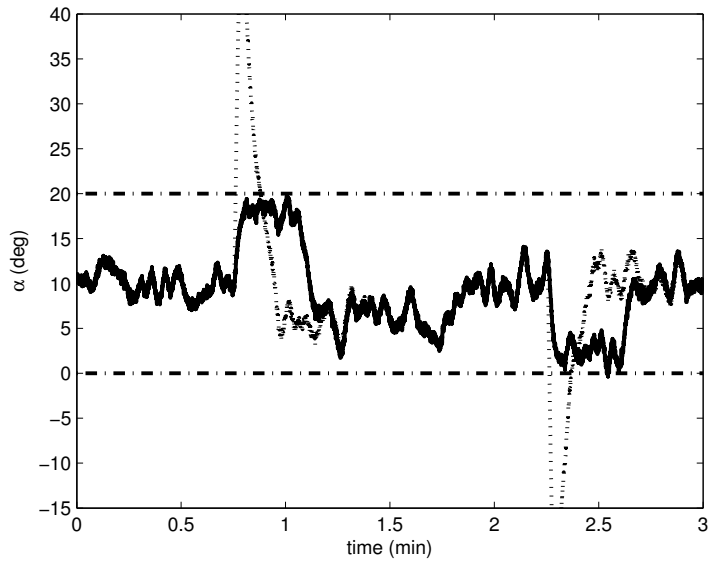


Figure 7.6: $\alpha(t)$ ungoverned (dotted) and governed (solid) responses plotted against constraints (dot-dashed)

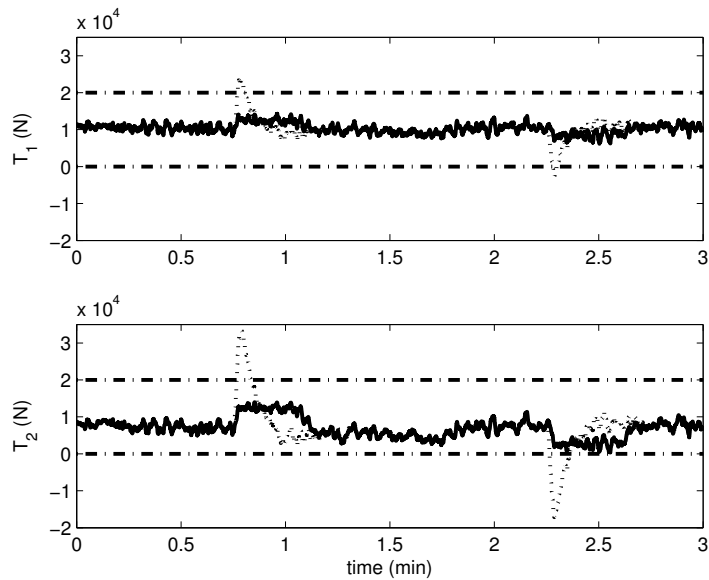


Figure 7.7: Forward (top) and aft (bottom) tension ungoverned (dotted) and governed (solid) responses plotted against constraints (dot-dashed); note that the magnitudes of negative tether tensions do not carry physical significance but rather merely reflect the fact that the tethers are slack

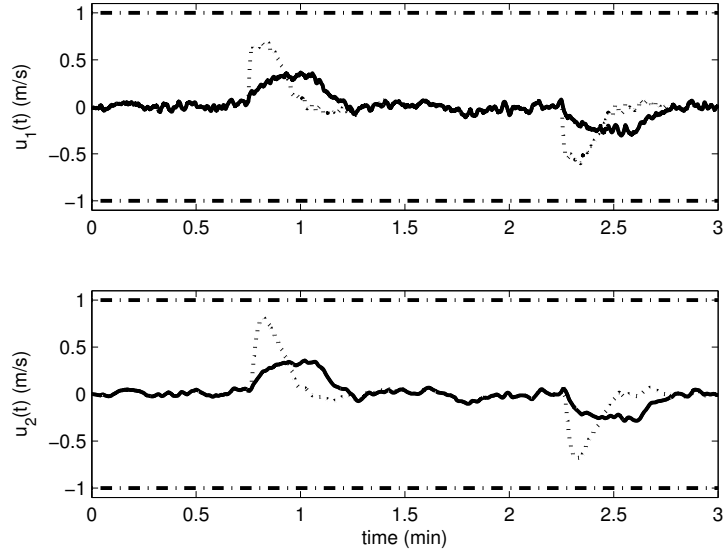


Figure 7.8: $\bar{u}_1(t)$ (top) and $\bar{u}_2(t)$ (bottom) uncontrolled (dotted) and controlled (solid) responses plotted against saturation limits (dot-dashed)

controller exhibits transient altitudes that exceed the FAA limitation of 2000ft above ground level. Furthermore, Fig. 7.6 shows that while the uncontrolled controller exhibits severe angle of attack $\alpha(t)$ violations upon altitude setpoint changes, the RG ensures that $\alpha(t)$ stays within acceptable bounds in order to prevent the loss of lift that results from stall or a nose-down configuration. Finally, Fig. 7.7 demonstrates that both tether tensions remain within acceptable bounds upon altitude changes, whereas the uncontrolled response exhibits slack tethers and excessive tether tensions at different times. It is important to note that although the linearized model generates negative tension, the magnitude of these negative values do not carry physical significance since they merely reflect slack tethers.

7.5 Nonlinear model simulation

In this section we apply a few modifications to the linear RG in order to use the RG for nonlinear constraint enforcement. Firstly, we develop an observer to estimate the output $y(t)$ and use the nonlinear model output as an input to the observer. The RG is consequently applied to the observer estimate. We also tighten the constraint on $\alpha(t)$ to the set $[3, 17]$ instead of $[0, 20]$ and lower the altitude constraint to 604m, because these two variables exhibit more sensitivity to the reference input close to the constraints than they do at the operating point.

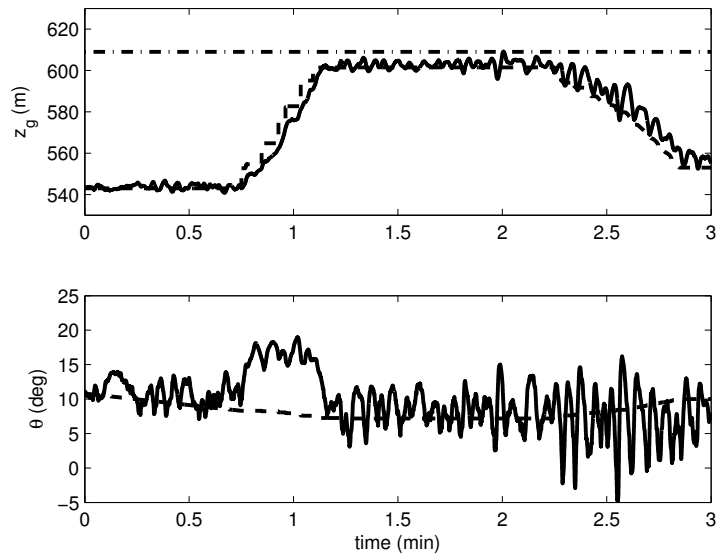


Figure 7.9: Nonlinear simulation: z_g and θ responses (solid) plotted against governed set-point $r(t)$ (dashed) and the altitude constraint (dot-dashed)

Furthermore, we do not present ungoverned response results because the application of the above controller without an RG results in nonrobust operation; specifically, its application leads the system to stall, which ultimately causes catastrophic loss of lift.

The results are presented in Figs. 7.9-7.12. The results show similar response properties to that found in the previous section, demonstrating that all state and control input constraints are successfully enforced by the RG. The success of the approach on the fully nonlinear model indicates promise for the practical application of the RG approach in future flight testing.

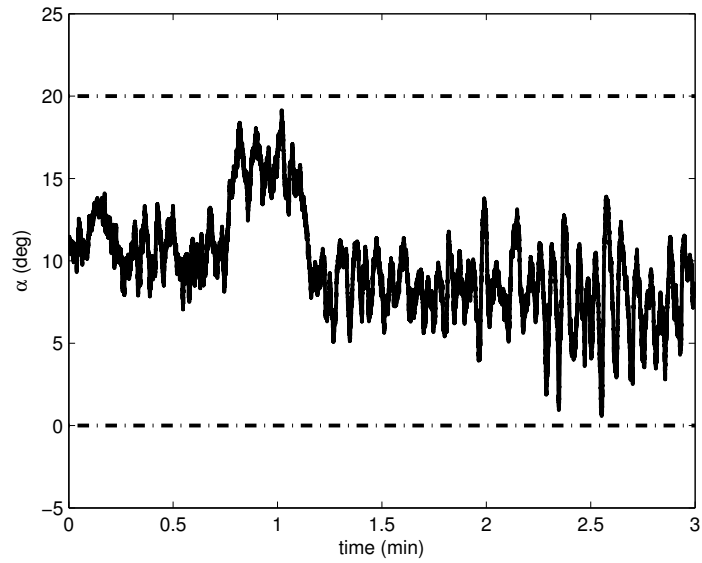


Figure 7.10: Nonlinear simulation: $\alpha(t)$ responses plotted against constraints (dot-dashed)

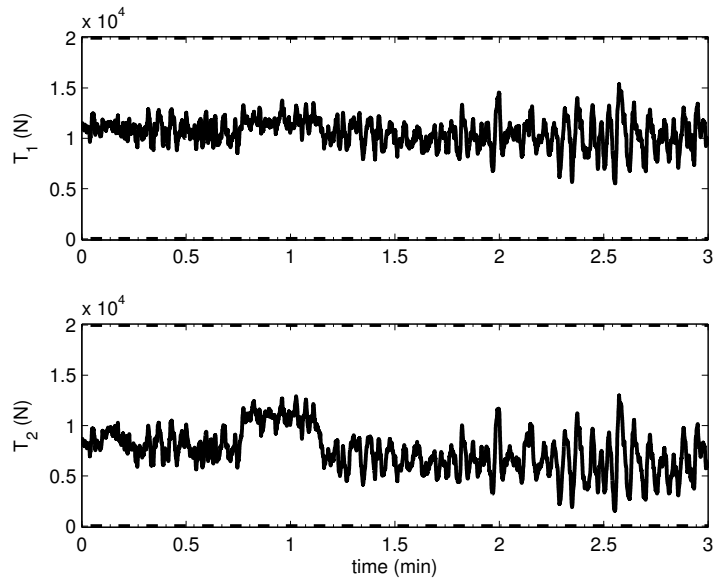


Figure 7.11: Nonlinear simulation: Forward (top) and aft (bottom) tension responses plotted against constraints (dot-dashed)

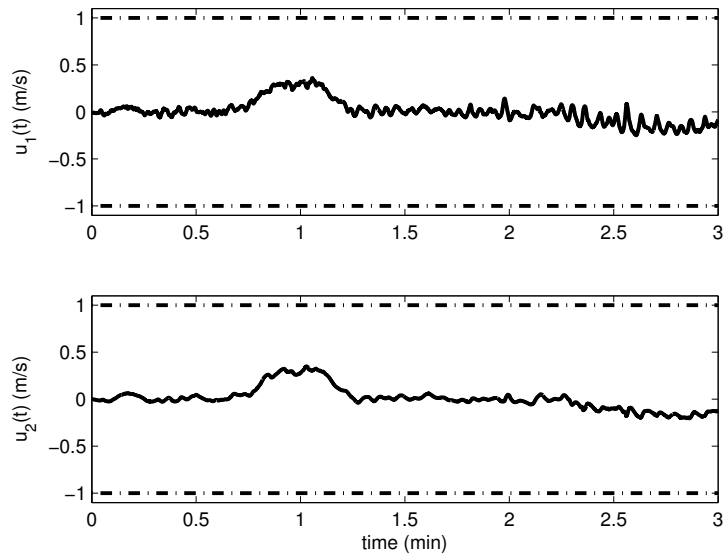


Figure 7.12: Nonlinear simulation: $\bar{u}_1(t)$ (top) and $\bar{u}_2(t)$ (bottom) responses plotted against saturation limits (dot-dashed)

CHAPTER 8

Reference governors for constrained spacecraft attitude control on $\text{SO}(3)$

8.1 Introduction

In this chapter, we consider an RG scheme for constrained control of spacecraft maneuvers that exploits predictions based on discrete-time models with dynamics that evolve on $\text{SO}(3)$. The scheme developed here uses a prediction model obtained using the Lie group variational integrator (LGVI) [99, 100, 101, 102, 103, 104, 105, 106]; this predictive model leads to improvements in prediction since it preserves conserved quantities of motion, such as momentum and energy.

The use of an LGVI can lead to large improvements in prediction [99] because the LGVI has been developed to preserve the underlying group structure of dynamics that evolve on Lie groups. Unlike standard integration schemes such as Runge-Kutta, the LGVI preserves conserved quantities of motion up to a bounded error. In the case of $\text{SO}(3)$, the LGVI achieves this by updating the rotation matrix by multiplying two matrices in $\text{SO}(3)$, thereby ensuring that the rotation matrix evolves on $\text{SO}(3)$ and the conserved quantities of motion are preserved. For other types of variational integrators which also have this property, see [107, 108].

Theoretical results presented in this chapter show recursive feasibility and convergence for the RG scheme. Furthermore, we show that the RG exhibits global convergence properties for all initial states satisfying feasibility properties with respect to constraints. This amounts to global rest-to-rest reorientation capability if there are no constraints; this conclusion is interesting since global stabilization on $\text{SO}(3)$ by smooth or even continuous time-invariant feedback laws cannot be achieved [47].

A simulation using the scheme is also reported. We simulate a rest-to-rest space-

craft attitude control maneuver, where the objective of the spacecraft attitude control problem is to reorient the spacecraft from a given attitude to the desired attitude.

The chapter is organized as follows. In Section 8.2, we describe the Lie group variational integrator that we employ for making predictions on $\text{SO}(3)$. In Section 8.3, we introduce the RG scheme. In Section 8.4, we present a simulation of a rotational maneuver.

8.2 Constrained LGVI dynamics

To account for the discrete-time character of RG updates and constraint enforcement at discrete-time instants, we exploit the LGVI model as a prediction model. The LGVI dynamics for a controlled rigid spacecraft on $\text{SO}(3)$ in discrete-time are given by [109, 102],

$$(h\Pi(t))^\times = \mathbf{F}(t)\mathbf{J} - \mathbf{J}\mathbf{F}(t)^\text{T}, \quad (8.1a)$$

$$\mathbf{C}(t+1) = \mathbf{C}(t)\mathbf{F}(t), \quad (8.1b)$$

$$\Pi(t+1) = \mathbf{F}(t)^\text{T}\Pi(t) + h\mathbf{T}(t), \quad (8.1c)$$

where $\Pi(t) \in \mathbb{R}^3$ is the angular momentum of the spacecraft expressed in the body frame, $\mathbf{F}(t) \in \text{SO}(3)$ is a one time-step change in $\mathbf{C}(t) \in \text{SO}(3)$, which is the spacecraft rotation matrix, $\mathbf{T}(t) \in \mathbb{R}^3$ is the applied torque, h is the discretization time-step, and $\mathbf{J} = \frac{1}{2} \text{tr}(\mathbf{J}_c)\mathbf{I} - \mathbf{J}_c$, where \mathbf{J}_c is the spacecraft inertia matrix. For subsequent ease of exposition, we define a new variable, $\mathbf{X}(t) = (\mathbf{C}(t), \mathbf{F}(t)) \in \text{SO}(3) \times \text{SO}(3)$.

The dynamics are subject to the state- and control-constraint,

$$(\mathbf{X}(t), \mathbf{T}(t)) \in \mathcal{C}, \quad \forall t \in \mathbb{Z}_+, \quad (8.2)$$

where $\mathcal{C} \subset \text{SO}(3) \times \text{SO}(3) \times \mathbb{R}^3$ is a compact set with nonempty interior.

The solution to (8.1) proceeds by first computing $\mathbf{F}(t)$ in (8.1a) from a given $\Pi(t)$ and then computing (8.1b) and (8.1c) based on this value. $\mathbf{F}(t)$ in (8.1a) can be computed by solving a continuous-time algebraic Riccati equation [110]. However, a special orthogonal solution $\mathbf{F}(t)$ to (8.1a) exists if and only if [110],

$$(h\Pi(t)^\times)^2 + 4\mathbf{J}^2 \succeq 0. \quad (8.3)$$

This implies that, in order to guarantee a solution to (8.1a) at the next time step,

the convex [47] condition (8.3) must be enforced at the current time-step, *i.e.*,

$$(h\Pi_{k+1}^\times)^2 + 4\mathbf{J}^2 \succeq 0. \quad (8.4)$$

Therefore, in addition to all other constraints, (8.4) is always included in the constraint set \mathcal{C} .

Remark 8.1. Condition (8.3) ensures the angular velocity $\Omega(t) = \mathbf{J}_c^{-1}\Pi(t)$ is small enough so there exists a solution $\mathbf{F}(t)$ corresponding to $\Omega(t)$. Physically, the change in rotation $\mathbf{F}(t)$ can correspond to an infinite number of values of $\Omega(t)$, but the solution to (8.1a) only corresponds to one.

The RG that we present in the following section utilizes (8.1) to propagate the given rotation and angular momentum in order to predict the constraint violation of the spacecraft and to ensure the tracking of a desired reference rotation.

8.3 Reference governor for SO(3)

Below we describe the required modifications of the nonlinear RG to the SO(3) setting while relying on [2, 3] for supporting theoretical results. The RG described in [3, 2] is applied to an asymptotically stable closed-loop nonlinear system, which consists of an open-loop plant and a stabilizing controller with the reference as an input. The dynamics of this system are of the form,

$$x(t+1) = f(x(t), v(t)), \quad (8.5)$$

where $x(t) \in \mathbb{R}^n$ is the state variable and $v(t) \in \mathbb{R}^m$ is a reference input. Given a desired reference input $r(t) \in \mathbb{R}^m$, the RG computes $v(t)$ according to (0.2) and where $\kappa(t) \in [0, 1]$ is maximized subject to constraints being satisfied for all $t \in \mathbb{Z}_+$ by the predicted response with $v(t+k|t) \equiv v(t)$, *i.e.*, while v is held constant. It is shown in [3, 2] that if,

$$v(t) \in \mathcal{V}, \quad (8.6)$$

where \mathcal{V} is a compact, nonempty, and convex set whose corresponding set of equilibrium points is contained in the interior of the set of all constraint-admissible equilibria, there exists a time t^* such that if the constraints are satisfied for all $t \in \mathbb{Z}_{t^*}$, then they are satisfied for all $t \geq t^*$.

8.3.1 Unconstrained closed-loop control law

Because the RG is applied to closed-loop systems, we need to develop a stabilizing nominal controller for the dynamics of the discrete-time model described in Section 8.2. The constraint admissible reference rotation is denoted $\mathbf{V}(t)$ and, for this controller, we use the almost-globally stabilizing continuous-time control law, which, in the unconstrained case, guarantees $\mathbf{C}(t) \rightarrow \mathbf{V}(t) \in \text{SO}(3)$ for almost every rotation $\mathbf{C}(t)$. The closed-loop control design is described in the subsequent paragraph.

At every time-step t , given $\mathbf{V}(t)$, we compute the attitude error, which evolves on $\text{SO}(3)$,

$$\mathbf{E}(t) = \mathbf{V}(t)^T \mathbf{C}(t). \quad (8.7)$$

We apply the feedback,

$$\mathbf{T}(t) = -\mathbf{K}\mathbf{\Pi}(t) - \mathbf{E}(t), \quad (8.8)$$

where $\mathbf{K} \in \mathbb{R}^{3 \times 3}$ is a positive-definite feedback gain and $\mathbf{E}(t)$ is given by,

$$\mathbf{E}(t)^\times = \mathbf{A}\mathbf{E}(t) - \mathbf{E}(t)^T \mathbf{A}, \quad (8.9)$$

for some symmetric positive-semidefinite matrix $\mathbf{A} \in \mathbb{R}^{3 \times 3}$, with three distinct eigenvalues. In continuous-time, where the state is $(\mathbf{C}(t), \Omega(t))$, (8.8) can be shown to be asymptotically stabilizing [111] on all of $\text{SO}(3) \times \mathbb{R}^3$ except for a set of measure zero, with stable equilibrium $\mathbf{E}(t) = \mathbf{I}$ and unstable equilibria given by the set $\mathcal{U}_{\mathbf{A}} = \{\mathbf{E}(t) \in \text{SO}(3) : \mathbf{E}(t)^\times = 0, \mathbf{E}(t) \neq \mathbf{I}\}$; the set on which the control is not stabilizing is the union of all stable manifolds for the unstable equilibria in $\mathcal{U}_{\mathbf{A}}$. In this work, we assume that the continuous-time result is preserved in the discrete-time case for sufficiently small time-step¹ h . Note that when \mathbf{A} is diagonal, then $\mathcal{U}_{\mathbf{A}} = \{\mathbf{C}_i(\pi) : i = 1, 2, 3\}$, where \mathbf{C}_i is an Euler rotation about the i -th axis by the angle π .

8.3.2 Determining $\mathbf{V}(t)$

Because $\text{SO}(3)$ is not closed under addition, the reference update equation (0.2) is not appropriate for references that are elements of the group. $\text{SO}(3)$ is closed under multiplication however, so we introduce a new update equation similar to (0.2), but

¹This appears to be the case based on simulation results; we leave a rigorous proof of this to future work.

based on multiplication and exponentiation instead of addition and multiplication,

$$\mathbf{V}(t) = (\mathbf{R}(t)\mathbf{V}(t-1)^T)^{\kappa(t)}\mathbf{V}(t-1) \in \mathcal{V}, \quad (8.10)$$

where $\mathcal{V} \subset \text{SO}(3)$ is the constraint set for the reference, which satisfies the convexity-like condition,

$$\mathbf{V}, \mathbf{V}' \in \mathcal{V} \implies (\mathbf{V}'\mathbf{V}^T)^\kappa \mathbf{V} \in \mathcal{V}, \quad \forall \kappa \in [0, 1]. \quad (8.11)$$

Note that the curve described by varying $\kappa(t) \in [0, 1]$ in (8.10) is the shortest geodesic connecting $\mathbf{V}(t-1)$ and $\mathbf{R}(t)$ [112]; also note that $\mathbf{V}(t) = \mathbf{V}(t-1)$ if $\kappa(t) = 0$ and $\mathbf{V}(t) = \mathbf{R}(t)$ if $\kappa(t) = 1$.

In order to maintain the system trajectory in the stable region, we impose an artificial constraint of the form,

$$(\mathbf{X}(t), \mathbf{V}(t)) \in \mathcal{W}, \quad (8.12)$$

where \mathcal{W} is positively invariant under the dynamics (8.1)-(8.2), (8.7)-(8.9), and $\mathbf{V}(t)$ held constant over the prediction horizon. The set \mathcal{W} can be chosen to be a sublevel set of the closed-loop Lyapunov function [113]. For example, let $\mathcal{W} = \{(\mathbf{X}, \mathbf{V}) : V(\mathbf{X}, \mathbf{V}) \leq c\}$, where $V(\mathbf{X}, \mathbf{V})$ is a Lyapunov function for the continuous-time analog to (8.1)-(8.2), (8.7)-(8.9) and $c < \inf_{\mathbf{X} \in \mathcal{U}_A} V(\mathbf{X}, \mathbf{I})$.

Thus at every time-step t , $\kappa(t)$ is obtained through numerical optimization by choosing the largest value of $\kappa(t)$ for which constraint admissibility can be guaranteed if the reference is kept constant for all future time-steps. In this way, we obtain a recursively feasible reference that guarantees constraint admissibility for all future time-steps. Specifically, we perform the following optimization online,

$$\begin{aligned} \max \{ \kappa(t) \in [0, 1] : \mathbf{V}(t+k|t) \equiv \mathbf{V}(t), \\ (8.1)-(8.2), (8.7)-(8.9), (8.12) \text{ are satisfied for all } t \in \mathbb{Z}_{t^s} \}. \end{aligned} \quad (8.13)$$

The optimization is performed through a bisection algorithm similar to [3, 2]. Note that the simulation is only performed until the time-instant $t^s - 1$, and this may not predict constraint violation for all future time. However, under suitable assumptions, such that if $t^s \geq t^*$ and all constraints are satisfied for all $t \in \mathbb{Z}_{t^s}$, they will also be satisfied for any $t \geq t^s$.

Due to the properties of $\text{SO}(3)$, for some pair $\mathbf{R}(t)$ and $\mathbf{V}(t-1)$, (8.10) may not have a unique solution. This occurs when $\mathbf{R}(t)$ is a cut point of $\mathbf{V}(t-1)$, *i.e.*,

$(\mathbf{R}(t)\mathbf{V}(t-1)^T)^2 = \mathbf{I}$ but $\mathbf{R}(t)\mathbf{V}(t-1)^T \neq \mathbf{I}$. In this case, both geodesics connecting $\mathbf{V}(t-1)$ and $\mathbf{R}(t)$ are equal in length and $\mathbf{R}(t)\mathbf{V}(t-1)^T = \text{Log } \pi\mathbf{N}^\times$, for some $\mathbf{N} \in \mathbb{R}^3$ where $\|\mathbf{N}\|_2 = 1$.²

By the definition of \mathcal{V} , both geodesics are contained in \mathcal{V} , so the choice of geodesic is arbitrary. Accordingly, our approach is to perturb the target reference by,

$$\mathbf{R}(t) := \exp(-\varepsilon\pi\mathbf{N}^\times)\mathbf{R}(t), \quad (8.14)$$

for some small $0 < \varepsilon < 1$, before performing the optimization (8.13). With this small modification of the reference, we guarantee a unique solution to (8.13).

We now present the online algorithm in Algorithm 3 for calculating $\mathbf{V}(t)$. In the algorithm, the initial state values are set to the current state estimates and κ_{cand} , a candidate $\kappa(t)$, is chosen. Simulations are then performed over a finite time horizon to determine if a constraint is violated. When κ_{cand} converges to a preset tolerance, the algorithm stops.

Algorithm 3: RG for SO(3)

input : $\mathbf{X}(t)$, $\mathbf{R}(t)$, $\mathbf{V}(t-1)$

output: $\mathbf{V}(t)$

$\kappa_{\text{max}} \leftarrow 1$;

$\kappa_{\text{min}} \leftarrow 0$;

if $(\mathbf{R}(t)\mathbf{V}(t-1)^T)^2 = \mathbf{I}$ and $\mathbf{R}(t)\mathbf{V}(t-1)^T \neq \mathbf{I}$ **then** $\mathbf{R}(t) \leftarrow \exp(-\varepsilon\pi\mathbf{N}^\times)\mathbf{R}(t)$;

$\kappa(t) \leftarrow 1$;

Simulate (8.1), (8.7)-(8.10) until $t = t^s$;

if $(\mathbf{X}(t), T(t)) \in \mathcal{C}$, $\forall t \in \mathbb{Z}_+$ **then** solutionNotFound \leftarrow false;

$\kappa_{\text{cand}} \leftarrow 1$;

while solutionNotFound **do**

$\kappa_{\text{cand}} \leftarrow \frac{\kappa_{\text{max}} + \kappa_{\text{min}}}{2}$;

$\kappa(t) \leftarrow \kappa_{\text{cand}}$;

Simulate (8.1), (8.7)-(8.10) until $t = t^s$;

if $(\mathbf{X}(t), T(t)) \in \mathcal{C}$, $\forall t \in \mathbb{Z}_+$ **then** $\kappa_{\text{min}} \leftarrow \kappa_{\text{cand}}$;

else $\kappa_{\text{max}} \leftarrow \kappa_{\text{cand}}$;

if $\kappa_{\text{max}} - \kappa_{\text{min}} < \text{tol}$ **then** solutionNotFound \leftarrow false;

$\mathbf{V}(t) \leftarrow (\mathbf{R}(t)\mathbf{V}(t-1)^T)^{\kappa_{\text{min}}}\mathbf{V}(t)$

Using the above algorithm, we show that under the assumption that $t^s \geq t^*$, the reference governor exhibits the properties of recursive feasibility and finite settling

²We define the map $\text{Log} : \text{SO}(3) \rightarrow \mathfrak{so}(3)$ as in [112] with an extension to the case when $\text{tr}(\mathbf{C}) = -1$. $\text{Log}(\mathbf{C}) = \frac{\theta}{2\sin\theta}(\mathbf{C} - \mathbf{C}^T)$ if $0 < |\theta| < \pi$, where $\text{tr}(\mathbf{C}) = 1 + 2\cos\theta$; if $\text{tr}(\mathbf{C}) = 3$, then $\text{Log}(\mathbf{C}) = 0$, and if $\text{tr}(\mathbf{C}) = -1$, then $\text{Log}(\mathbf{C}) = \pi\mathbf{N}^\times$.

time.

Proposition 8.2. *Assume that $\mathbf{R}(t) \equiv \mathbf{R}$ is constant for $t \in \mathbb{Z}_+$, $\mathbf{V}(-1)$ is feasible for (8.13), and $t^s \geq t^*$.*

Then the following holds: (i) The control scheme described by Algorithm 3 is recursively feasible, i.e., the solution $\mathbf{V}(t) = \mathbf{V}(t-1)$ is always feasible for (8.13); (ii) the scheme ensures finite-time convergence to a constraint-admissible reference, i.e., there exists a $t^c \in \mathbb{Z}_+$ such that $\mathbf{V}(t) = \tilde{\mathbf{R}} \in \mathcal{V}$ for all $k \geq t^c$; (iii) if $\mathbf{R} \in \mathcal{V}$, then $\tilde{\mathbf{R}} = \mathbf{R}$.

Proof. The proof follows from the theorems and propositions in [3, 2], with a modification needed due to the step (8.14) in Algorithm 3 to show that we are always able to avoid antipodal points by redefining the admissible and desired references according to the algorithm.

Specifically, if $\mathbf{R}\mathbf{V}(t-1)^T = \exp(\pi\mathbf{N}^\times)$, then before modification, $\exp(-\varepsilon\pi\mathbf{N}^\times)\mathbf{R} \cdot \mathbf{V}(t-1)^T = \exp(-\varepsilon\pi\mathbf{N}^\times)\exp(\pi\mathbf{N}^\times) = \exp((1-\varepsilon)\pi\mathbf{N}^\times) \neq \exp(\pi\mathbf{N}^\times)$. Therefore, if $\kappa(t) \neq 0$ for some $t \in \mathbb{Z}_+$, then $\mathbf{R}\mathbf{V}(t'-1)^T \neq \exp(\pi\mathbf{N}^\times)$ for all $t' \geq t$, if not, then $\tilde{\mathbf{R}} = \mathbf{V}(t-1)$. \square

8.4 Numerical simulation results

In this section, we consider a spacecraft with inertia matrix $\mathbf{J}_c = \text{diag}(10, 8, 8)$ and discretization time-step $h = 0.1$. In the figures, we plot the orientation maneuvers on the sphere S^2 , where the vector $[x \ y \ z]^T$, corresponding to the first column of $\mathbf{C}(t)$, is plotted in green; the second is in blue; and the third is in red. These vectors correspond to the alignments of body fixed frame axes relative to an inertial frame.

The objective is to achieve tracking of an equilibrium reference signal, while simultaneously satisfying spacecraft constraints. We consider two constraints to be enforced by the RG: a pointing inclusion constraint and a thrust limit. The pointing inclusion constraint is given as a constraint that the spacecraft point in the direction of a fixed target, such as the Earth; this inclusion constraint may also be considered as an exclusion constraint, requiring the spacecraft not point outside of the inclusion zone. For example, in order to avoid damage to the photosensitive equipment, we may require that the spacecraft not point towards the Sun. The inclusion constraint that we consider here is that the spacecraft point within 60° of the fixed axis, e_3 . This can be expressed as a constraint on the (3, 3) entry of the matrix $\mathbf{C}(t)$,

$$\mathbf{C}_{33}(t) \geq \cos 60^\circ = 0.5. \quad (8.15)$$

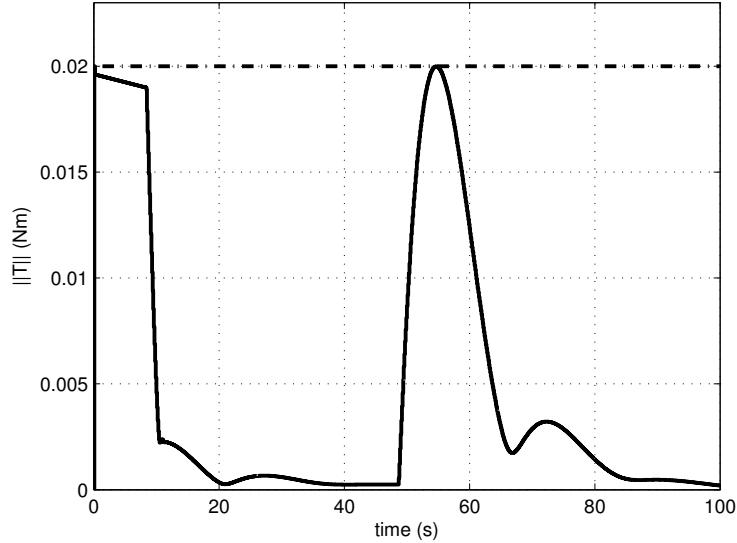


Figure 8.1: $\|T(t)\|_2$ (solid) response plotted against the torque constraint (dot-dashed)

The other constraint is a limit on the thrust force, which is expressed as,

$$\|T(t)\|_2 \leq 0.02. \quad (8.16)$$

We choose the set \mathcal{V} as a compact set, the elements of which result in equilibria that strictly satisfy (8.15) in steady state.

Figs. 8.1-8.4 present simulation results corresponding to the reference governor simulation with closed-loop control gains $\mathbf{A} = \text{diag}(0.1, 0.2, 0.3)$ and $\mathbf{K} = 0.2\mathbf{I}$. The reference governor modifies the reference to command the rotation, while enforcing all constraints, from an initial condition close to the inclusion constraint boundary to the reference rotation $\mathbf{R}(t) \equiv \mathbf{I}$. The only constraint that becomes active in the closed-loop trajectory is the control constraint, which is plotted in Fig. 8.1; the corresponding time history of the angular velocity is plotted in Fig. 8.2; that of the reference governor parameter κ_k is plotted in Fig. 8.3 and shows that the reference governor modifies the desired rotation signal until the desired reference is admissible. In Fig. 8.4, we plot the orientation maneuver of the spacecraft along with the trajectory of the admissible reference $\mathbf{V}(t)$.

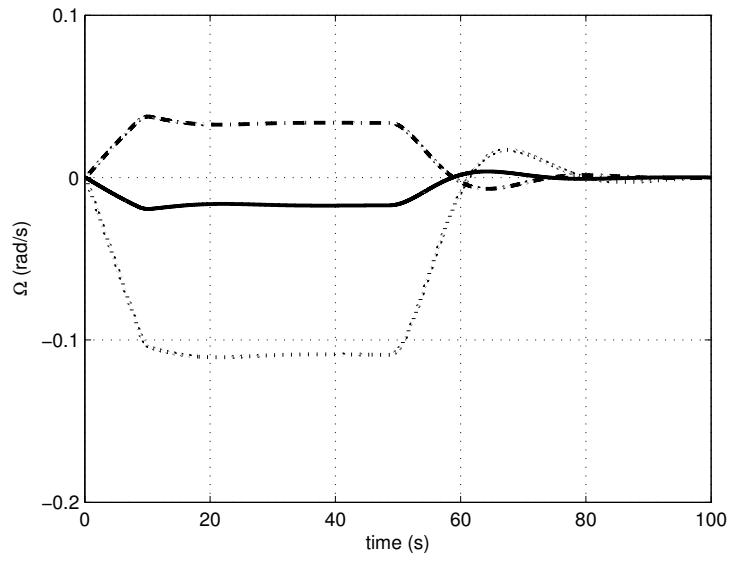


Figure 8.2: $\Omega_1(t)$ (solid), $\Omega_2(t)$ (dot-dash), and $\Omega_3(t)$ (dotted) responses

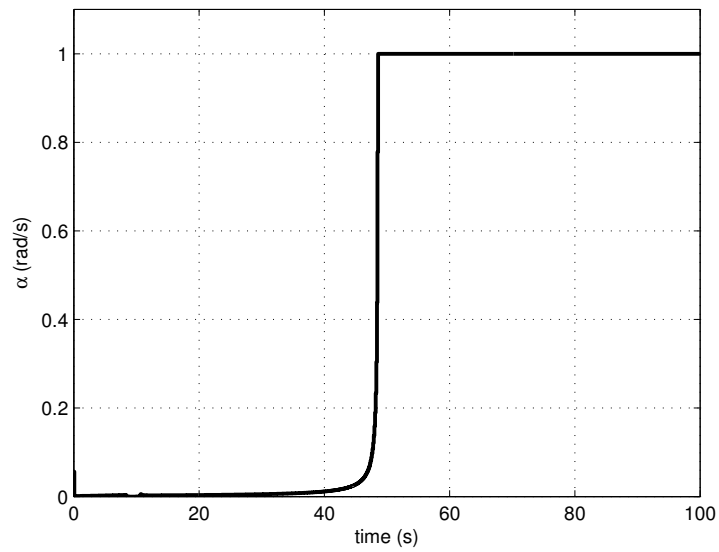


Figure 8.3: $\kappa(t)$ response

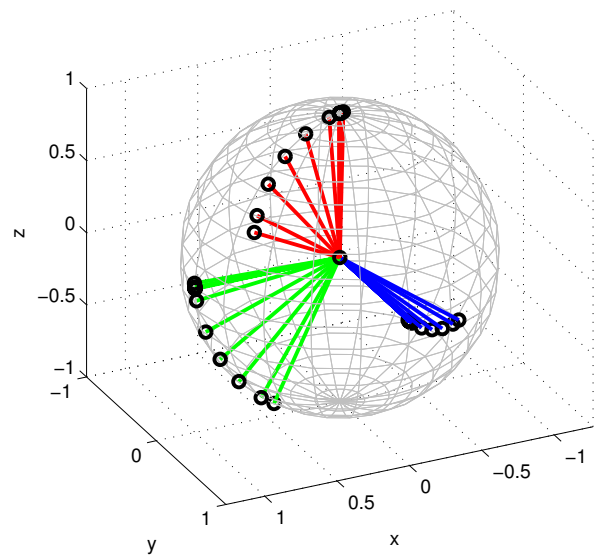


Figure 8.4: Orientation maneuver plotted at 10s increments

Conclusions and future work

Conclusions

This dissertation has focused on the theoretical developments and practical applications of RGs and related schemes. The RG and ECG theory has been extended in various ways. In particular, we have developed a theory for governors applied to reduced order and decentralized systems. We have also developed prioritized governor schemes and schemes for the case where a linear system is subject to nonlinear constraints. We also derived results for the case of governors applied to systems that track time-varying references or enforce time-dependent constraints. Three applications were considered. The first was the enforcement of the compressor surge constraint in turbocharged gasoline engines. The second was the enforcement of constraints for a flying wind-energy system. The third was the enforcement of spacecraft attitude constraints, in which case the dynamics evolve on the Lie group $SO(3)$. In the first application, we successfully tested the RG in an experimental vehicle, while in the second and third application we simulated the RG on nonlinear models.

The main developments and results are summarized below for each of the above developments.

Reduced-order reference governors and extended command governors

We presented an approach to implementing RGs and ECGs based on reduced-order models while guaranteeing that constraints are enforced for the full-order system. Our approach takes advantage of a system decomposition into fast and slow states and a reduced-order model design that reflects the dynamics of the slow states with tightened constraints. We have extended the theory to include observers and handle observer errors. Finally, we presented numerical examples; the first example was a turbocharged gasoline engine and the second was an infinite-dimensional system that was motivated by applications to control of very flexible aircraft.

Reference governors for decentralized systems

We presented two different decentralized constrained control methods that exploit RG techniques. The first design is for systems of lower-order that are connected over a network, where it is feasible for every subsystem to reconstruct the full state but where there is a delay in communicating the other subsystems' reference inputs. The second design is for higher-order systems, where the constraint enforcement by every subsystem is handled through a partition of the constraint set, so that the satisfaction of every constraint partition ensures that the full constraint is enforced overall. Numerical simulations using these methods were presented and showed that they enforced constraints in a decentralized manner. The first method was applied to an aircraft engine and the second to a mass-spring-damper, and appropriate simulation results were reported.

Command governors for prioritized constraints and reference governors for prioritized references

We presented two strategies in applying the theories of RGs and CGs to constrained systems subject to prioritization. The first scheme is applicable to soft constraints which are satisfied in order of priority by applying the CG to slack variables that augment the constraints. The second scheme considers an RG applied to a prioritized sequence of inputs whose goal is to maintain the set-points with highest priority as close as possible to their desired values. Theoretical results and simulations have been presented for both schemes.

Reference governors for linear systems subject to nonlinear constraints

We considered applications of the RG to linear system models but with nonlinear constraints. This case frequently occurs in practice, including when feedback linearization is used. We discussed different cases: convex, convex-quadratic, MLD (specifically if-then), and concave constraints. The response properties of the RG are based on previous work [2], but the computations can be arranged elegantly and in the same spirit as the explicit solution [7] for the linear RG with linear constraints. Finally, using the developed ideas, we presented an effective treatment of constraints in the examples of spacecraft rendezvous as well as in an electromagnetically actuated mass-spring-damper.

Reference and command governors for systems with slowly time-varying references and time-dependent constraints

We considered the application of RGs and CGs to systems subject to slowly-varying reference inputs and slowly-varying constraints. The use of constraint-admissible λ -contractive sets was exploited in place of invariant sets in the ordinary theory. This was done to guarantee that the system can respond quickly enough to changes in either the desired reference or constraints.

In the case of slowly-varying references, we showed constraint adherence and finite-time convergence of the admissible reference to the desired reference, *i.e.*, the usual RG and CG convergence properties, have been generalized to the case of time-varying references. We also showed that we are able to enforce time-dependent constraints and guarantee recursive feasibility if the constraints vary slowly enough. The results of numerical simulations were also presented for each case.

Reference governors for the enforcement of compressor surge constraints

We considered the application of a linear RG to the enforcement of surge constraints in a turbocharged vehicle engine. Two strategies were proposed. The first was an inner-loop RG strategy that governed the throttle actuator. The second was an outer-loop RG strategy that governed the desired air mass. After appropriate modifications that took system nonlinearities into account, both strategies were able to enforce the surge constraints; however, the inner-loop RG required gain scheduling on engine speed to do so. Experimental results from vehicle tests were presented showing surge mitigation in both cases.

Reference governors for airborne wind energy systems

We presented an RG-based approach for guaranteeing that critical flight constraints are satisfied for a wind energy system. We detailed the modifications made to the RG in order to apply it to a nonlinear longitudinal dynamic model and we demonstrated the satisfaction of critical altitude, tether tension, and angle of attack constraints in the presence of realistic set-point variations and wind disturbance inputs through simulation.

Reference governors for constrained spacecraft attitude control on $SO(3)$

We considered the problem of applying an RG to the constrained control of spacecraft attitude dynamics. The RG uses the LGVI to update the predicted trajectory

on $\text{SO}(3)$. We showed that the RG guarantees constraint admissibility and convergence to the desired equilibrium and presented numerical results illustrating these properties.

Future work

Synthesis of decentralized schemes

It is clear that the two decentralized methods considered in Chapter 2 are not mutually exclusive. A natural extension is to change the second scheme to the scheme where the subsystem RGs communicate on a network with some delay. In such a case, there would be no need to partition Y , but each subsystem would need to handle modified versions of the constraints (2.7).

Furthermore, we are able to extend the case of decentralized RGs coupled with an observer to the case of multiple delays. The development of this would be similar to that of RGs for network control systems subject to observer delay as in [49].

Designing ordinary RGs using maximal contractive sets

Ordinary RGs use O_∞ , which has been constructed to include *all* references reachable in steady-state. Computationally this may take a long time, and methods of approximating O_∞ have been created for this reason. An alternative method of approximating O_∞ may be to consider a set with properties similar to O_∞^λ , which includes only the set of references which are guaranteed to exponentially approach the desired reference faster than a certain rate $\lambda < 1$. This approximation is smaller than O_∞ and as a result may be computed more quickly. As $\lambda \rightarrow 1$, the approximation likely approaches O_∞ ; however, this result remains to be shown.

Designing the auxiliary dynamics (\bar{C}, \bar{A}) in the ECG

The choice of auxiliary dynamics in the case of the ECG is unclear. Based on experience and numerical simulations, it appears that we obtain good performance when choosing the eigenvalues of \bar{A} to coincide with that of the system dynamics A . Furthermore, consider the optimal control problem of minimizing $\sum_{t=0}^{\infty} (r - v(t))^T R (r - v(t))$ subject to the dynamics (0.1) where A is invertible. When constraints are not active,

the controller dynamics are of the form,

$$\begin{aligned}\bar{x}(t+1) &= A^{-\text{T}}\bar{x}(t), \\ v(t) &= -R^{-1}B^{\text{T}}A^{-\text{T}}\bar{x}(t) + r,\end{aligned}$$

which is similar to the auxiliary dynamics (0.13). Since $A^{-\text{T}}$ is unstable, if A is asymptotically stable then the above cannot be used as an auxiliary subsystem, yet the connection is still interesting. The best choice of \bar{C} and \bar{A} requires more attention.

RGs for Lie groups and manifolds

The main idea behind the modified RG in Chapter 8 is that it varies the reference $\mathbf{V}(t)$ along the geodesic connecting $\mathbf{V}(t-1)$ and $\mathbf{R}(t)$ on $\text{SO}(3)$. This is an extension of the ordinary RG, which varies the reference $v(t)$ along the line segment connecting $v(t-1)$ and $r(t)$ in \mathbb{R}^n . Such an extension could naturally be made to any smooth manifold, provided at least one geodesic exists between any two points on a manifold.

BIBLIOGRAPHY

- [1] G. Goodwin, M. Seron, and J. A. De Doná, *Constrained Control and Estimation: An Optimization Approach*. London, England: Springer, 2005.
- [2] E. Gilbert and I. Kolmanovsky, “Nonlinear tracking control in the presence of state and control constraints: A generalized reference governor,” *Automatica*, vol. 38, no. 12, pp. 2063–2073, 2002.
- [3] A. Bemporad, “Reference governor for constrained nonlinear systems,” *IEEE Trans. Autom. Control*, vol. 43, no. 3, pp. 415–419, 1998.
- [4] D. Angeli, A. Casavola, and E. Mosca, “On feasible set-membership state estimators in constrained command governor control,” *Automatica*, vol. 37, no. 1, pp. 151–156, 2001.
- [5] I. Kolmanovsky and E. G. Gilbert, “Theory and computation of disturbance invariant sets for discrete-time linear systems,” *Math. Problems Eng.*, vol. 4, no. 4, pp. 317–367, 1998.
- [6] E. G. Gilbert and C. J. Ong, “Linear systems with hard constraints and variable set points: Their robustly invariant sets,” Department of Mechanical Engineering, National University of Singapore, Singapore, Tech. Rep. C08-2002, 2008.
- [7] E. G. Gilbert and I. Kolmanovsky, “Fast reference governors for systems with state and control constraints and disturbance inputs,” *Int. J. Robust Nonlinear Control*, vol. 9, no. 15, pp. 1117–1141, 1999.
- [8] E. G. Gilbert and C.-J. Ong, “Constrained linear systems with hard constraints and disturbances: An extended command governor with large domain of attraction,” *Automatica*, vol. 47, no. 2, pp. 334–340, 2011.
- [9] P. Kamasouris, M. Athans, and G. Stein, “Design of feedback control systems for stable plants with saturating actuators,” in *Proc. IEEE Conf. Decision and Control*, Austin, TX, Dec. 1988, pp. 469–479.
- [10] —, “Design of feedback control systems for unstable plants with saturating actuators,” in *Proc. IFAC Symp. Nonlinear Control Syst. Design*, Capri, Italy, Jun. 1989, pp. 302–307.

- [11] P. Kapasouris and M. Athans, “Control systems with rate and magnitude saturation for neutrally stable open loop systems,” in *Proc. IEEE Conf. Decision and Control*, Honolulu, HI, Dec. 1990, pp. 3404–3409.
- [12] E. G. Gilbert and K. T. Tan, “Linear systems with state and control constraints: The theory and application of maximal output admissible sets,” *IEEE Trans. Autom. Control*, vol. 36, no. 9, pp. 1008–1020, 1991.
- [13] K. T. Tan, “Maximal output admissible sets and the nonlinear control of linear discrete-time systems with state and control constraints,” Ph.D. dissertation, University of Michigan, Ann Arbor, 1991.
- [14] E. G. Gilbert, I. Kolmanovsky, and K. T. Tan, “Nonlinear control of discrete-time linear systems with state and control constraints: A reference governor with global convergence properties,” in *Proc. IEEE Conf. Decision and Control*, Lake Buena Vista, FL, Dec. 1994, pp. 144–149.
- [15] —, “Discrete-time reference governors and the nonlinear control of systems with state and control constraints,” *Int. J. Robust Nonlinear Control*, vol. 5, no. 5, pp. 487–504, 1995.
- [16] A. Bemporad and E. Mosca, “Constraint fulfilment in control systems via predictive reference management,” in *Proc. IEEE Conf. Decision and Control*, Lake Buena Vista, FL, Dec. 1994, pp. 3017–3022.
- [17] —, “Nonlinear predictive reference governor for constrained control systems,” in *Proc. IEEE Conf. Decision and Control*, New Orleans, LA, Dec. 1995, pp. 1205–1210.
- [18] A. Bemporad, A. Casavola, and E. Mosca, “Nonlinear control of constrained linear systems via predictive reference management,” *IEEE Trans. Autom. Control*, vol. 42, no. 3, pp. 340–349, 1997.
- [19] A. Casavola, E. Mosca, and D. Angeli, “Robust command governors for constrained linear systems,” *IEEE Trans. Autom. Control*, vol. 45, no. 11, pp. 2071–2077, 2000.
- [20] A. Casavola, E. Mosca, and M. Papini, “Control under constraints: An application of the command governor approach to an inverted pendulum,” *IEEE Trans. Contr. Syst. Technol.*, vol. 12, no. 1, pp. 193–204, 2004.
- [21] I. Kolmanovsky and J. Sun, “Parameter governors for discrete-time nonlinear systems with pointwise-in-time state and control constraints,” *Automatica*, vol. 42, no. 5, pp. 841–848, 2006.
- [22] F. Borrelli, P. Falcone, J. Pekar, and G. Stewart, “Reference governor for constrained piecewise affine systems,” *J. Process Control*, vol. 19, no. 8, pp. 1229–1237, 2009.

- [23] E. Garone and F. Tedesco, “Sensorless supervision of linear dynamical systems: The feed-forward command governor approach,” *Automatica*, vol. 47, no. 7, pp. 1294–1303, 2011.
- [24] A. Casavola, E. Garone, and F. Tedesco, “Improved feed-forward command governor strategies for constrained discrete-time linear systems,” *IEEE Trans. Autom. Control*, vol. 59, no. 1, pp. 216–223, 2014.
- [25] S. Di Cairano and I. Kolmanovsky, “Rate limited reference governor for network controlled systems,” in *Proc. American Control Conf.*, Baltimore, MD, Jun. 2010, pp. 3704–3709.
- [26] —, “Further developments and applications of network reference governor for constrained systems,” in *Proc. American Control Conf.*, Montreal, QC, Jun. 2012, pp. 3907–3912.
- [27] I. Kolmanovsky, U. Kalabić, and E. Gilbert, “Developments in constrained control using reference governors,” in *Proc. Nonlinear Model Predictive Control Conf.*, Noordwijkerhout, Netherlands, Aug. 2012, pp. 282–290.
- [28] I. Kolmanovsky, E. Garone, and S. Di Cairano, “Reference and command governors: A tutorial on their theory and automotive applications,” in *Proc. American Control Conf.*, Portland, OR, Jun. 2014, pp. 226–241.
- [29] R. Miller, I. V. Kolmanovsky, E. G. Gilbert, and P. Washabaugh, “Control of constrained nonlinear systems: A case study,” *IEEE Control Syst. Mag.*, vol. 20, no. 1, pp. 23–32, 2000.
- [30] S.-R. Oh and S. K. Agrawal, “A reference governor-based controller for a cable robot under input constraints,” *IEEE Trans. Control Syst. Technol.*, vol. 13, no. 4, pp. 639–645, 2005.
- [31] C. Peterson, A. Juanzemis, M. Baldwin, M. Holzinger, and I. Kolmanovsky, “Model predictive control and extended command governor for improving robustness of relative motion guidance and control,” in *Proc. AAS/AIAA Space Flight Mech. Meeting*, Santa Fe, NM, Jan. 2014, pp. AAS–14–249.
- [32] I. V. Kolmanovsky, E. G. Gilbert, and H. E. Tseng, “Constrained control of vehicle steering,” in *Proc. IEEE Conf. Control Applicat.*, St. Petersburg, Russia, Jul. 2009, pp. 571–581.
- [33] J. Sun and I. Kolmanovsky, “Load governor for fuel cell oxygen starvation protection: A robust nonlinear reference governor approach,” *IEEE Trans. Control Syst. Technol.*, vol. 13, no. 6, pp. 911–920, 2005.
- [34] A. Vahidi, I. Kolmanovsky, and A. Stefanopoulou, “Constraint handling in a fuel cell system: A fast reference governor approach,” *IEEE Trans. Control Syst. Technol.*, vol. 15, no. 1, pp. 86–98, 2007.

- [35] V. Tsourapas, J. Sun, and A. Stefanopoulou, “Incremental step reference governor for load conditioning of hybrid fuel cell and gas turbine power plants,” *IEEE Trans. Control Syst. Technol.*, vol. 17, no. 4, pp. 756–767, 2009.
- [36] S. Jade, E. Hellström, J. Larimore, A. G. Stefanopoulou, and L. Jiang, “Reference governor for load control in a multicylinder recompression HCCI engine,” *IEEE Trans. Control Syst. Technol.*, vol. 22, no. 4, pp. 1408–1421, 2014.
- [37] S. D. Jade, “Transient load-speed control in multi-cylinder recompression HCCI engines,” Ph.D. dissertation, University of Michigan, Ann Arbor, 2014.
- [38] U. V. Kalabić, I. V. Kolmanovsky, and E. G. Gilbert, “Reduced order extended command governors,” *Automatica*, vol. 50, no. 5, pp. 1466–1472, 2014.
- [39] U. V. Kalabić, J. H. Buckland, S. L. Cooper, S. K. Wait, and I. V. Kolmanovsky, “Reference governors for enforcing compressor surge constraints,” *IEEE Trans. Control Syst. Technol.*, submitted for publication.
- [40] U. Kalabić, I. Kolmanovsky, J. Buckland, and E. Gilbert, “Reduced order reference governor,” in *Proc. IEEE Conf. Decision and Control*, Maui, HI, Dec. 2012, pp. 3245–3251.
- [41] U. Kalabić and I. Kolmanovsky, “Decentralized constraint enforcement using reference governors,” in *Proc. IEEE Conf. Decision and Control*, Florence, Italy, Dec. 2013, pp. 6415–6421.
- [42] U. Kalabić, Y. Chitalia, J. Buckland, and I. Kolmanovsky, “Prioritization schemes for reference and command governors,” in *Proc. European Control Conf.*, Zurich, Switzerland, Jul. 2013, pp. 2734–2739.
- [43] U. Kalabić, I. Kolmanovsky, and E. Gilbert, “Reference governors with nonlinear constraints,” in *Proc. IEEE Conf. Decision and Control*, Orlando, FL, Dec. 2011, pp. 2680–2686.
- [44] U. Kalabić and I. Kolmanovsky, “Reference and command governors for systems with slowly time-varying references and time-dependent constraints,” in *Proc. IEEE Conf. Decision and Control*, Los Angeles, CA, Dec. 2014, pp. 6701–6706.
- [45] U. Kalabić, I. Kolmanovsky, J. Buckland, and E. Gilbert, “Reference and extended command governors for control of turbocharged gasoline engines based on linear models,” in *Proc. IEEE Int. Conf. Control Applicat.*, Denver, CO, Sep. 2011, pp. 319–325.
- [46] U. Kalabić, C. Vermillion, and I. Kolmanovsky, “Reference governor design for computationally efficient attitude and tether tension constraint enforcement on a lighter-than-air wind energy system,” in *Proc. European Control Conf.*, Zurich, Switzerland, Jul. 2013, pp. 1004–1010.

- [47] U. Kalabić, R. Gupta, S. D. Cairano, A. Bloch, and I. Kolmanovsky, “Constrained spacecraft attitude control on $SO(3)$ using reference governors and nonlinear model predictive control,” in *Proc. American Control Conf.*, Portland, OR, Jun. 2014, pp. 5586–5593.
- [48] Q. Li, U. V. Kalabić, and I. V. Kolmanovsky, “Fast reference governors for second-order linear systems with constraints and an input time-delay,” *Automatica*, vol. 50, no. 2, pp. 641–645, 2014.
- [49] S. Di Cairano, U. V. Kalabić, and I. V. Kolmanovsky, “Reference governor for network control systems subject to variable time-delay,” *Automatica*, to be published.
- [50] Q. Li, U. Kalabić, and I. Kolmanovsky, “Predictor-based reference governor for second-order linear constrained systems operated over a communication network,” in *Proc. World Congress Intelligent Control Autom.*, Shenyang, China, Jun. 2014, pp. 1700–1704.
- [51] T. Polóni, U. Kalabić, K. McDonough, and I. Kolmanovsky, “Disturbance canceling control based on simple input observers with constraint enforcement for aerospace applications,” in *Proc. IEEE Conf. Control Applicat.*, Antibes, France, Sep. 2014, pp. 158–165.
- [52] L. Meirovitch, *Fundamentals of Vibrations*. Longrove, IL: Waveland Press, 2010.
- [53] M. J. Dillsaver, C. E. S. Cesnik, and I. V. Kolmanovsky, “Gust load alleviation control for very flexible aircraft,” in *Proc. AIAA Atmospheric Flight Mech. Conf.*, Portland, OR, Aug. 2011, AIAA-2011-6368.
- [54] R. Skelton, *Dynamic Systems Control: Linear Systems Analysis and Synthesis*. New York: Wiley, 1988.
- [55] M. J. Dillsaver, U. V. Kalabić, I. V. Kolmanovsky, and C. E. S. Cesnik, “Constrained control of very flexible aircraft using reference and extended command governors,” in *Proc. American Control Conf.*, Washington, DC, Jun. 2013, pp. 1608–1613.
- [56] J. Lunze, *Feedback Control of Large Scale Systems*. Upper Saddle River, NJ: Prentice Hall, 1992.
- [57] J.-H. Kim, S. Lall, W. Merrill, and A. Behbahani, “A computational approach for decentralized control of turbine engines,” in *Proc. IEEE Conf. Decision and Control*, Atlanta, GA, Dec. 2010, pp. 346–351.
- [58] A. Behbahani, B. Wood, D. Benson, A. Berner, B. Hegwood, J. Dejager, W. Rhoden, B. Ohme, J. Sloat, and C. Harmon, “Technology requirements and development for affordable high-temperature distributed engine controls,” in *Proc. Int. Instrumentation Symp.*, San Diego, CA, Jun. 2012, pp. 305–321.

- [59] Distributed Engine Controls Working Group. (2015) Distributed engine controls working group (DECWG). [Online]. Available: <http://www.decwg.org>
- [60] F. Tedesco, A. Casavola, and E. Garone, “A distributed parallel command governor strategy for the coordination of multi-agent networked systems,” in *Proc. IFAC Nonlinear Model Predictive Control Conf.*, Noordwijkerhout, Netherlands, Aug. 2012, pp. 478–483.
- [61] H. Richter, *Advanced Control of Turbofan Engines*. New York: Springer, 2012.
- [62] S. Di Cairano, D. Yanakiev, A. Bemporad, I. V. Kolmanovsky, and D. Hrovat, “Model predictive idle speed control: Design, analysis, and experimental validation,” *IEEE Trans. Control Syst. Technol.*, vol. 20, no. 1, pp. 84–97, 2011.
- [63] A. Weiss, I. V. Kolmanovsky, and W. Merrill, “Incorporating risk into control design for emergency operation of turbo-fan engines,” in *Proc. Infotech@Aerospace Conf.*, St. Louis, MO, Mar. 2011, AIAA-2011-1591.
- [64] E. C. Kerrigan and J. M. Maciejowski, “Soft constraints and exact penalty functions in model predictive control,” in *Proc. UKACC Int. Conf. Control*, Cambridge, England, Sep. 2000.
- [65] —, “Designing model predictive controllers with prioritised constraints and objectives,” in *Proc. IEEE Int. Symp. Comput. Aided Control Syst. Design*, Glasgow, Scotland, Sep. 2002, pp. 33–38.
- [66] K. M. Sobel and E. Y. Shapiro, “A design methodology for pitch pointing flight control systems,” *J. Guidance Control Dynamics*, vol. 8, no. 2, pp. 181–187, 1985.
- [67] A. Isidori, *Nonlinear Control Systems*. New York: Springer-Verlag, 1989.
- [68] A. Bemporad and M. Morari, “Control of systems integrating logic, dynamics and constraints,” *Automatica*, vol. 35, no. 3, pp. 407–427, 1999.
- [69] B. Wie, *Spacecraft Dynamics and Control*, 2nd ed. Reston, VA: AIAA, 2010.
- [70] E. Hartley, “Model predictive control for spacecraft rendezvous,” Ph.D. dissertation, University of Cambridge, England, 2010.
- [71] H. Park, S. Di Cairano, and I. V. Kolmanovsky, “Linear quadratic model predictive control approach to spacecraft rendezvous and docking,” in *Proc. AAS/AIAA Space Flight Mech. Meeting*, New Orleans, LA, Feb. 2011, AAS-11-142.
- [72] L. Singh, S. Bortolami, and L. Page, “Optimal guidance and thruster control in orbital approach and rendezvous for docking using model predictive control,” in *Proc. AIAA Guidance Navigation Control Conf.*, Toronto, ON, Aug. 2010, AIAA-2010-7754.

- [73] W. H. Clohessy and R. S. Wiltshire, “Terminal guidance system for satellite rendezvous,” *J. Aerospace Sci.*, vol. 27, no. 9, pp. 653–658, 1960.
- [74] W. Fehse, *Automated Rendezvous and Docking of Spacecraft*. Cambridge, England: Cambridge University Press, 2003.
- [75] J. Hong, I. A. Cumming, P. D. Washabaugh, and D. S. Bernstein, “Stabilization of a mass and spring system with electromagnetic actuation,” in *Proc. IEEE Int. Conf. Control Applicat.*, Hartford, CT, Oct. 1997, pp. 189–194.
- [76] F. Blanchini and S. Miani, *Set-Theoretic Methods in Control*. New York: Birkhäuser, 2008.
- [77] M. Herceg, M. Kvasnica, C. N. Jones, and M. Morari, “Multi-parametric toolbox 3.0,” in *Proc. European Control Conf.*, Zurich, Switzerland, Jul. 2013, pp. 502–510.
- [78] N. Watson and M. Janota, *Turbocharging the Internal Combustion Engine*. London: Macmillan, 1982.
- [79] U. Kalabić and I. Kolmanovsky, “Inner-loop reference governors: Placing reference governors inside the control loop using passivity,” in *Proc. IEEE Conf. Decision Control*, submitted for publication.
- [80] O. Leufven and L. Eriksson, “Time to surge concept and surge control for acceleration performance,” in *Proc. IFAC World Congress*, Seoul, South Korea, Jul. 2008, pp. 2063–2068.
- [81] L. Eriksson, L. Nielsen, J. B. rd, J. Bergström, F. Petersson, and P. Andersson, “Modeling of a turbocharged SI engine,” *Annu. Reviews Control*, vol. 26, no. 1, pp. 129–137, 2002.
- [82] L. Eriksson, “Modeling and control of turbocharged SI and DI engines,” *Oil & Gas Sci. Technol.*, vol. 62, no. 4, pp. 523–538, 2007.
- [83] J. H. Buckland, “Estimation methods for turbocharged spark ignition engines,” Ph.D. dissertation, University of Michigan, Ann Arbor, 2009.
- [84] P. Williams, B. Lansdorp, and W. Ockels, “Optimal cross-wind towing and power generation with tethered kites,” *J. Guidance Control Dynamics*, vol. 31, no. 1, pp. 81–93, 2008.
- [85] F. Canale, L. Fagiano, and M. Milanese, “High altitude wind energy generation using controlled power kites,” *IEEE Trans. Control Syst. Technol.*, vol. 18, no. 2, pp. 279–293, 2010.
- [86] L. Fagiano, “Control of tethered airfoils for high-altitude wind energy generation,” Ph.D. dissertation, Polytechnic University of Turin, Italy, 2009.

- [87] A. Ilzhofer, B. Houska, and M. Diehl, “Nonlinear MPC of kites under varying wind conditions for a new class of large-scale wind power generators,” *Int. J. Robust Nonlinear Control*, vol. 17, no. 17, pp. 1590–1599, 2007.
- [88] S. Gros, M. Zanon, and M. Diehl, “Orbit control for a power generating airfoil based on nonlinear MPC,” in *Proc. American Control Conf.*, Montreal, QC, Jun. 2012, pp. 137–142.
- [89] S. Wrage and S. Brabeck, “Wind energy plant with a steerable kite,” Patent US7504741, Mar. 17, 2009.
- [90] S. Griffith, W. Hua, C. Hardham, P. Lynn, and J. McBride, “Controlling power extraction for wind power generation,” Patent US7656053, Aug. 3, 2010.
- [91] C. Vermillion, T. Grunnagle, and I. Kolmanovsky, “Modeling and control design of a lighter-than-air wind energy system,” in *Proc. American Control Conf.*, Montreal, QC, Jun. 2012, pp. 5813–5818.
- [92] C. Vermillion, T. Grunnagle, R. Lim, and I. Kolmanovsky, “Model-based plant design and hierarchical control of a prototype lighter-than-air wind energy system, with experimental flight test results,” *Trans. Control Syst. Technol.*, vol. 22, no. 2, pp. 531–542, 2014.
- [93] R. Weng, K. Balasubramanian, C. Vermillion, and I. Kolmanovsky, “Model predictive longitudinal control of a lighter-than-air wind energy system,” in *Proc. ASME Dynamic Syst. Control Conf.*, Fort Lauderdale, FL, Oct. 2012, DSCC2012-8613.
- [94] C. L. Archer and K. Caldeira, *Atlas of High Altitude Wind Power*. Stanford, CA: Carnegie Institute for Science, 2008.
- [95] —, “Global assessment of high-altitude wind power,” *Energies*, vol. 2, no. 2, pp. 307–319, 2009.
- [96] P. Dewdney, M. Nahon, and B. Veidt, “The large adaptive reflector: A giant radio telescope with an aero twist,” *Canadian Aeronautics Space J.*, vol. 48, no. 4, pp. 239–250, 2002.
- [97] M. Nahon, G. Gilardi, and C. Lambert, “Dynamics/control of a radio telescope receiver supported by a tethered aerostat,” *J. Guidance Control Dynamics*, vol. 25, no. 6, pp. 1107–1115, 2002.
- [98] “Flying qualities of piloted airplanes,” U.S. Military Spec. MIL-F-8785C, 1980.
- [99] T. Lee, N. H. McClamroch, and M. Leok, “A Lie group variational integrator for the attitude dynamics of a rigid body with applications to the 3D pendulum,” in *Proc. IEEE Int. Conf. Control Applicat.*, Toronto, ON, Aug. 2005, pp. 962–967.

- [100] —, “Attitude maneuvers of a rigid spacecraft in a circular orbit,” in *Proc. American Control Conf.*, Minneapolis, MN, Jun. 2006, pp. 1742–1747.
- [101] T. Lee, M. Leok, and N. H. McClamroch, “Lie group variational integrators for the full body problem in orbital mechanics,” *Celestial Mech. Dynamical Astronomy*, vol. 98, no. 2, pp. 121–144, 2007.
- [102] —, “Optimal attitude control of a rigid body using geometrically exact computations on $SO(3)$,” *J. Dynamical Control Syst.*, vol. 14, no. 4, pp. 465–487, 2008.
- [103] T. Lee, “Computational geometric mechanics and control of rigid bodies,” Ph.D. dissertation, University of Michigan, Ann Arbor, 2008.
- [104] A. M. Bloch, I. I. Hussein, M. Leok, and A. K. Sanyal, “Geometric structure-preserving optimal control of the rigid body,” *J. Dynamical Control Syst.*, vol. 15, no. 3, pp. 307–330, 2009.
- [105] N. Nordkvist and A. K. Sanyal, “Attitude feedback tracking with optimal attitude state estimation,” in *Proc. American Control Conf.*, Baltimore, MD, Jun. 2010, pp. 2861–2866.
- [106] N. A. Chaturvedi, A. K. Sanyal, and N. H. McClamroch, “Rigid body attitude control: Using rotation matrices for continuous, singularity-free control laws,” *IEEE Control Syst. Mag.*, vol. 31, no. 3, pp. 30–51, 2011.
- [107] J. E. Marsden and M. West, “Discrete mechanics and variational integrators,” *Acta Numerica*, vol. 10, pp. 357–514, 2001.
- [108] D. V. Zenkov, M. Leok, and A. M. Bloch, “Hamel’s formalism and variational integrators on a sphere,” in *Proc. IEEE Conf. Decision Control*, Maui, HI, Dec. 2012, pp. 7504–7510.
- [109] J. Moser and A. Veselov, “Discrete versions of some classical integrable systems and factorization of matrix polynomials,” *Commun. Math. Physics*, vol. 139, no. 2, pp. 217–243, 1991.
- [110] J. R. Cardoso and F. S. Leite, “The Moser-Veselov equation,” *Linear Algebra Applicat.*, vol. 360, no. 1, 2003.
- [111] A. Sanyal, A. Forsbury, N. Chaturvedi, and D. S. Bernstein, “Inertia-free spacecraft attitude tracking with disturbance rejection and almost global stabilization,” *J. Guidance Control Dynamics*, vol. 32, no. 4, pp. 1167–1178, 2009.
- [112] M. Moakher, “Means and averaging in the group of rotations,” *SIAM J. Matrix Anal. Applicat.*, vol. 24, no. 1, pp. 1–16, 2002.
- [113] T. Lee, “Geometric tracking control of the attitude dynamics of a rigid body on $SO(3)$,” in *Proc. American Control Conf.*, San Francisco, CA, Jun. 2011, pp. 1200–1205.